JOURNAL OF CAVE AND KARST STUDIES

August 2010
Volume 72, Number 2
ISSN 1090-6924
A Publication of the National Speleological Society

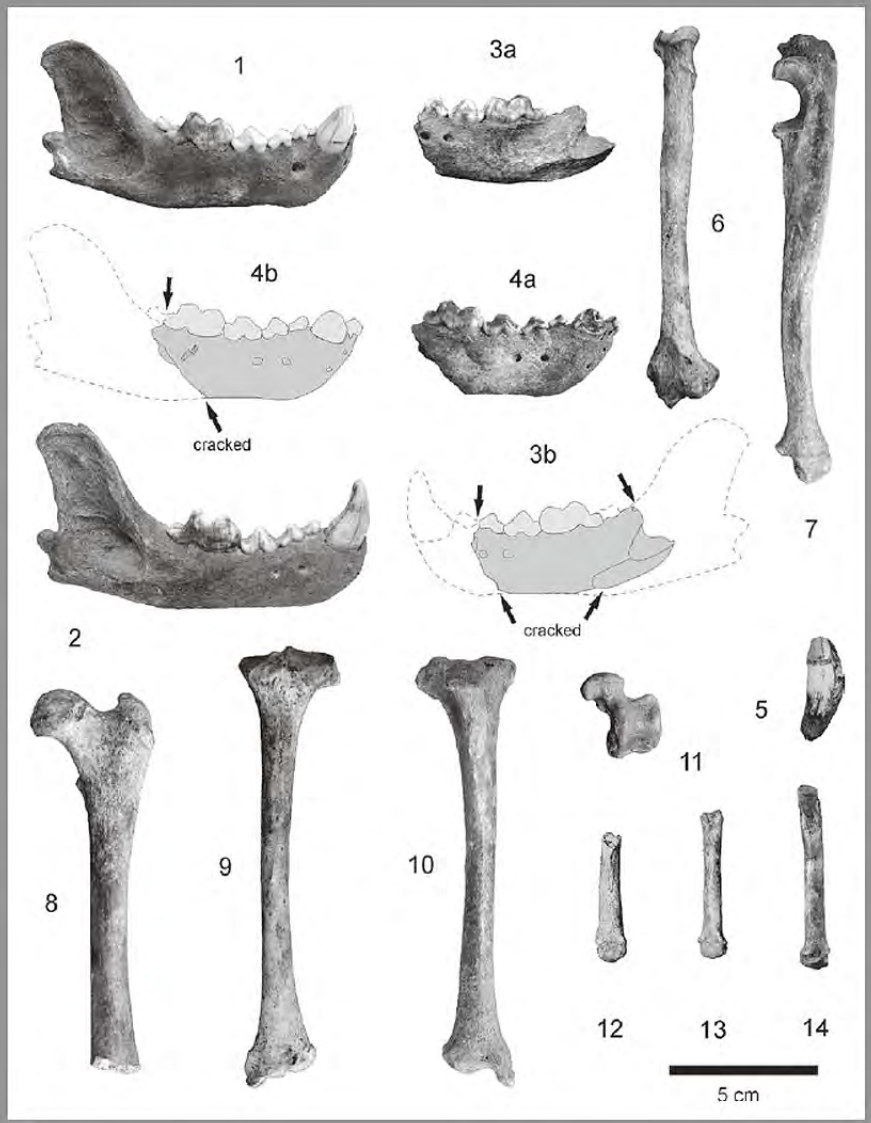

IN THIS ISSUE:

Czech Republic Wolverine bones, a new Harvestman from West Virginia, Secondary minerals in Hawai'ian Volcanic Caves, and more...

Published By
The National Speleological Society

The *Journal of Cave and Karst Studies* (ISSN 1090-6924, CPM Number #40065056) is a multi-disciplinary, refereed journal published three times a year by the National Speleological Society, 2813 Cave Avenue, Huntsville, Alabama 35810-4431 USA; Phone (256) 852-1300; Fax (256) 851-9241, email: nss@caves.org; World Wide Web: http://www.caves.org/pub/journal/.
Check the *Journal* website for subscripion rates. Back issues and cumulative indices are available from the NSS office.

POSTMASTER: send address changes to the *Journal of Cave and Karst Studies*, 2813 Cave Avenue, Huntsville, Alabama 35810-4431 USA.

The *Journal of Cave and Karst Studies* is covered by the following ISI Thomson Services Science Citation Index Expanded, ISI Alerting Services, and Current Contents/Physical, Chemical, and Earth Sciences.

Front cover: Plate 4 from Diedrich and Copeland in this issue.

W.J. Waterstrat, J.E. Mylroie, A.M. Owen, and J.R. Mylroie – Coastal caves in Bahamian eolian calcarenites: differentiating between sea caves and flank margin caves using quantitative morphology. *Journal of Cave and Karst Studies,* v. 72, no. 2, p. 61–74. DOI: 10.4311/jcks2009es0086

COASTAL CAVES IN BAHAMIAN EOLIAN CALCARENITES: DIFFERENTIATING BETWEEN SEA CAVES AND FLANK MARGIN CAVES USING QUANTITATIVE MORPHOLOGY

WILLAPA J. WATERSTRAT, JOHN E. MYLROIE, ATHENA M. OWEN, AND JOAN R. MYLROIE
Department of Geosciences, Mississippi State University, Mississippi State, MS 39762 USA, willapajames@hotmail.com, mylroie@geosci.msstate.edu, dinosaurgoddess@yahoo.com, jmylroie@deanas.msstate.edu

Abstract: Coastal areas on carbonate islands commonly contain two types of caves: sea caves developed by wave erosion processes, and flank margin caves developed by dissolution at the edge of the fresh-water lens. Differentiating sea caves and flank margin caves in coastal settings is important, but can it be done reliably and quantitatively? Current methods use the degree of intricate wall-rock dissolution and the presence or absence of dense calcite speleothems to separate the two cave types. This study reports how analysis of cave maps creates three separate tools to differentiate coastal caves: area to perimeter ratio, entrance width to maximum width ratio, and rectangle short axis to long axis ratio. The study also presents some of the first sea cave data from eogenetic carbonate islands, specifically eolian calcarenites. The morphological and geometrical comparisons between Bahamian flank margin cave and sea cave maps using the three tools allows the two cave types to be statistically differentiated. The Bahamian sea cave data were also compared to sea cave data from California and Maine to demonstrate that Bahamian sea caves have a unique quantitative signature based on the youth and homogeneity of the host eolian calcarenite rock. The Bahamian sea cave data also indicate that sea cave formation may not be solely determined by differential rock weaknesses, as reported in the literature, but may also be a result of wave dynamics such as constructive interference.

INTRODUCTION

On carbonate islands such as the Bahamas, there exists a mechanism for producing dissolutional caves adjacent to coastlines at or near sea level. Dissolution occurs in the phreatic environment of a floating Ghyben-Herzberg-Dupuit fresh-water lens as a result of: 1) mixing with vadose fresh water descending to the lens, and mixing with phreatic marine water below the lens; 2) oxidation of organics trapped at the density interfaces at the top and bottom of the lens; and 3) the increased flow velocity associated with the distal lens margin (Mylroie and Mylroie, 2007). This dissolutional environment results in caves that are unique to these island/coastal carbonate settings. Termed flank margin caves (Mylroie and Carew, 1990), these caves exhibit a morphology that is very different from epigenic stream caves, but very similar to that observed in hypogenic caves (Mylroie and Mylroie, 2007; Palmer, 1991; 2007). As seen in Figures 1 and 2, flank margin caves commonly consist of oval chambers separated by thin bedrock walls, maze-like passages, undulating ceilings and floors, bedrock pillars, and complex wall morphology. The dissolutional bedrock morphology and interior deposits of flank margin caves lack evidence of high-speed turbulent flow, such as ablation scallops or sediment bedforms typical of epigenic stream caves (Mylroie and Carew, 1995).

Because the locations of flank margin caves are linked with sea-level position, they record Quaternary glacioeustatic sea-level changes in the tectonically-stable Bahamas. Most enterable flank margin caves are found at approximately 2–4 m above present sea level, which, after allowing for isostatic subsidence (Carew and Mylroie, 1995a), corresponds with the height of the last interglacial sea-level highstand (~125 ka, MIS 5e). The caves are developed in Quaternary eolian calcarenites (or eolianites), composed of well-sorted, fine-grained sands lacking secondary structural features. A full discussion of Bahamian geology and karst processes can be found in Carew and Mylroie (1995b; 1997), Mylroie and Mylroie (2007), and Mylroie and Carew (2008).

Sea caves are also common features of the littoral zone on rocky coastlines with cliffs. Bahamian sea caves lack the internal complexity of flank margin caves (Figs. 3 and 4). In order for sea caves to form, Moore (1954) argued that: "The prerequisite conditions of [sea] cave formation are: 1) the presence of a sea cliff which is in direct contact with the erosive forces of waves and currents; 2) the exposed face of the cliff must contain certain geologic structures, or textures, which will allow the establishment of differential erosion; 3) the rock of which the cliff is composed must be of sufficiently resistant nature so as to prevent rapid formation of a protective beach at its base." A protective beach attenuates wave energy, and resistant rock allows for a sizeable cavity to form without collapse. Sea caves have

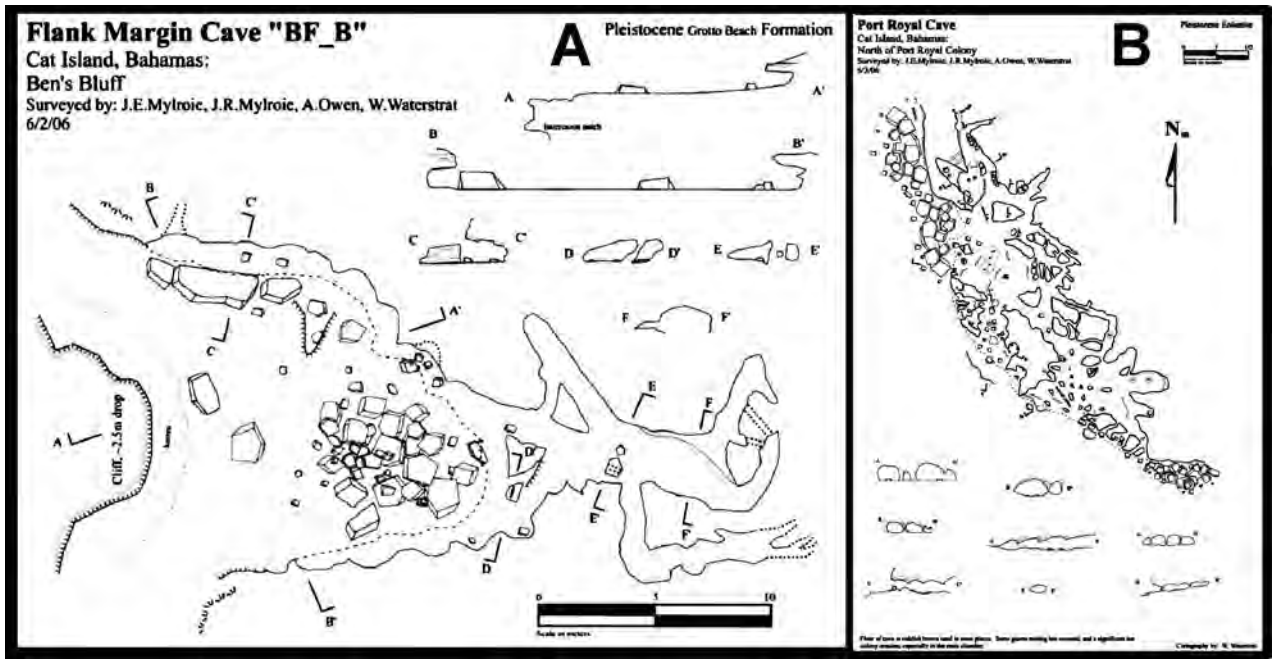

Figure 1. Maps of typical Bahamian flank margin caves currently located in coastal settings where wave action has breached into them. A) BF_B Cave, Cat Island, Bahamas. B) Port Royal Cave, Cat Island, Bahamas. Both caves were surveyed as part of the research for this paper and were added to the Roth (2004) Bahamian flank margin cave database.

therefore been considered to usually form when wave action exploits a pre-existing weakness of the rock, causing differential erosion to produce a cave. It is important to note that even in carbonate rocks, differential erosion is largely due to mechanical weathering and not necessarily to dissolution as in traditional karst caves. Weakness in the rock may be due to primary or secondary structures (Moore, 1954). Initial rock weaknesses caused by secondary structures such as joints and faults have a large effect on the shape, size, and extent of the resulting cave (Bunnell, 1988), as is clearly shown in the fault controlled, elongate sea caves of Santa Cruz Island (Fig. 5). However, in this study, Bahamian sea caves are shown to form in carbonate rocks with little or no existing secondary structural weaknesses. Eolianites are an extremely homogenous and uniform rock; their greatest heterogeneity occurs at their top contacts, where paleosols occur. Sea caves developing well below these paleosols are forming in a very uniform material.

Flank margin caves and sea caves form a cave category called coastal caves. As both cave types develop at or near sea level, they can be used for sea-level indicators. However, because flank margin caves are hypogenic in character (Palmer, 1991), and form without an entrance, they are only found when erosion and denudation has intersected them. Alternatively, sea caves must form along an actively eroding cliffline in a shoreline setting (Fig. 6). Sea caves are expressed in the surface environment as they originate, but flank margin caves are not expressed at the surface until some degree of subsequent surface denudation has occurred (Fig. 7).

The Quaternary has been a time during which sea levels have been lower than at present about 85% of the time, and flank margin caves found above sea level today formed within the short time window of Quaternary sea-level highstands (Mylroie and Mylroie, 2007). In the Bahamas, coastal caves that developed during past sea-level highstands (in the vicinity of today's sea-level elevation) have spent significant time in the subaerial environment during lower glacioeustatic sea levels. As a result, their exhumations are attributable to significant amounts of surface denudation (Fig. 7B). The degree of surface denudation can determine if a coastal cave is truncated or removed. Sea caves, forming open to the coast, are vulnerable to complete removal by a degree of surface denudation that would only truncate a flank margin cave developed at the same time (Fig. 7C). Therefore, successful differentiation between flank margin caves and sea caves can help document the degree of denudation (Fig. 7D). Because the time of cave formation is known (125 ka), the denudation rate can be estimated. Denudation is greatly affected by climate. Therefore, given that cave formation and denudation are so closely linked in time, the amount of denudation expressed by cave truncation and erosion is a paleoclimatic indicator.

Flank margin caves, because they form in the distal margin of the fresh-water lens, contain information about the configuration, discharge, and other properties of that lens. Flank margin cave configurations, sizes, and locations have been successfully used to determine past fresh-water lens properties in carbonate islands (Mylroie et al., 2008).

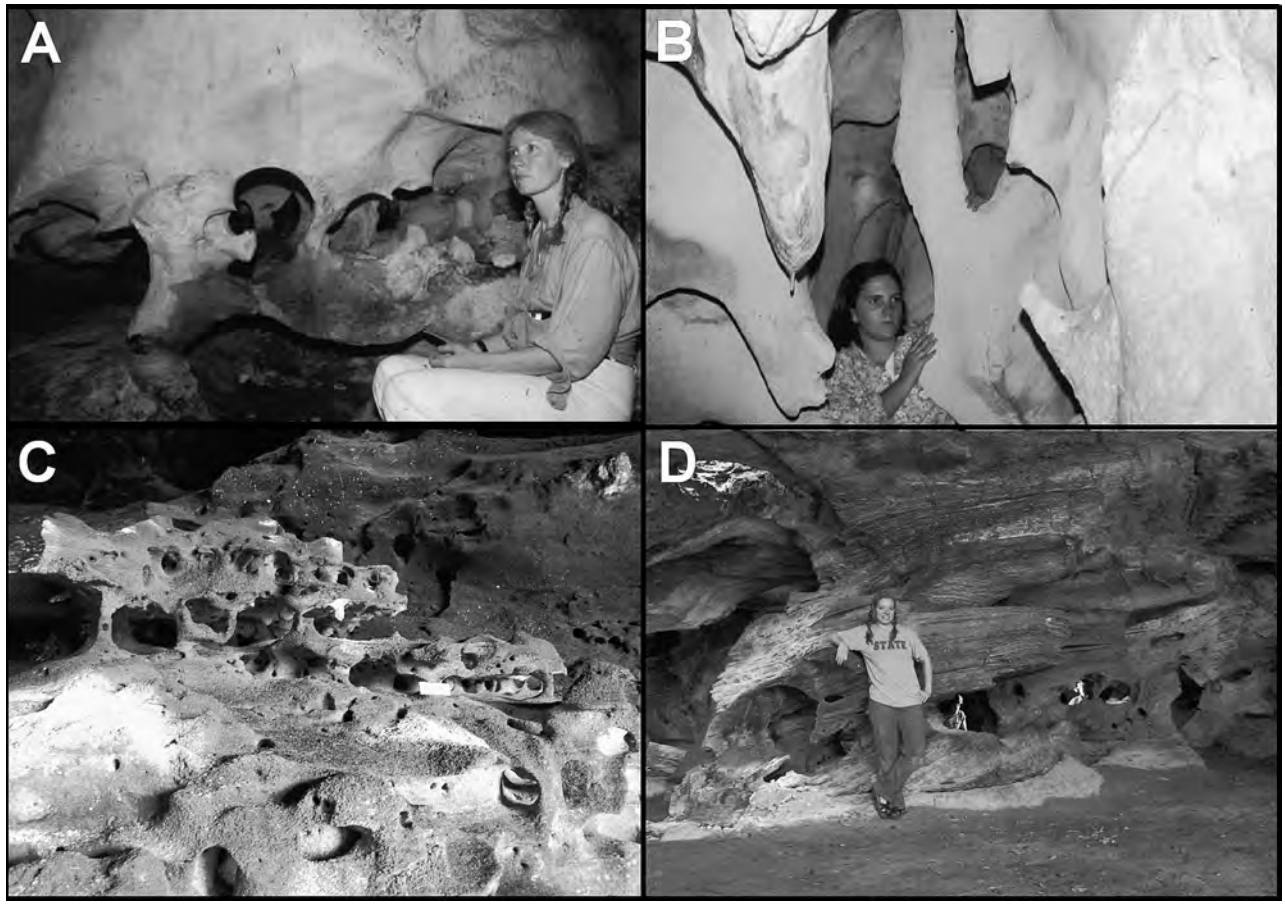

Figure 2. Images of dissolutional features typical of flank margin caves in the Bahamas and globally. Sea caves do not display the delicate bedrock sculpture seen here. A) Harry Oakes Cave, New Providence Island. B) Lighthouse Cave, San Salvador Island. C) Temple of Athena Cave, Crooked Island (scale bar is 10 cm long). D) Babylon Cave, Acklins Island; note figures visible through holes in the bedrock pillar.

The configuration of a fresh-water lens is controlled by rock properties such as porosity and permeability, and climate factors such as precipitation and evapotranspiration; if the rock properties are known, paleolens configuration can assist paleoclimatic interpretation. Therefore, determining whether a coastal cave is a flank margin cave or a true sea cave has important implications in regard to denudational processes, and as a result, paleoclimate for that region.

Speleothems have been used to differentiate sea caves from flank margin caves (Mylroie and Carew, 1991). Speleothems, especially calcite precipitates such as stalactites, stalagmites, and flowstone are usually diagnostic of development inside an enclosed cave environment. For well-ordered, dense calcite precipitation, the cave environment has to be atmospherically restricted enough to allow CO_2 diffusion, as opposed to evaporation, to dominate the calcite precipitation. Open sea caves are unlikely to provide such an environment, whereas flank margin caves, especially prior to erosional breaching, do provide such an environment (Mylroie and Carew, 1991). In open, evaporative environments, calcite precipitates tend to be porous, crumbly and tuffaceous (Taboroši et al., 2006). Therefore, the existence of well-developed calcite speleothems in truncated cave chambers (Fig 8A), and even in remnant notches (Fig 8B), can be an indicator that denudational processes have breached a dissolutional cave. However, wave action on a small, breached flank margin cave could strip out speleothems, and lead an observer to an incorrect interpretation that the cave remnant was an abandoned sea cave. Sea caves in carbonate rocks, especially ones abandoned as a result of sea-level change or coastal dynamics, such as beach or spit formation, might be able to create a calcite precipitation environment, especially if the entrance has become restricted by sedimentation or breakdown. Speleothems in such caves could result in the cave being misinterpreted as dissolutional in origin. Some of the pitfalls in using calcite speleothems as indicators of cave origin are discussed in Taboroši et al. (2006). As with any scientific inquiry, multiple lines of evidence should be utilized to make an interpretation of sea cave versus flank margin cave origin.

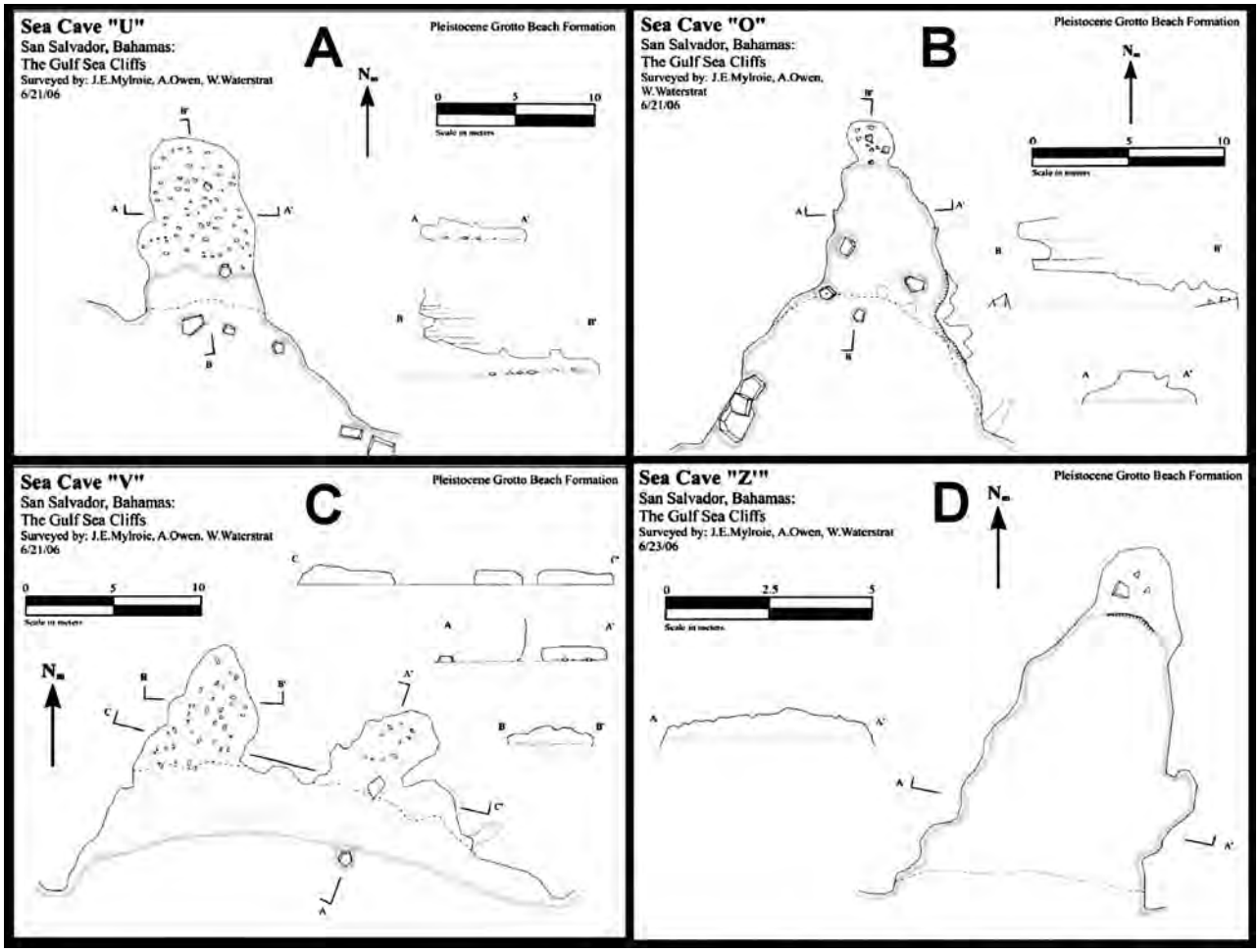

Figure 3. Maps of typical sea caves from San Salvador, Bahamas. Note the simplicity of the caves compared to Figure 1. All examples from the southern coast of San Salvador Island. A) Sea Cave "U". B) Sea Cave "O". C) Sea Cave "V". D) Sea Cave "Z".

The morphological parameters presented in this paper (Fig. 2 compared to Fig. 4), supported by independent evidence such as calcite speleothems, can strengthen the interpretation of coastal cave origin.

METHODOLOGY

Flank margin caves have been widely studied in recent years, and an extensive database of maps exists for them; 66 Bahamian flank margin cave maps were obtained from Roth (2004). However, sea caves, especially in carbonate rocks, have received little attention. There are numerous sea caves on the U.S. west coast and these have been documented in places such as the California Channel Islands (Bunnell, 1988). For this study, 98 maps of sea caves from Santa Cruz Island, California were scanned from Bunnell (1988). Additionally, eight sea caves (active and relict) from Mount Desert Island, Maine were scanned from Nardacci (2002). Forty-four Bahamian sea caves were surveyed and mapped on several trips to the Bahamas between 2005 and 2007, with the majority of them surveyed in June 2006. Additional flank margin caves were mapped on Cat Island, Bahamas, as part of this study (Fig. 1). The surveys were done with a fiberglass tape and Suunto compass and inclinometer, following the protocols of Dasher (1994). Sketches were done with a high degree of detail and accuracy because cave maps for both flank margin caves (Fig. 1) and sea caves (Fig. 3) were the basis for subsequent morphometric analyses.

In order to quantify the distinctions between flank margin caves and sea caves, a series of morphometric parameters were created (Roth, 2004; Roth et al., 2006; Waterstrat, 2007). From the cave maps, several measurements were taken: (1) perimeter (excluding the length of the entrance dripline); (2) area (enclosed by the walls and dripline); (3) entrance width; (4) maximum width (roughly parallel to entrance measurement); and (5) the length of the axes of the smallest possible rectangle to enclose the entire cave. These measurements are shown for a coastal cave map in Figure 9. Computer programs were used to

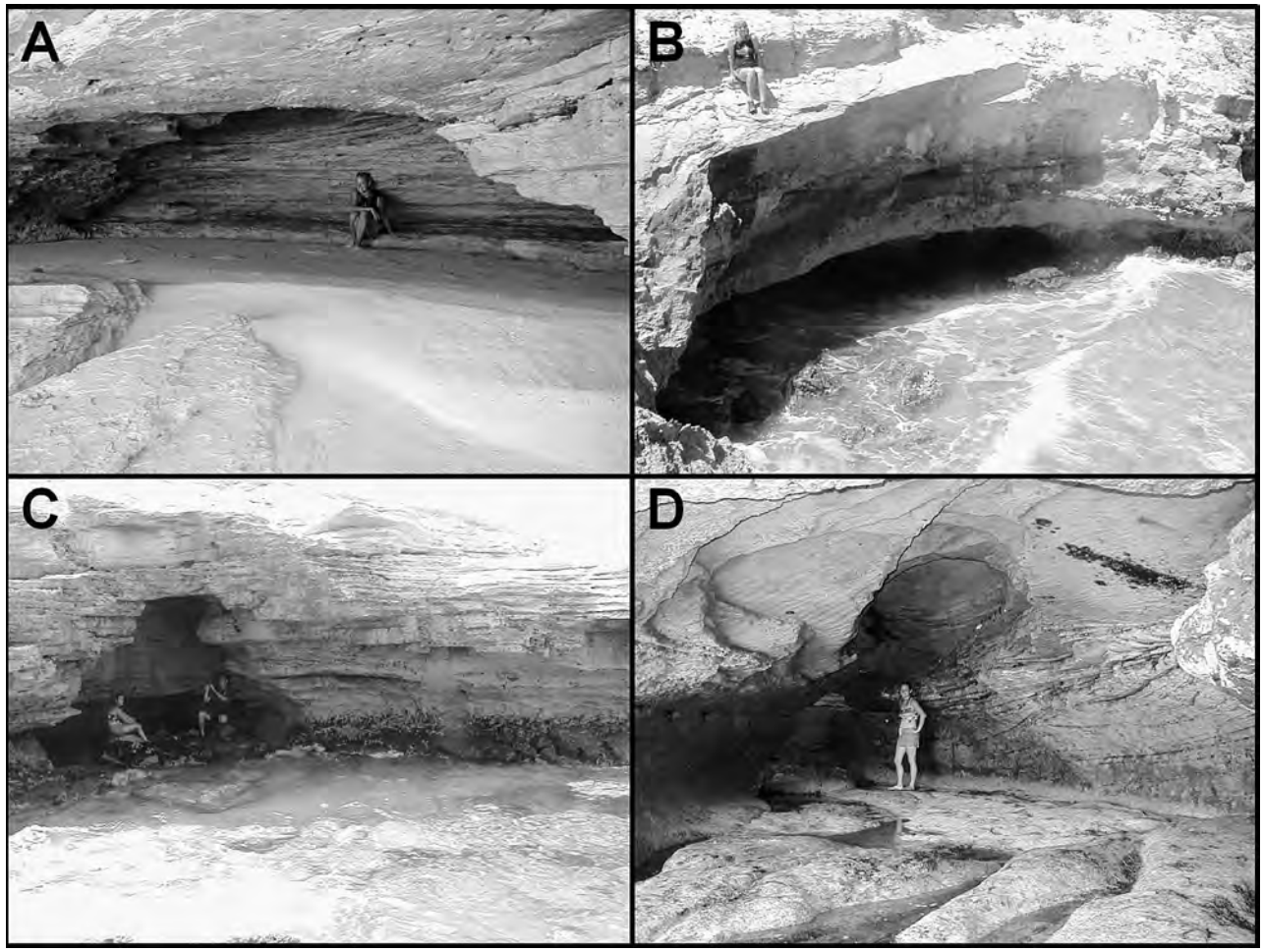

Figure 4. Images of typical sea caves from San Salvador Island, Bahamas. Note the large entrances, and the simplicity of the bedrock wall configuration as a result of mechanical carving by wave action. A) Sea cave in coastal cliffs north of Grotto Beach, southwest side of the island. B) Sea cave in coastal cliffs west of The Gulf, south side of the island. C) Sea cave in coastal cliffs at North Point, northeast side of the island. D) Sea Cave at Cut Cay, the truncated northern tip of North Point, northeast side of the island (note wind ripples exposed in the eolian beds of the cave roof). Sea caves shown in A and B are developed in Late Pleistocene beach, back beach and eolian calcarenites (Grotto Beach Formation). Sea caves shown in C and D are developed in Holocene eolian calcarenites (Rice Bay Formation). The sea caves in the Holocene rocks are unlikely to be breached flank margin caves, as the rocks have only been in existence for ~5,000 years (Carew and Mylroie, 1995b; 1997), providing a control for the morphometric analysis of sea cave maps.

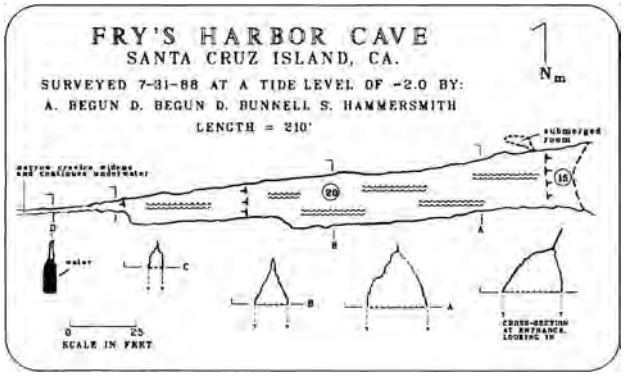

Figure 5. A Fault-controlled sea cave from Santa Cruz Island (after Bunnell, 1988).

generate the cave area and perimeter values from scanned cave maps. Initially Autocad® was used by Roth (2004) for the 66 caves in her database. For this study NIH 1.62f (freely available software from the National Institutes of Health (NIH)) was used because it is a simple and faster program to operate. Comparison testing demonstrated the two programs produce identical results. Because these measurements are dependent on the overall size of the cave, they must be normalized to allow for comparisons of individual caves and groups of caves. Therefore, the following ratios were used: (1) area to perimeter ratio (A/P); (2) entrance width to maximum width (E/M); and (3) rectangle short/long axes (S/L). The use of these metrics, developed for sea cave/flank margin cave comparisons by

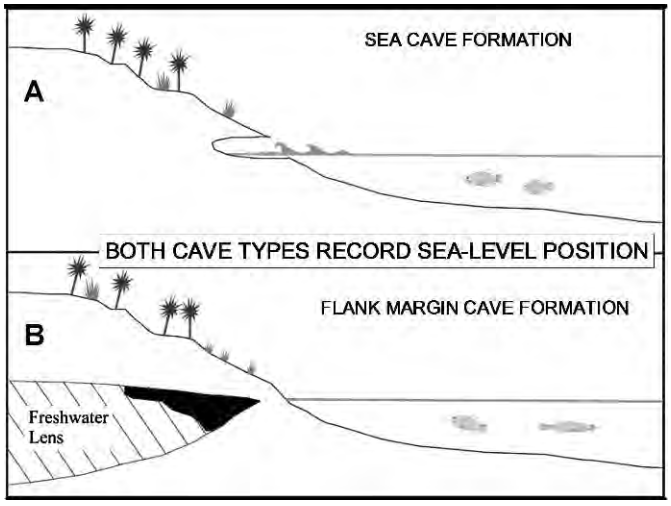

Figure 6. Diagram demonstrating the position of development of sea caves (A) and flank margin caves (B). Assuming the sea-level highstand shown is glacioeustatic from MIS 5e ~ 125 ka, the events shown in Figure 7 can be considered.

Waterstrat (2007), have been successfully applied to a comparison of sea caves and flank margin caves on the limestones of coastal Puerto Rico (Lace, 2008). For this study, each comparison was first examined using analysis of variance, and a *t*-test was used to determine statistical significances (*p* values).

Area to Perimeter Ratio (A/P)

Coastal caves tend to be chambers and collections of chambers, rather than long linear features, as is typical of dendritic stream caves. As a result, areal footprint as determined from the cave map is the best measure of coastal cave size, as opposed to simply summing the length of survey shots as is commonly done for ranking the size of stream caves (Mylroie, 2007). Because of the way flank margin caves form (by intersection of ever-enlarging voids), they are expected to have a complex, and therefore long, perimeter for their individual area (Labourdette et al., 2007). As a result, the ratio of area to perimeter is an indication of the complexity of the perimeter. Flank margin caves are expected to have lower A/P ratios, reflecting their complex perimeters (Figs. 1 and 2). Sea caves should have higher A/P ratios, which illustrates their less convoluted perimeters as a result of genesis by mechanical erosion because block detachment yields planar walls and wave abrasion smoothes wall irregularities (Figs. 3 and 4).

Entrance Width to Maximum Width (E/M)

Flank margin caves form with no entrance to the surface. They are expressed only when they have been breached by hillslope retreat, intersected by vadose shafts, or exposed by collapse (Figs. 7 and 8). Because of this phenomenon, a very large cave may have only a very small entrance. Sea caves, however, are dependent on wave energy for their formation, so the entrance is usually the widest point of the cave. Comparing the ratio of entrance width to maximum width yields values between zero and one. If the ratio is one, the entrance is the widest point of the cave, as expected for most sea caves. If the ratio is smaller than one, the entrance is narrower than the widest point of the cave. Ratios much smaller than one are expected for flank margin caves that are largely intact.

Rectangle Short/Long Axes (S/L)

For each cave map, a smallest-possible rectangle that would enclose the entire cave was created and the length of each axis recorded. By creating a ratio of the short axis over the long axis, values range from near zero to one. The more elongate a cave is, the lower this ratio becomes. As the ratio approaches one, the axes approach the same length, and therefore a square with no elongation. Because many sea caves in California are controlled by faults and joints (Bunnell, 1988), they were expected to yield low S/L values (Fig. 5).

Comparison Controls

In order to make quantitative comparisons, sea caves and flank margin caves had to be initially identified and characterized by other means. To establish origin as a flank margin cave, the maps from caves that could not be sea caves were utilized as controls. For example, if a flank margin cave was enterable only by a vertical dissolution shaft or vertical collapse, a sea cave origin was highly unlikely. The same could be said for a flank margin cave entered by way of a small entrance, which then opened into a very large chamber. Wave energy would not have been able to create such a chamber with only a single tiny orifice for wave energy access. The young age of flank margin caves (late Pleistocene), and their development as chambers within the fresh-water lens means that the cave walls are not masked by sediment, breakdown, or massive speleothems as is common in continental epigenic caves. The bedrock wall of a typical flank margin cave can be observed throughout the cave, and can demonstrate that there are no blocked, large entrances that could have once been used by wave energy. Dense calcite speleothems, and wall rock morphology (Fig. 2) provide additional independent evidence of dissolutional origin.

The control case for sea caves was provided by sea caves developed in Holocene eolianites on San Salvador. These Holocene eolianites are 5,000 years old or less (Carew and Mylroie, 1995b; 1997), and therefore, could not host relict flank margin caves from an earlier sea-level highstand.

For both sea caves and flank margin caves, the control cave set plotted separately in the quantitative study, allowing the unknown caves to be properly classified. Each unknown cave carried independent information, such as presence or absence of calcite speleothems, and complex or simple wall morphology, that supported the initial

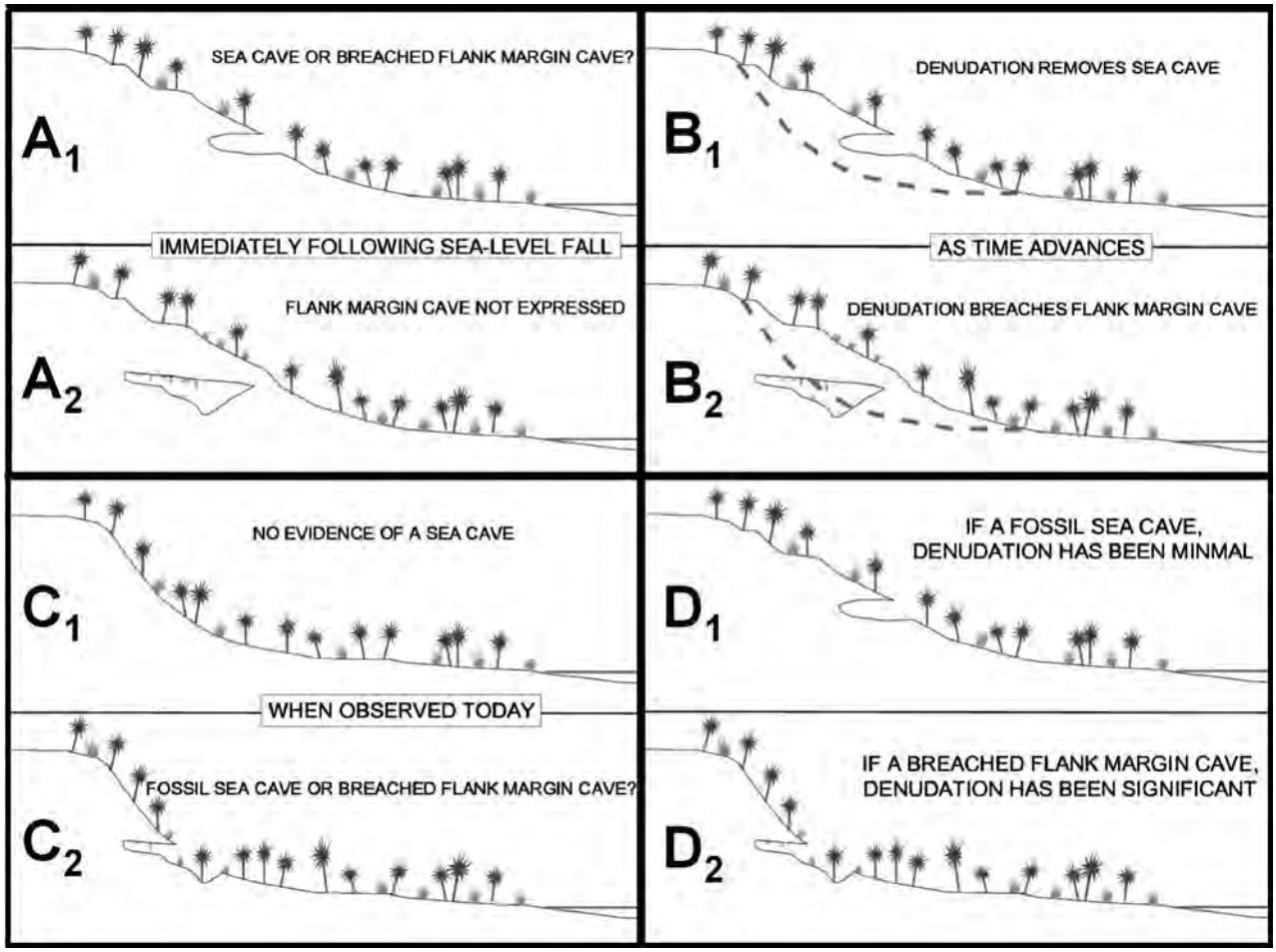

Figure 7. Sequential diagram to show the response of sea caves and flank margin caves to surficial denudation processes. A). Immediately following sea level fall (glacioeustatic in the Bahamas, after the end of MIS 5e), sea caves are expressed (A_1), but flank margin caves are cryptic (A_2). B) Denudation of meters to tens of meters (dashed line) completely removes sea caves (B_1), and opens previously cryptic flank margin caves (B_2). C) As a result of the denudation shown in (B), no evidence remains of sea cave development (C_1), and the caves remaining are breached flank margin caves (C_2). D) If speleothem and morphometric analysis allow the cave types to be distinguished, then the amount of denudation, and therefore the paleoclimatic conditions necessary for that denudation, can be determined (D_1 versus D_2).

classification based on the control set, and as will be shown, the quantitative morphology. As has been noted, breached flank margin caves in coastal zones can be invaded and modified by wave action, creating a transitional form. Also, a sea cave as it enlarges inland may intersect pre-existing karst features. An example is shown in Figure 9, where a small dissolution pit has been intersected by sea cave growth, seen in the northeast portion of the cave.

Results

The cave maps used from all literature sources and from surveys conducted in the Bahamas are available online from Waterstrat (2007). The parameters presented above were used to compare Bahamian flank margin caves with sea caves from San Salvador, because they occur in the same rock types. Sea caves from California and Maine were also compared to sea caves from San Salvador to examine potential cave differences caused by different rock types and locations. These latter two groups form in crystalline rocks and are structurally controlled to varying degrees. San Salvador sea caves, however, form in Quaternary carbonates without guiding secondary structural weaknesses (Mylroie and Mylroie, 2009). The ability of this technique to distinguish between cave types is demonstrated below.

Area to Perimeter Ratio (A/P)

As previously mentioned, area to perimeter ratio is a measure of the complexity of the perimeter for a given size (based on area) of cave. Area to perimeter ratio is useful for differentiating between Bahamian flank margin caves (FM) and San Salvador sea caves (SSSC), between San

Figure 8. Relict calcite vadose speleothems visible in open caves and notches from an inland area at Grotto Beach, San Salvador Island, Bahamas. A) Dripping Rock Cave, with massive stalactites partially entombed in recent sands. B) Calcite column at Pink Grotto Cave, fully exposed to the open. This area was initially mapped as containing a fossil bioerosion notch (B) with fossil sea caves (A), but has been reinterpreted as breached flank margin caves (Mylroie and Carew, 1991; Florea, et al., 2004).

Salvador sea caves and Santa Cruz sea caves (SCSC), and between San Salvador sea caves and Maine sea caves (MSC), with greater than 95% confidence (Table 1). Santa Cruz sea caves and Maine sea caves can be distinguished with >90% confidence using A/P values.

The four cave groups can be distinguished when A/P values are plotted against cave areas (i.e., cave sizes) (Fig. 10). Examining only the Bahamian flank margin caves that are within the 300-m^2-size range (the typical size range of San Salvador sea caves, representing 41 flank

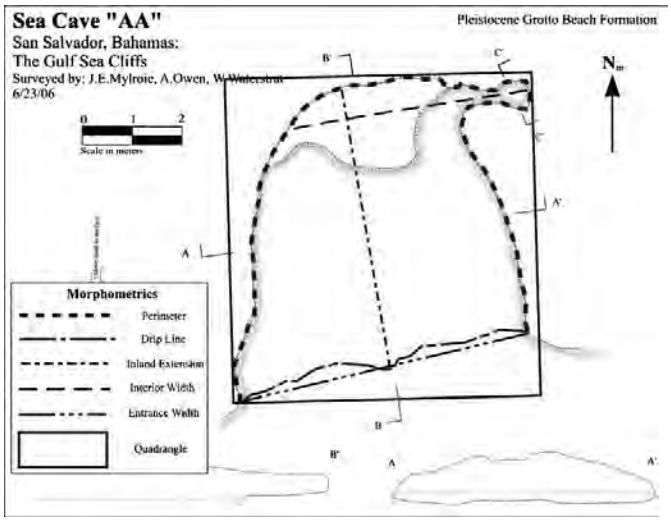

Figure 9. Map of Sea Cave AA, showing how perimeter, area, entrance width, interior cave width, inland extension, and enclosing box length and width were measured.

margin caves) (Fig. 11), the San Salvador sea caves have a higher A/P values than Bahamian flank margin caves. This result shows that for a given area, the perimeter of the San Salvador sea caves is smaller (therefore smoother), which is expected for voids generated by wave energy.

Area to perimeter (A/P) ratio is one of the best tools for differentiating between the various cave types. When comparing ratios for flank margin caves and the sea caves of San Salvador, they are distinct with better than 95% confidence ($p = 0.012$), based on the Student's *t*-test. Differentiating between the various sea caves from different regions (San Salvador, Santa Cruz California, and Maine) is also possible. The A/P ratio shows that San Salvador sea caves are distinct from Santa Cruz sea caves with more than 99% confidence ($p = 0.001$). Maine sea caves are found to be distinct from San Salvador sea caves with more than 95% confidence ($p = 0.016$). Finally, Santa Cruz sea caves are distinct from Maine sea caves with ~95% confidence ($p = 0.063$).

ENTRANCE WIDTH VS. MAXIMUM WIDTH (E/M)

The entrance width vs. maximum interior width parameter (E/M ratio) is an indicator of the type of cave origin. Flank margin caves form with no entrance, and are entered only by later erosional intersection, so are expected to have small E/M values. Sea caves usually have relatively wide entrances because they form by mechanical erosion, and wave energy attenuates further into the cave, which limits littoral erosive power and typically leads to generally an inland tapering of sea caves (Moore, 1954). However, flank margin caves may have wide entrances if enough

Table 1. Area to perimeter ratio differentiation results. FM = Flank Margin; SSSC = San Salvador Sea Cave; SCSC = Santa Cruz Sea Cave; and MSC = Maine Sea Cave.

A/P Ratio	FM vs. SSSC	SSSC vs. SCSC	SSSC vs. MSC	SCSC vs. MSC
p value	0.012	5.4×10^{-16}	0.016	0.063
Mean	2.26/1.67	1.668/3.954	1.668/2.610	3.954/2.610
Std. Dev.	1.642/0.735	0.735/2.191	0.735/1.681	2.191/1.681

erosion has occurred to breach into a large cave chamber. This parameter is useful for differentiating between all groups except San Salvador sea caves and Maine sea caves with better than 95% confidence (Table 2). San Salvador sea caves and Maine sea caves have a similar E/M morphology despite being found in rocks of different types and ages.

Only a few Bahamian flank margin caves have an E/M value of one (Fig. 12). Most flank margin caves are shown to have a much lower E/M value than San Salvador sea caves (mean = 0.524 for flank margin caves, 0.933 for San Salvador sea caves). Using this parameter, these two caves types can be differentiated with better than 99% confidence. Other groups (with the exception of Maine sea caves vs. San Salvador sea caves) can be confidently differentiated with this parameter as well.

Rectangle Short/Long Axes (S/L)

The rectangle measurement is described in the methodology section. Once again, the size of the rectangle is a measurement of cave size because it depends on area. Thus, in order to use this measurement for comparison, we examine the ratio of the lengths of the short and long axes of the rectangle (Table 3). With a square rectangle, the ratio will be 1. As the rectangle becomes exceptionally elongate, the ratio approaches zero. When we examine only those caves with an area of less than 300 m^2 (Fig. 13), differences are apparent. In Figure 13, the ratio has been reversed, with long axis over short axis to allow a greater separation of the points for visual analysis. In this figure presentation mode, Santa Cruz sea caves commonly exhibit large long axis to short axis ratios, which is a reflection of their fault-controlled elongation.

Based on S/L ratio, Bahamian flank margin caves are distinct from San Salvador sea caves with 99% confidence. Flank margin caves have a lower mean ratio (0.535 for flank margin caves vs. 0.701 for San Salvador sea caves). When comparing the various types of sea caves, this metric also does an excellent job in distinguishing between the elongate, fault-controlled sea caves of Santa Cruz Island and the other less-elongate sea caves from San Salvador, but not as well with sea caves from Maine.

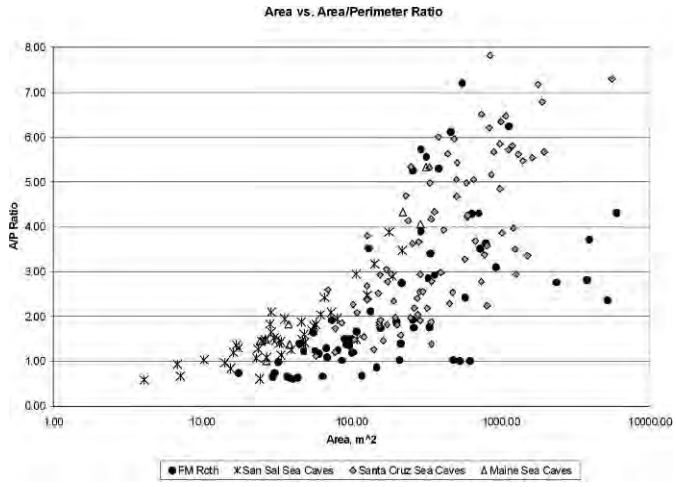

Figure 10. A/P vs. Area. Cross patterns are San Salvador sea caves, solid circles are Bahamian flank margin caves, filled diamonds are Santa Cruz sea caves, and light triangles are Maine sea caves. Visually, the separation of Bahamian flank margin caves (solid circles) from Bahamian sea caves (cross pattern) and Maine sea caves (open triangles) is apparent, but isolated overlaps occur. Statistics shown in Table 1.

Discussion

Bahamian Flank Margin Caves vs. San Salvador Sea Caves

Bahamian flank margin caves are distinct in shape from the sea caves of San Salvador. As predicted, the A/P ratio for Bahamian flank margin caves is significantly lower than

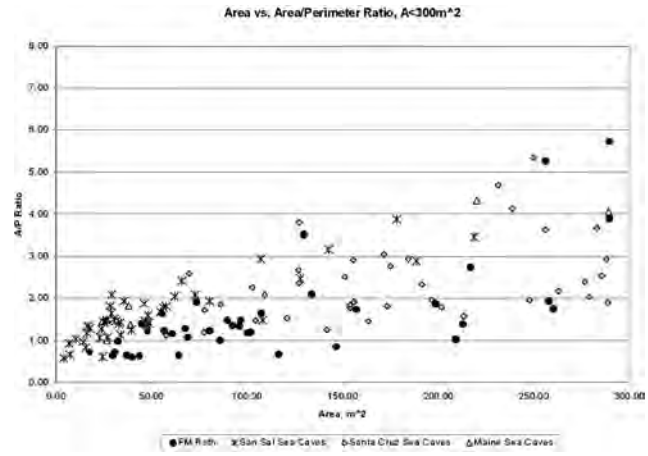

Figure 11. A/P vs. Area for caves <300m^2. Cross patterns are San Salvador sea caves, solid circles are Bahamian flank margin caves, filled diamonds are Santa Cruz sea caves, and light triangles are Maine sea caves.

Table 2. Entrance width vs. maximum width results. FM = Flank Margin; SSSC = San Salvador Sea Cave; SCSC = Santa Cruz Sea Cave; and MSC = Maine Sea Cave.

E/M Ratio	FM vs. SSSC	SSSC vs. SCSC	SSSC vs. MSC	SCSC vs. MSC
p value	3.7×10^{-13}	1.8×10^{-4}	0.38	7.2×10^{-4}
Mean	0.524/0.933	0.933/0.803	0.933/0.968	0.803/0.968
Std. Dev.	0.349/0.148	0.148/0.250	0.148/0.090	0.250/0.090

that of San Salvador sea caves. Given two caves of the same size, a flank margin cave is expected to have a more complex (i.e., longer) perimeter, which reflects its dissolutional formation by intersection of ovular voids (Figs. 1 and 2). Sea caves are expected to have much smoother walls, and therefore, shorter perimeters (Figs. 3 and 4). Thus, when comparing the A/P ratios for these two cave types, flank margin caves should have a lower ratio than a sea cave of the same size (area). However, smaller flank margin caves often have a rather simple perimeter. This is because they may only form by the enlargement and intersection of a few voids, instead of many. Small flank margin caves, when breached by wave action, are also more likely to experience wave scour of their entire interior, which can remove some passage wall complexity (and speleothems). Though most of the San Salvador sea caves fall within this small size range (<300 m^2), they can still be shown to be distinct from flank margin caves, even though Figure 10 shows that sea caves and flank margin caves plot closer together when they are smaller in area.

The techniques described in Waterstrat (2007), using area and perimeter measurements to differentiate seas caves and flank margin caves has, as noted earlier, been adapted (Fig. 14) to coastal carbonates on Puerto Rico

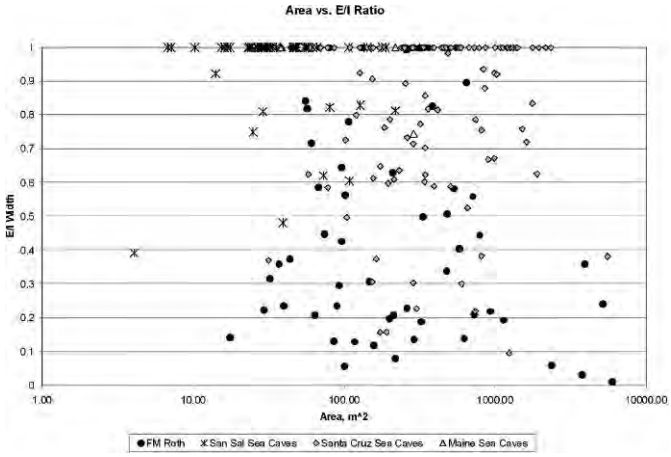

Figure 12. E/M vs. Area. Note that few Bahamian flank margin caves have an E/M ratio near 1. Cross patterns are San Salvador sea caves, solid circles are Bahamian flank margin caves, filled diamonds are Santa Cruz sea caves, and light triangles are Maine sea caves. Statistics shown in Table 2.

(Lace 2008, his Fig. 6). Lace (2008) arranged his plots slightly differently, placing perimeter on the vertical axis and area on the horizontal axis, but the results plot similar to the A/P ratio versus area graphs shown in this paper (e.g. Figs. 10 and 11). This entirely independent study has demonstrated that sea caves and flank margin caves can be reliably differentiated from maps of similar areal footprint in a coastal carbonate setting other than in the Bahamas. Note that as cave size decreases, differentiating Puerto Rican sea caves from flank margin caves becomes more difficult, for reasons noted previously.

The ratio of the short and long axes of the rectangle is also a useful parameter for differentiating between Bahamian flank margin caves and San Salvador sea caves. Flank margin caves tend to have a smaller ratio. This means that they tend to be more elongate than San Salvador sea caves. This elongation is a function of the dissolutional formation of flank margin caves and their dependence on the freshwater lens position. Because the lens position and mixing front are dependent on sea level and distance to the coastline, flank margin caves are more likely to extend laterally along the coast than to extend inland, in order to follow the geochemically-active lens margin (Labourdette et al., 2007). This coast-parallel development is illustrated by several flank margin caves that wrap around the coastline, yet do not extend far inland (Mylroie and Mylroie, 2007). The sea caves of San Salvador, however, form voids that are enclosed by a less elongate rectangle. There is an apparent visual trend in Figure 13 for smaller flank margin caves to have an axis ratio closer to one. This result is a consequence of their small area not showing elongation parallel to the lens margin because the caves are not large enough to have exceeded the landward dimensions of the favorable lens-margin dissolution zone. As they get larger, they can link up only parallel to the coast and the inland limit of growth forces the lateral elongation. The size distribution of flank margin caves with an axis ratio close to one may indicate the width of the geochemically-active zone of the lens margin, a demonstration of lens dynamics and potentially paleoclimate at the time of cave development.

The ratio of entrance width to maximum interior width was the next parameter examined to differentiate cave types. When the entrance width is the widest point of the cave, the ratio is one. When entrances are small compared to the maximum interior width, the ratio approaches zero. Most San Salvador sea caves have a ratio of nearly one

Table 3. Rectangle short/long axes ratio results. FM = Flank Margin; SSSC = San Salvador Sea Cave; SCSC = Santa Cruz Sea Cave; and MSC = Maine Sea Cave.

S/L Ratio	FM vs. SSSC	SSSC vs. SCSC	SSSC vs. MSC	SCSC vs. MSC
p value	1.2×10^{-5}	8.2×10^{-9}	0.028	0.44
Mean	0.535/0.701	0.701/2.88	0.701/0.547	2.88/0.547
Std. Dev.	0.204/0.171	0.171/1.873	0.171/0.207	1.873/0.207

(mean = 0.933), reflecting the observation that their entrances are almost always the widest point of the cave. Flank margin caves are expected to have a smaller value because they can be large voids with small entrances formed from breaching by hillslope retreat or vadose intersection (pit entrances). However, in some cases, more than half of a flank margin cave may have been eroded away. In these instances, the entrance becomes the widest point. Significant denudation of flank margin caves (E/M ~ 1) was demonstrated on Tinian Island, Marianas, as shown in Figure 15 (Stafford et al., 2005, modified from their Fig. 11), by use of entrance versus maximum width ratios. Apparently, most of the Bahamian flank margin caves in this study are not this extensively eroded, because their E/M values are low (mean = 0.524). The Tinian carbonates are older than those in the Bahamas and have been tectonically uplifted so their probable ages are likely greater, or the local climate creates a faster denudation rate (Stafford et al., 2005).

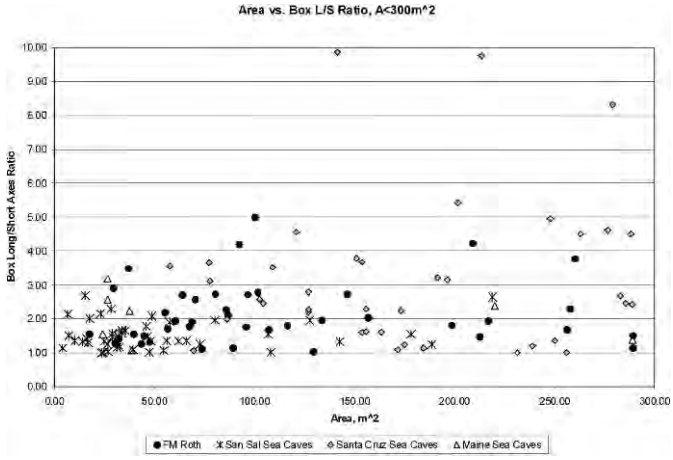

Figure 13. Area vs. L/S for caves less than 300 m^2; the ratio has been inverted to increase visual separation of points. Note that Santa Cruz sea caves tend to have higher ratios with this inverted ratio presentation of long axis over short axis, reflecting their fracture elongation. Bahamian and Maine sea caves show a lack of elongation. Cross patterns are San Salvador sea caves, solid circles are Bahamian flank margin caves, filled diamonds are Santa Cruz sea caves, and light triangles are Maine sea caves. Statistics shown in Table 3.

San Salvador Sea Caves vs. Santa Cruz Sea Caves

Because all sea caves form mostly by the erosive action of littoral wave energy, it might be expected that they will have similar morphologies. However, structural controls can have a considerable effect on their morphology. The sea caves of Santa Cruz occur in extensively faulted and jointed rocks. This preexisting weakness strongly guides their morphology and results in many long, linear caves (Bunnell, 1988). Their A/P values are then much different from that of the San Salvador sea caves and they can be readily differentiated.

Additionally, Santa Cruz sea caves exhibit smaller ratios of S/L values for the rectangle fitting procedure, which reflects the elongation of many caves there. This again illustrates their fault/joint-controlled morphology. The penetrative faulting and related jointing creates a weakness that is readily exploited by wave energy, in otherwise resistant rocks. This results in generally elongate caves. Sometimes several faults are involved and the cave morphology becomes more complex, but the faults still

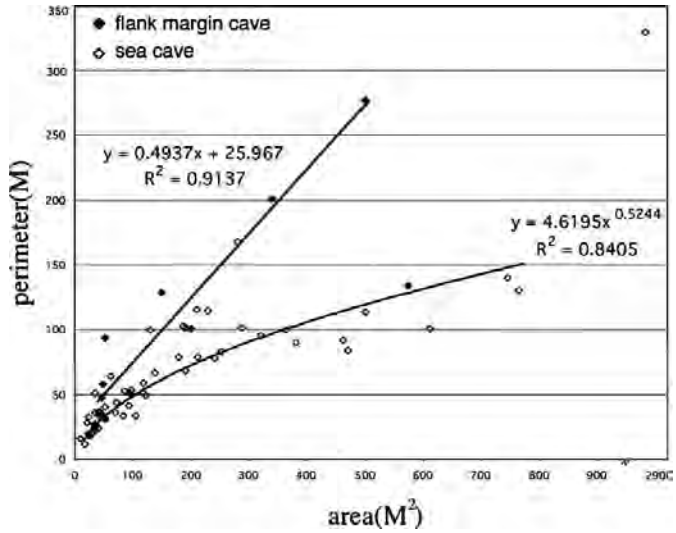

Figure 14. Plot of cave perimeter versus cave area for coastal caves of Puerto Rico, using the protocols established by Waterstrat (2007). Flank margin caves are solid diamonds, sea caves are open diamonds. Note the divergence of the plots as cave size increases (after Lace, 2008, his figure 6). Note also that cave perimeter is on the vertical axis, and cave area on the horizontal axis in this plot.

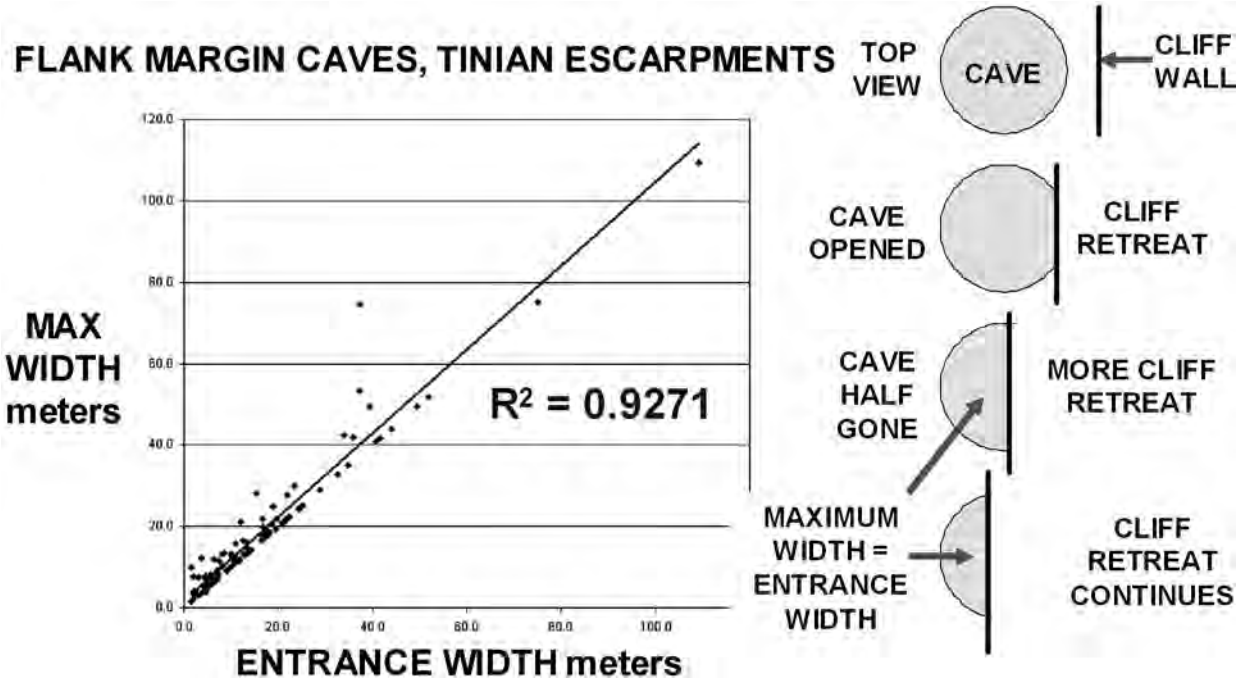

Figure 15. Plot of maximum width versus entrance width for flank margin caves on Tinian Island, Commonwealth of the Northern Mariana Islands. There are no points in the lower right hand portion of the graph because no cave can have an entrance width greater than its maximum width. A few caves plot in the upper left, indicating that the interior chamber is wider than the entrance. The vast majority of caves fall on the 45° line, indicating that the cave is 50%, or more, denuded such that the maximum width is the entrance width. Modified from Stafford et al. (2005). Tinian flank margin caves are denuded to a greater degree than in the Bahamas.

apparently guide their formation. Because the host rocks are otherwise resistant, the largest documented sea caves in the world are found here. Santa Cruz sea cave elongation is oriented inland; San Salvador flank margin cave elongation is oriented parallel to the coast.

E/M values also proved valuable for differentiating these two cave types. A number of the Santa Cruz caves have multiple entrances and can have intersecting passages. Though many Santa Cruz Caves simply taper in width from their entrance to the back wall (resulting in an E/M ratio of 1; see Fig. 5), some of them are long and narrow, but open up into a larger chamber at the intersection of faults. Painted Cave, the largest sea cave in the world, is a good example of this phenomenon (Bunnell, 1988) These intersections helps explain why Santa Cruz sea caves have a lower E/M value (mean = 0.803) than most San Salvador sea caves, which have a ratio close to 1 (mean = 0.933). San Salvador sea caves have a consistent morphology that simply tapers in width inward from the maximum width at the entrance.

San Salvador Sea Caves vs. Maine Sea Caves

Despite what at first glance appears to be similar morphology, San Salvador sea caves and Maine sea caves proved to be significantly different. Both of these groups of caves are formed in rocks that, as in the Bahamas are either absent of apparent guiding structural features like faults or joints, or as in Maine, have only a few such features. They exhibit a generally rectilinear outline with the entrance as the widest point. Despite these similarities, they are still distinguishable from each other by A/P values, and the S/L values. However, E/M values are not a good means of differentiating between these two cave types.

Santa Cruz Sea Caves vs. Maine Sea Caves

Comparing Santa Cruz sea caves with Maine sea caves is useful for illustrating the importance of joint control on the morphology of sea caves. Both groups are formed in broadly similar rocks (i.e., crystalline), yet they exhibit distinctly different morphologies. As previously mentioned, Santa Cruz sea caves are fault/joint-controlled and tend to be very elongate, although some complexity exists. Maine sea caves are formed in rocks that, while they may contain a fault or a dike, are absent of extensive jointing and exhibit a less elongate overall shape. These differences reflect the active (Santa Cruz) versus passive (Maine) tectonic setting of these two locations. Despite these apparent differences and average S/L values (2.88 for Santa Cruz caves, 0.547 for Maine sea caves), they are not significantly different according to the *t*-test performed. This is surprising, but is probably explained by the very different sample sizes (98 Santa Cruz caves, 8 Maine caves).

The A/P values and the E/M values have been shown to be useful for telling these two caves apart.

The Quaternary eolianite geology of the Bahamian sea caves is quite different from that of the harder, denser, and more structurally deformed rocks that make up the sea caves in Maine and the California channel islands. It is thus no surprise that differences in sea cave shape result.

Conclusions

This study makes comparisons between flank margin caves and various types of sea caves. Forty-four sea caves were surveyed and mapped on San Salvador. Additionally, three coastal flank margin caves were surveyed and mapped on Cat Island, Bahamas and added to the existing Roth (2004) database. Various morphometrics (perimeter, area, dripline length, entrance width, maximum interior width, and inland extension) were measured for comparison between caves.

The new sea cave data were compared to an existing and updated morphometric database for flank margin caves compiled by Roth (2004). Both coastal cave types developed in the same rocks and in similar environments, but formed by entirely different processes. Because of their coastal localities (including former shorelines from a previous highstand), these coastal caves are easy to misinterpret. However, the use of morphometric techniques allowed for confident differentiation between these two coastal cave types.

Cave maps were obtained for 98 sea caves in California (Bunnell, 1988) and eight sea caves from Maine (Nardacci, 2002). These sea caves are formed in crystalline rocks and perhaps are not comparable to flank margin caves developed in soluble rocks. However, the California and Maine sea caves form by the same littoral processes as the San Salvador sea caves (Waterstrat, 2007). Traditionally, sea cave morphology has been explained by differential susceptibility of the rock to erosion (e.g., faults and joints) (Moore, 1954). The Santa Cruz sea caves are extensively faulted and jointed and their morphology has clearly been guided by these structures, as illustrated by their pronounced elongation. The sea caves of San Salvador, however, contain none of these initial weaknesses so some other method must explain their formation. The same appears to be true with Maine sea caves, although sufficient field observations have not been conducted to verify this. Therefore, some other process must be responsible for the differential erosion that results in sea cave formation at specific locations on a uniform coastline like San Salvador. It is unlikely that all the sea caves found on San Salvador are breached and modified flank margin caves because so many sea caves occur in Holocene rocks, which are too young to contain flank margin caves. The morphometric analyses reported here agree with traditional techniques, such as wall morphology and speleothem presence, used to separate the two cave types. Wave focusing as a result of interaction with submerged topography, constructive and destructive wave interference, wave refraction, and wave diffraction might be the mechanisms. Previous sea cave classification has been based on secondary structural controls such as faults and joints, but this study has shown that sea caves form in Bahamian eolianites lacking such structures. As in hydrology, the properties of the water (e.g., water viscosity in aquifers, wave energy for sea caves) need to be considered as well as the rock properties. Porosity and permeability are not enough to explain groundwater flow in an aquifer; in a like manner, rock structure alone is not enough to explain sea cave formation in coastal cliffs.

All four groups of caves in this study were found to be distinct from each other using several morphometric parameters. This outcome reinforces the usefulness of these tools in the classification of coastal caves. Coupled with interior bedrock sculpture and speleothem occurrence, flank margin caves can be differentiated from sea caves by morphometric techniques, and the paleoclimatic information carried by each coastal cave assessed. Recent increased interest in sea caves, and the maps produced (e.g., Bunnell, 2008; 2009), may allow a larger sea cave database to be assembled. From such data, questions concerning rock qualities versus wave energy in the generation of sea caves can be assessed.

Acknowledgments

The authors acknowledge the Gerace Research Centre, San Salvador Island, Bahamas, for logistical support of field operations. Mississippi State University supplied resources to support the research. Dave Bunnell, Pat Kambesis, and Mike Lace provided important input to the project. Lee Florea and an anonymous reviewer made many useful suggestions that improved the manuscript.

References

Bunnell, D., 1988, Sea caves of Santa Cruz Island, Santa Barbara, Cal., McNally and Loftin, 123 p.

Bunnell, D., 2008, Vertical sea caving: NSS News, v. 66, no. 10, p. 11–18.

Bunnell, D., 2009, Return to Santa Cruz Island: NSS News, v. 67, no. 1, p. 12–19.

Carew, J.L., and Mylroie, J.E., 1995a, Quaternary tectonic stability of the Bahamian Archipelago: Evidence from fossil reefs and flank margin caves: Quaternary Science Reviews, v. 14, p. 145–153.

Carew, J.L., and Mylroie, J.E., 1995b, A stratigraphic and depositional model for the Bahaman Islands, *in* Curran, H.A., and White, B., eds., Terrestrial and Shallow Marine Geology of the Bahamas and Bermuda, Geological Society of America Special Paper 300, p. 5–31.

Carew, J.L., and Mylroie, J.E., 1997, Geology of the Bahamas, *in* Vacher, H.L., and Quinn, T.M., eds., Geology and hydrogeology of carbonate islands, Developments in sedimentology, Amsterdam, Elsevier, v. 54, p. 91–139.

Dasher, G.R., 1994, On Station: A complete handbook for surveying and mapping caves, Huntsville, Ala, National Speleological Society, 242 p.

Florea, L.J., Mylroie, J.E., and Price, A., 2004, Sedimentation and porosity enhancement in a breached flank margin cave: Carbonates and Evaporites, v. 19, p. 75–85.

Labourdette, R., Lascu, I., Mylroie, J., and Roth, M., 2007, Process-like modeling of flank margin caves: From genesis to burial evolution: Journal of Sedimentary Research, v. 77, p. 965–979.

Lace, M.J., 2008, Coastal cave development in Puerto Rico: Journal of Coastal Research, v. 24, no. 2, p. 508–518.

Moore, D.G., 1954, Origin and development of sea caves: National Speleological Society Bulletin, v. 16, p. 71–76.

Mylroie, J.E., 2007, Cave surveys, cave size, and flank margin caves: Compass and Tape, v. 17, no. 4, p. 8–16.

Mylroie, J.E., and Carew, J.L., 1990, The flank margin model for dissolution cave development in carbonate platforms: Earth Surface Processes and Landforms, v. 15, p. 413–424.

Mylroie, J.E., and Carew, J.L., 1991, Erosional notches in Bahamian carbonates: Bioerosion or groundwater dissolution?, *in* Bain, R.J., ed., Proceedings of the 5th Symposium on the Geology of the Bahamas, Port Charlotte, Fla, Bahamian Field Station, p. 185–191.

Mylroie, J.E., and Carew, J.L., 1995, Chapter 3, Karst development on carbonate islands, *in* Budd, D.A., Harris, P.M., and Saller, A., eds., Unconformities and porosity in carbonate strata, American Association of Petroleum Geologists Memoir 63, p. 55–76.

Mylroie, J.E., and Carew, J.L., 2008, Field guide to the geology and karst geomorphology of San Salvador Island, San Salvador, Bahamas, Gerace Research Centre, 88 p.

Mylroie, J.E., and Mylroie, J.R., 2007, Development of the carbonate island karst model: Journal of Cave and Karst Studies, v. 69, p. 59–75.

Mylroie, J.E., and Mylroie, J.R., 2009, Caves of the Bahamas; Guidebook for excursion no. 82, 15th International Congress of Speleology: Huntsville, Ala., National Speleological Society, 76 p.

Mylroie, J.E., Mylroie, J.R., Jenson, J.W., and MacCracken, R.S., 2008, Fresh-water lens anisotropy and flank margin cave development Fais Island, FSM, *in* Freile, D., and Park, L., eds., Proceedings of the 13th Symposium on the geology of the Bahamas and Other carbonate regions, San Salvador, Bahamas, Gerace Research Centre, p. 135–139.

Nardacci, M.L., 2002, A Guide to the geology and caves of the Acadian Coast, 2002 NSS Convention, Camden, Maine, National Speleological Society, 91 p.

Palmer, A.N., 1991, Origin and morphology of limestone caves: Geological Society of America Bulletin, v. 103, no. 1, p. 1–21, doi:10.1130/0016-7606(1991)103<0001:OAMOLC>2.3.CO;2.

Palmer, A.N., 2007, Cave geology, Dayton, Ohio, Cave Books, 454 p.

Roth, M.J., 2004, Inventory and geometric analysis of flank margin caves of the Bahamas [MSc. thesis], Mississippi State, Mississippi State University, 117 p. http://library.msstate.edu/etd/show.asp?etd=etd-07062004-164930

Roth, M.J., Mylroie, J.E., Mylroie, J.R., Ersek, V., Ersek, C.C., and Carew, J.L., 2006, Flank margin cave inventory of the Bahamas, *in* Davis, R.L., and Gamble, D.W., eds., Proceedings of the 12th Symposium on the Geology of the Bahamas and Other Carbonate Regions, San Salvador, Bahamas, Gerace Research Center, p. 153–161.

Stafford, K.W., Mylroie, J.E., Taboroši, D., Jenson, J.W., and Mylroie, J.R., 2005, Karst development on Tinian, Commonwealth of the Northern Mariana Islands: Controls on dissolution in relation to the carbonate island karst model: Journal of Cave and Karst Studies, v. 67, no. 1, p. 14–27.

Taboroši, D., Mylroie, J.E., and Kirakawa, K., 2006, Stalactites on tropical cliffs: Remnants of breached caves or subaerial tufa deposits?: Zeitschrift für Geomorphologie, v. 50, p. 117–139.

Waterstrat, W.J., 2007, Morphometric differentiation of flank margin caves and littoral, or sea caves [MSc. thesis], Mississippi State, Mississippi State University, 201 p. http://library.msstate.edu/etd/show.asp?etd=etd-04052007-150907

W.B. White – Secondary minerals in volcanic caves: data from Hawai'i. *Journal of Cave and Karst Studies,* v. 72, no. 2, p. 75–85. DOI: 10.4311/jcks2009es0080

SECONDARY MINERALS IN VOLCANIC CAVES: DATA FROM HAWAI'I

WILLIAM B. WHITE
Materials Research Institute and Department of Geosciences, The Pennsylvania State University, University Park, PA 16802, wbw2@psu.edu

Abstract: Lava tube caves contain a variety of secondary minerals formed by seepage waters extracting components from the overlying soils and basalt and depositing them as crusts, crystals, and small speleothems in the underlying tubes. Fifty one specimens were analyzed in the course of a reconnaissance of a selection of caves on Hawai'i. Many of these were from caves at low elevation where the cave environment is wet and at ambient temperature. Some were from a cave at 2900 meters on Mauna Loa where conditions were much drier. Minerals in hot fumarole caves in the Kilauea Caldera were observed but not sampled. Mineral identifications were made by X-ray diffraction with some assistance from a scanning electron microscope with energy dispersive X-ray detector for rough chemical analysis. Calcite is surprisingly common, appearing in the form of small coralloids and other crusts and coatings. Gypsum is common as crusts and as puffballs. Two other sulfate salts, thenardite and mirabilite, were identified. Two unusual mineral deposits contained the transition metal ions vanadium and copper. Bright olive-green patches in Lama Lua Cave were characterized as a hydrated copper-vanadium silicate with composition $Mg_2Cu_4(VO_4)_2Si_5O_{13}(H_2O)_{5.6}$. Although the mineral produced a high quality X-ray diffraction pattern, the pattern did not match any minerals in the database. The blue-green stalactites in the Kapuka Kanohina system are a non-crystalline hydrated copper silicate coating lava stalactites.

INTRODUCTION

The term volcanic cave includes lava tubes, tumulous caves, fracture caves, volcanic vents and other cavernous openings produced by volcanic processes. Decoration of these caves can be broadly separated into two categories. Primary decorations are those features formed at the same time or in the closing stages of the process that formed the caves themselves (there seems to be some argument as to whether or not such features should be called speleothems). These include lava stalactites, lava stalagmites and other features formed by dripping and freezing of lava (Baird et al., 1985). Secondary decorations are mineral deposits that formed after the primary cave opening had cooled or at least partially cooled. Some of these result from steam and volcanic gases in fumarole caves and other openings that are still well above regional ambient temperatures, although below that of the original lava. Others result from the leaching of material by infiltrating groundwater and the subsequent deposition of minerals in underlying lava tubes. Although investigations of secondary minerals in volcanic caves are less numerous than investigations of minerals in limestone caves, the number of observed minerals is surprisingly large (Hill and Forti, 1997; Forti, 2000; 2005;). The reason for the mineralogical diversity is the variety of environments in volcanic settings, each with a unique set of conditions for mineral deposition (Forti, 2005).

Cavers exploring the lava tube systems on Hawai'i (the Big Island) have long noticed a variety of speleothems, some of which look much like the speleothems from limestone caves. They have also reported several brightly-colored unknown minerals. The present paper presents the results of a reconnaissance investigation during which samples were analyzed from nine caves, mostly at low elevation.

FIELD INVESTIGATIONS, SAMPLING, AND ANALYTICAL METHODS

The results reported in this paper are based on 51 samples collected during January 2005. Particularly interesting mineralized areas were pointed out by the cavers doing the exploration and mapping. Small samples, masses generally in the range of a few grams, were collected in sealed sample bottles. Great care was taken to do minimal damage to the caves. Previously broken fragments from the floor were used whenever possible. No further precautions were taken to preserve the samples, although samples that had been wet in the cave remained wet when the samples were removed from the bottles in the laboratory.

All samples were examined under a binocular microscope. Selected portions of each sample were ground to powder that was then used to obtain X-ray powder diffraction patterns. The instrument was a Scintag diffractometer with a CuKα X-ray source. Powder patterns were matched by a computer search routine with the reference patterns in the database of the International Committee for Powder Diffraction Standards. Paper copy of the X-ray patterns could be inspected visually for anomalous features.

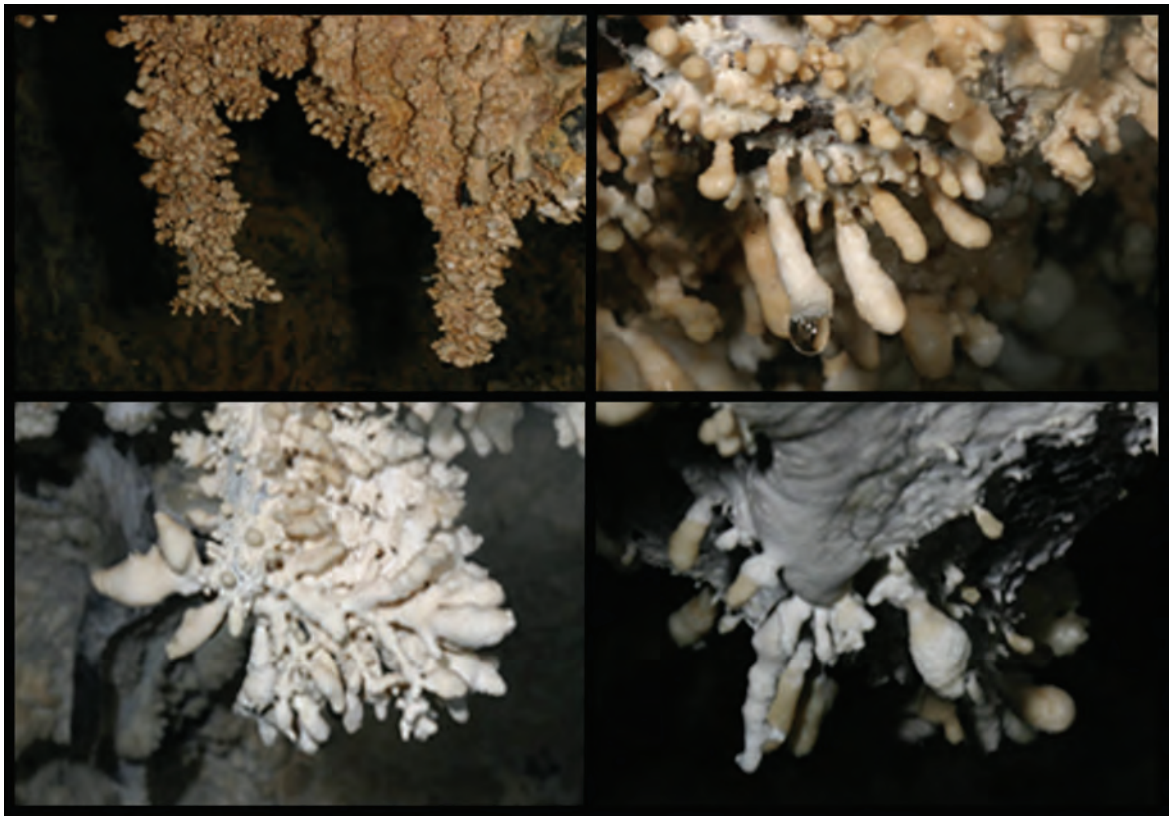

Figure 1. A representative selection of coralloid speleothems from Puff Ball Hall, Hualalai Ranch System. Individual coralloids are in the range of 1–3 cm in length.

For most of the samples, the X-ray diffraction patterns provided an unambiguous identification. However, two brightly colored samples required more extensive characterization tools. In addition to X-ray, these samples were also examined in a scanning electron microscope with an attachment to determine rough elemental composition by energy dispersive X-ray spectroscopy. For the Lama Lua olive-green coating, a more accurate chemical analysis was obtained with a Cameca Electron Microprobe. Infrared spectra were also obtained using a Nicholet Fourier transform spectrometer to provide additional structural information.

MINERAL DESCRIPTIONS AND IDENTIFICATION

Although similar features appear in many of the caves, it is convenient to organize the results according to the cave from which the key specimens were obtained.

THE HUALALAI RANCH SYSTEM AND OTHER KONA AREA CAVES

The Hualalai Ranch System has been mainly explored by cavers from the Butler Cave Conservation Society. Detailed exploration and survey has spliced together many previously unconnected fragments to produce 27.63 km of survey as of 2007. The sampling was concentrated in Puff Ball Hall, a highly mineralized area. In this part of the cave are various white coatings, white masses of material on the floor, white puff balls, and many coralloid type deposits. Twelve samples were collected in this section of the Hualalai Ranch System with a view of obtaining a representative cross section of the mineralogy.

Figure 1 displays a selection of typical coralloids. X-ray diffraction shows that the coralloids are composed of well-crystallized calcite. They are layered, generally colored tan to brown, and have no obvious differences from coralloids found in limestone caves. X-ray diffraction measurements revealed that many of the crusts and the loose powder on the floors are also calcite. The positions of the diffraction lines were close to those for pure $CaCO_3$ in all samples, showing that the magnesium content of the calcite is low. Palmer and Palmer (2006) estimated 2.2 mole percent magnesium in a sample from Refuge Cave (Kapuka-Kanohina System). Some samples of the loose, granular material from the floor produced calcite X-ray patterns on which were superimposed broader and weaker peaks that indicated a second phase of montmorillonite or a related smectite mineral (Fig. 2). Consistent with this interpretation is the somewhat sticky texture noted when the samples were ground in preparation for X-ray diffraction measurements.

The puff balls of Puff Ball Hall consist of button-shaped speleothems ranging from one to two cm in

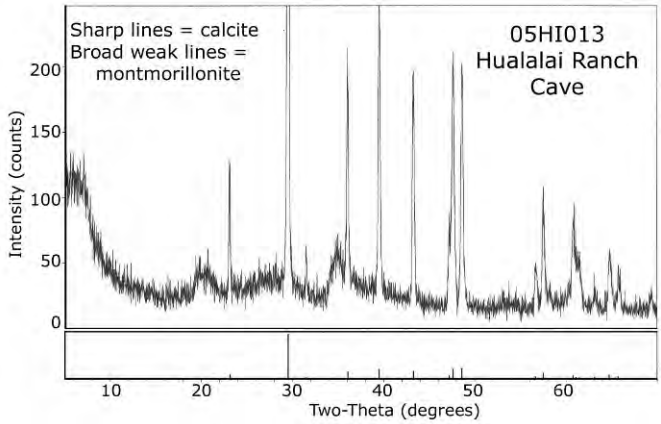

Figure 2. X-ray powder diffraction pattern of sample 05HI013, loose white powder from ledges on the walls of Puff Ball Hall, Hualalai Ranch System. The sharp diffraction peaks are due to calcite; the weaker, broader, and more noisy peaks are due to montmorillonite.

diameter (Fig. 3). X-ray diffraction shows that the puff balls have outer crusts of gypsum but the inside of the speleothems consists largely of calcite. Pure gypsum was found only in loose fragments and in some of the crusts and loose powders on the floors and ledges. As a guideline, hard nodular speleothems are calcite; soft fluffy speleothems are gypsum. No evidence was found for any other minerals, in spite of the fairly intensive sampling in this limited area.

A few samples were analyzed from other caves in the North Kona District. The results are:

Bee Cave (Davis, 2006), loose powder from floor: gypsum

Black Pellet Cave (Medville, 2005), white granular powder from floor: gypsum

Kiholo Bay Cave (Medville, 2006a), 0.5–1 cm lumps of chalky white powder in some parts and orange fine-grained crystals in other parts. X-ray shows a mixture of 80% gypsum and 20% calcite.

Lama Lua Cave

Lama Lua Cave is a 5523-m-tube in a 2100 year pahoehoe flow about 22 km north of Kailua-Kona. The main tube extends 3350 m down slope from the Lama Lua entrance (Medville, 2006b; Medville and Davis, 2007). Sampling was done through the Lama Lua entrance, an 8 m overhanging puka.

The first chamber below the puka is well decorated with coralloids very similar in appearance to those found in the Hualalai Ranch System. The area is wet and dripping. X-ray diffraction shows that three samples collected here consist entirely of well-crystallized calcite. One sample had a white mushy material coating over the coralloid, but the mushy material was also calcite. These samples exhibited a white luminescence under long wave (365 nm) ultraviolet light.

Figure 3. Two examples of puff balls from Puff Ball Hall, Hualalai Ranch System. Puffballs are about one cm in diameter.

The layered structure of these speleothems is not intrinsically different from the cave coral found in limestone caves.

About 500 m down tube from the entrance are several patches of olive-green mineral that appears to be sprayed onto the lava (Fig. 4). The deposits are thin layers completely coating upward-facing breakdown and some are related to fractures. The uniform coating implies that the coating is younger than the rockfall. Parts of these deposits are on broken slabs of breakdown so it was possible to collect several small chips from both mineralized areas. The mineral is in the form of a thin hard coating that was almost impossible to scrape from the underlying basalt. Examination by binocular microscope showed that the coating was spread uniformly over the vesicles in the underlying basalt. Under the microscope, the color and grain morphology appeared to be uniform suggesting that only one mineral was present. A scanning electron microscope image of the intact coating on a small chip of rock showed only featureless grains.

The X-ray emission spectrum, measured with the energy-dispersive detector on the SEM gives a rough chemical analysis (Fig. 5). The dominant elements in the green coating are Ca, Si, V, and Cu with some Fe and Al. By use of a diamond grinding bit on a miniature drill, it

Figure 4. Green mineral patches in Lama Lua Cave.

was possible to obtain a few milligrams of relatively pure coating material, although the possibility of some contamination from the underlying rock cannot be eliminated. The scraping produced a sharp and very complex X-ray diffraction pattern (Table 1). The infrared spectrum of the scraping (Fig. 6) shows that the mineral is hydrated and that it is a silicate.

A quantitative chemical analysis was obtained on individual grains with the electron microprobe (Table 2). The general agreement between the seven analyses further supports the hypothesis that the coating consists of a single mineral. The analyst reported vanadium as V_2O_3, but both the color and the oxidizing environment of the cave make it more likely that vanadium is present in the pentavalent state. With a readjustment of V_2O_3 to V_2O_5, the mean composition of the green mineral can be calculated (Table 3). Weight concentrations were converted to mole fractions and these were normalized to produce a chemical formula. The total of the metal oxides is only 89.85%. It can be assumed that the remaining 10.15% is water and/or OH^- because the IR spectrum shows that the mineral is hydrated. The band at 1650 cm^{-1} in the infrared spectrum

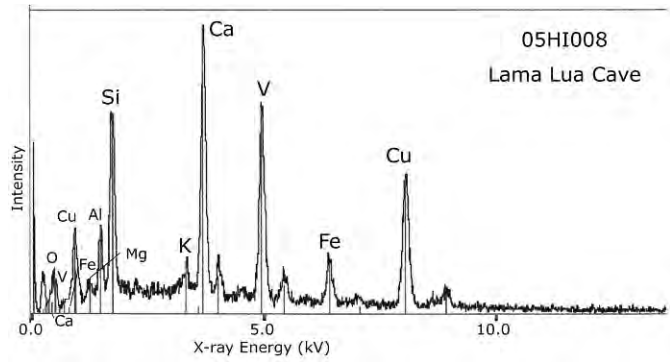

Figure 5. X-ray emission spectrum of the green mineral from Lama Lua Cave.

shows that at least some H_2O is present, but the intense, broad OH-stretching band does not distinguish between OH^- and H_2O, so both could be present. The formula was calculated assuming H_2O resulting in $Mg_2Cu_4(VO_4)_2$-$Si_5O_{13}(H_2O)_{5.6}$ as the composition.

The rounding of the subscripts in Table 3 is within the accuracy of the chemical analyses, especially if it is assumed that Al substitutes for Si. The placement of Ca in the formula is not known, although it could substitute for Mg. Forti (2005) commented that minerals of the vanadate family had not been reported from volcanic caves, so the Lama Lua occurrence is of interest.

Specific mineral identification of the green Lama Lua phase has proved elusive. Evidence given above suggests a single phase with chemical composition close to the constructed formula. The most uncertainty is associated with the H_2O/OH content, but the metal ratios should be accurate. The X-ray diffraction pattern has many lines, some with low intensities (Table 1). To avoid the possibility that some of the weak lines are due to minor quantities of other phases, only those reflections with intensity greater than 20 were inserted in the search routine of the X-ray data base, with the constraint of the chemical composition. There were no matches. There is the possibility that the green deposit in Lama Lua Cave is a new mineral, but a much more comprehensive characterization of the material will be needed before it can be proposed as such.

THE KIPUKA-KANOHINA SYSTEM

The Kipuka-Kanohina System in an interconnected set of caves located in Kula Kai View Estates, about 70 km south of Kailua-Kona and 30 km north of South Point. At 26.5 km, it is one of the longest lava tube complexes on the island (Elhard and Herrera, 2004; Coons, 2004). Two sections of the cave were investigated: the Kula Kai Caverns show cave and passages of the cave accessible from the Tapa Street entrance.

Kula Kai Caverns has an assortment of white coatings. Some of these are stringy deposits draped down the walls and have a distinctly organic appearance. Five samples

Table 1. X-ray powder diffraction data for green Lama Lua specimen 05HI008.

2-Theta	D (Å)	Intensity I/I_{100}
8.8	10.037	15.6
12.28	7.202	54.8
15.16	5.84	6.4
17.3	5.121	6
19.94	4.449	8.6
21.54	4.121	5.3
21.96	4.044	53.9
23.64	3.761	30.2
24.12	3.687	12.9
24.44	3.64	18
25.62	3.474	33.3
26.4	3.373	14.3
26.72	3.334	6.7
27.82	3.205	100
28.42	3.138	14.4
29.5	3.025	29.1
29.78	2.997	62.8
30.32	2.946	35.7
30.8	2.901	17.6
33.12	2.703	32.9
33.74	2.654	15.8
34.98	2.563	13.8
35.62	2.518	38.1
36.54	2.457	7.1
36.77	2.442	5.4
37.17	2.417	5.1
37.7	2.384	8.5
39.04	2.306	5.9
39.27	2.292	6
39.46	2.282	5.7
40.82	2.209	7.4
41.95	2.152	5
42.36	2.132	15
44.48	2.035	74.6
49.33	1.846	6.6
49.62	1.836	8.7
50.76	1.797	5.7
51.44	1.775	4.5
52.02	1.757	4.3
52.34	1.747	30
54.09	1.694	5.2
58.26	1.582	4.4
61.07	1.516	4.2
61.23	1.513	4.8
62.38	1.487	6.5
62.62	1.482	6.8
64.02	1.453	4.5
64.71	1.459	4.1
66.31	1.408	3.8
68.99	1.36	4.7
84.75	1.143	11.5
85.03	1.14	10.5
85.73	1.132	4.2
87.56	1.113	3.6
88.63	1.103	4.1
88.94	1.1	5.5

were collected from different parts of the cave. All were soft and mushy and difficult to grind for X-ray analysis. The X-ray patterns for all five samples showed well-crystallized calcite, some with a trace of gypsum. These speleothems have been referred to as moonmilk and they certainly have the physical appearance and texture of moonmilk. However, no trace of the usual moonmilk minerals (hydrated magnesium carbonates such as hydromagnesite) were detected. To the extent that moonmilk is a textural term and not a mineralogical term, it is legitimate to call these coatings moonmilk, but those examined, at least, are calcite moonmilk.

A sample of the chalk-white blobs about one cm in diameter was collected from the wall near the blue-green stalactites. The individual crystals were too small to resolve under the binocular microscope. The speleothem was wet, sticky and had a stringy character. Nevertheless, the X-ray pattern was that of well-crystallized calcite superimposed on a broad maximum typical of non-crystalline material (Fig. 7). There may well be an organic substructure to the stringy speleothems with an overgrowth of calcite, which is the only phase that would produce an X-ray diffraction pattern. X-ray patterns of other stringy deposits also exhibited a very broad hump indicating the presence of amorphous material

In the Kipuka Kanohina Cave System occur bright blue-green stalactites (Fig. 8). These were confirmed to be a copper mineral by Elhard and Coons (2004), who published a color photograph. The speleothems are located about 400 m down-tube from the Tapa Street Entrance in a section where the passage walls are polished shiny-black lava. It was possible to get permission from the land owner to remove one 2-cm-long stalactite. There were several surprises when the specimen reached the laboratory. Unlike the green coating in Lama Lua, the Kipuka Kanohina specimen had dried in transit and essentially fell off of the underlying stalactite as a loose powder. The blue-green material was a coating over a normal black lava stalactite. The 2-cm stalactite easily yielded a few milligrams of powder. The next surprise was the X-ray diffraction pattern. The sample didn't have one. The blue-green material was non-crystalline at the X-ray diffraction scale. The X-ray emission spectrum showed that the dominant elements are Si and Cu with smaller amounts of Ca and Al (Fig. 9). A spatial scan of X-ray emission

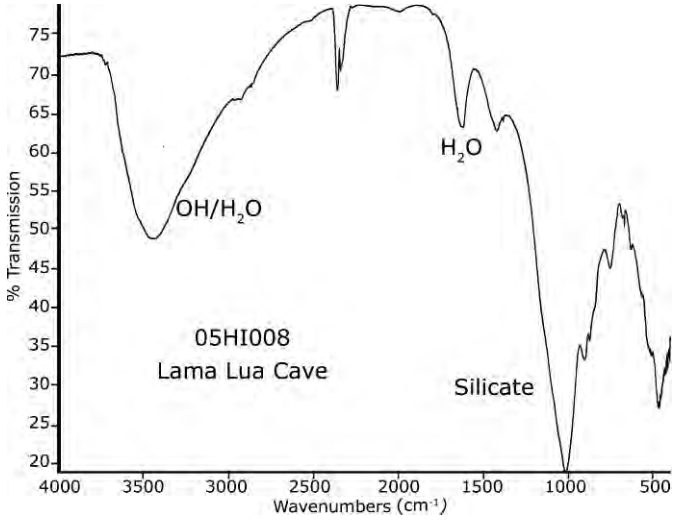

Figure 6. Infrared absorption spectrum for green mineral from Lama Lua Cave. One mg of scraping was ground with 200 mg KBr and vacuum cold-pressed into a transparent pellet for transmission measurement on a Nicholet Fourier Transform spectrometer.

over the area of an SEM image shows that the elemental distribution is highly uniform, indicating a single non-crystalline phase (Fig. 10). Overall, the blue-green coating is a nearly pure copper silicate. However, because it is non-crystalline, it is technically not a mineral. The infrared spectrum (Fig. 11) shows that the phase is highly hydrated, so it can be best described as a copper silicate gel. The chemical composition is similar to chrysocolla, $(Cu,Al)_2H_2Si_2O_5(OH)_4 \cdot nH_2O$, but lacks crystallinity.

HIGH ALTITUDE CAVES ON MAUNA LOA

There are many lava tubes, some mineralized, on the north side of Mauna Loa in the general area of Relay Junction (Medville, 1997). One of the most interesting caves was found high on Mauna Loa. It is reached from the side road that leads from the Saddle Road to the NOAA Observatory. About 6 km along contour from Relay Junction there is the black 1843 pahoehoe flow bounded on both sides by more recent brown aa flows. Less than one kilometer downslope from the road, there is a string of pukas that mark the route of a collapsed tube. One of these first appeared to be a simple collapse structure with a small alcove at the downslope end. However, at the upper end was another collapse into a lower tube. The lower tube continued downslope beneath the upper collapse until it choked off at about 60 m (Fig. 12). It is here called Sample Cave and it is unknown whether or not the cave has been previously cataloged.

There is a pile of white powder on the floor of the small alcove at the downslope end of the collapsed upper tube and white crusts on the walls. The white powder is thenardite, Na_2SO_4; the crusts are gypsum. Thenardite also appears as a wall coating at places in the puka where the surface is protected from direct rainfall. Thenardite is the dehydration product of mirabilite, $Na_2SO_4 \cdot 10H_2O$, a highly water-soluble mineral that occurs in some extremely dry limestone caves. A sample of the floor crust near the entrance of the lower tube contained a mixture of about 60% thenardite, 20% gypsum and 20% mirabilite. A sample from another cave high on Mauna Loa also contained a mixture of mirabilite and thenardite. These caves, high on the volcano, are sufficiently dry to preserve these water-soluble salts. There is an equilibrium between mirabilite and thenardite that depends on both temperature and water vapor partial pressure (White, 1997). The hydration state of any specific specimen will depend on the exact

Table 3. Normalization of the chemical analysis of sample 05HI006 to a chemical formula.

Oxide	Mean Wt (%)	Mole Fraction	Normalized
CuO	31.97	0.402	3.98
V_2O_5	18.37	0.101	1.00
K_2O	0.07	0.001	0.01
Al_2O_3	1.25	0.012	0.12
SiO_2	29.47	0.491	4.86
MgO	7.98	0.198	1.96
CaO	0.74	0.013	0.13
Total	89.85		
H_2O	10.15	0.564	5.58

Rounded composition: $2MgO \cdot 4CuO \cdot V_2O_5 \cdot 5SiO_2 \cdot 5.6H_2O$

Table 2. Electron microprobe analysis of green Lama Lua specimen 05HI006. All elements reported as weight percent of the specified oxide.

Grain	CuO	V_2O_3	K_2O	Al_2O_3	SiO_2	MgO	CaO
1	33.551	16.368	0.037	1.277	27.866	7.378	0.853
2	35.437	17.799	0.064	1.137	26.465	7.390	0.645
3	32.056	14.958	0.055	1.066	28.891	7.725	0.684
4	32.045	14.202	0.106	1.449	30.453	7.818	0.690
5	28.005	13.584	0.054	1.402	31.554	8.400	0.603
6	31.276	14.833	0.066	1.128	29.933	8.695	0.625
7	31.416	14.526	0.099	1.270	31.127	8.469	1.058

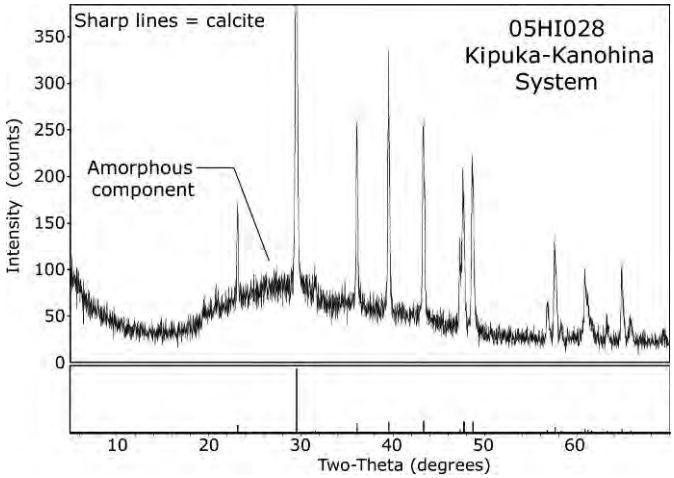

Figure 7. X-ray diffraction pattern for specimen 05HI028, white stringy material from the Kipuka Kanohina System.

amount of moisture in the local environment and may well change between wet and dry seasons.

The entrance area of the lower tube is encrusted with masses of crystals, some pure white and some tinged with yellow and orange (Fig. 13). A breakdown block at the cave entrance is coated with clear crystals up to a centimeter across (Fig. 14). Of the three samples analyzed by X-ray diffraction, all gave clean patterns of well-crystallized gypsum. Sample Cave has the most dramatic display of crystals of any of the caves examined, but the mineral is the same gypsum found in many limestone caves.

Dendritic clusters of clear crystals a few millimeters in length were observed in Red Spirit Pit. These proved to be gypsum although with a more acicular habit than those observed in Sample Cave.

Caves of the Kilauea Caldera

Kilauea Caldera contains dozens of small fumarole and tumulous caves. Some of these were steaming with a strong smell of SO_2 and maybe some HCl. Air temperature in some reached the range of 50 °C. There are white coatings on many of the caves and some of the fumaroles are depositing clear yellowish crystals (Fig. 15). White Stalactite Cave is a shallow trench with a short tunnel with walls coated by thick white and yellow crystals. In the absence of a collecting permit, it was not possible to obtain samples and the mineralogical characterization of these deposits remains a project for the future. The size and morphology of the clusters of crystals are similar to the gypsum crystals observed in Sample Cave. The yellow color might be due to small amounts of included elemental sulfur.

Discussion and Conclusions

Overall, 51 samples were obtained from nine caves. Of these 51 samples, 22 were calcite and 15 were gypsum. Calcite appeared as coralloids, as crusts, and as the stringy white masses from the Kipuka Kanohina System. Gypsum sand and crusts were found in the Hualalai Ranch System, the Kipuka Kanohina System, Bee Cave, Black Pellet Cave, Kiholo Bay Cave, Sample Cave, and Red Spirit Pit. Except for the copper and vanadium minerals, the secondary speleothems in this group of lava tube caves are not intrinsically different from speleothems found in many limestone caves. However, the most common features of limestone caves, calcite stalactites, stalagmites, and flowstone, were not observed. Although calcite was the most common mineral observed, it always appeared in the form of coralloids, moonmilk, or powdery crusts.

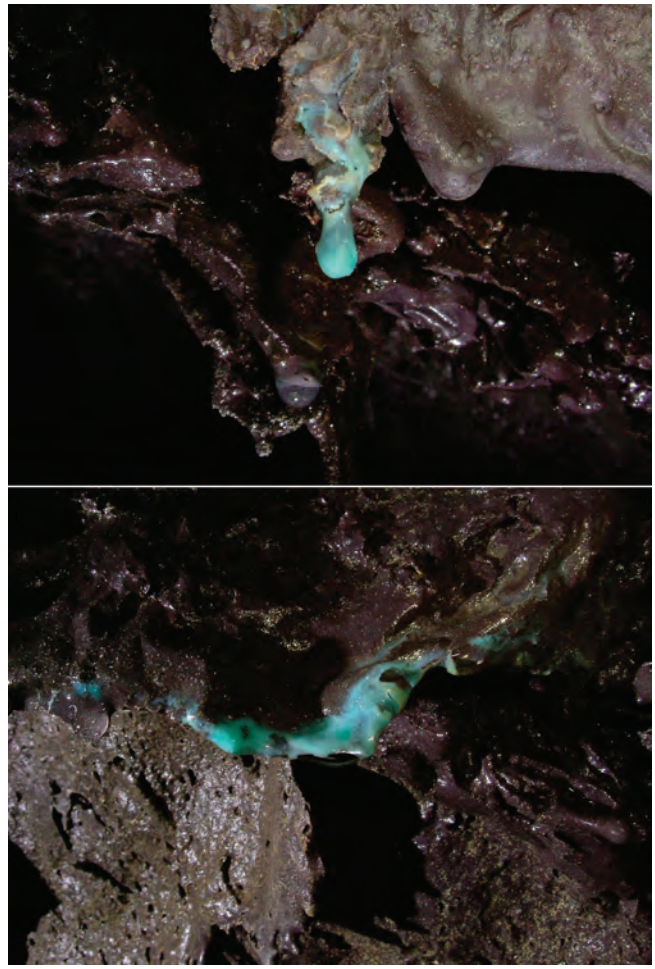

Figure 8. Photographs of the blue-green stalactites in the Kipuka-Kanohina System.

Sulfate Minerals

The presence of sulfate salts is the result of evaporation of the seepage waters that enter the caves, especially caves that are still hot. When the caves cool and are wetted from rainfall seepages, as is true of most of the low altitude caves, only the ubiquitous gypsum survives. The more highly soluble salts only survive in the higher and drier caves. Thenardite and mirabilite, which convert rapidly into each other depending on temperature and moisture

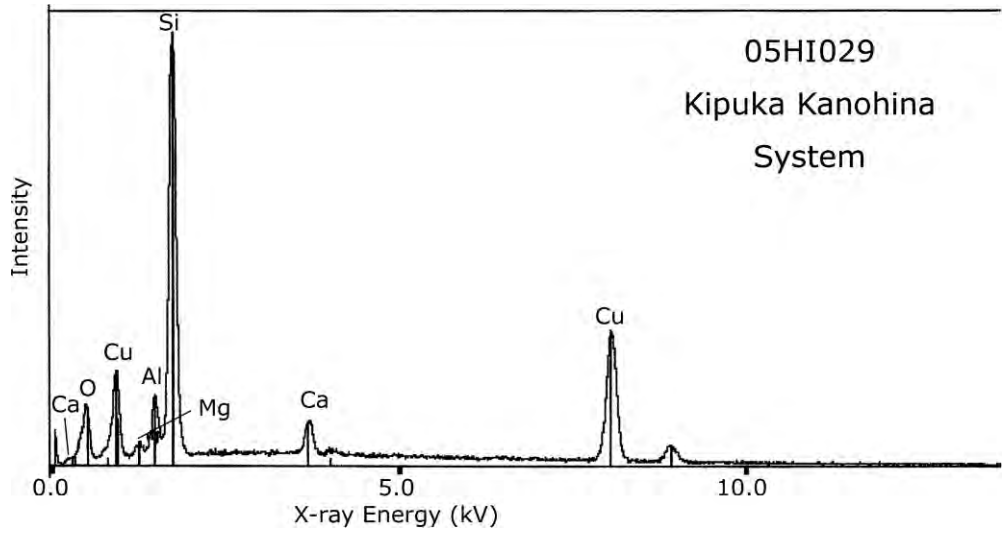

Figure 9. X-ray emission spectrum of the blue green coating from lava stalactites (sample 05HI029).

content, were found in this investigation and have been reported in other caves such as Lae'apuki (Porter, 2000). In addition, Lae'apuki Cave contains large and extensive speleothems of blödite, $Na_2Mg(SO_4)_2 \cdot 4H_2O$, and kainite, $KMg(SO_4)Cl \cdot 3H_2O$. Unpublished mineral analyses of the USGS's Hawaiian Volcano Observatory also list hydroglauberite, $Na_{10}Ca_3(SO_4)_8 \cdot 6H_2O$.

As noted by Forti (2005), these highly water-soluble minerals are transient phases. As the host lava tubes cool to ambient conditions, these minerals dissolve and are lost.

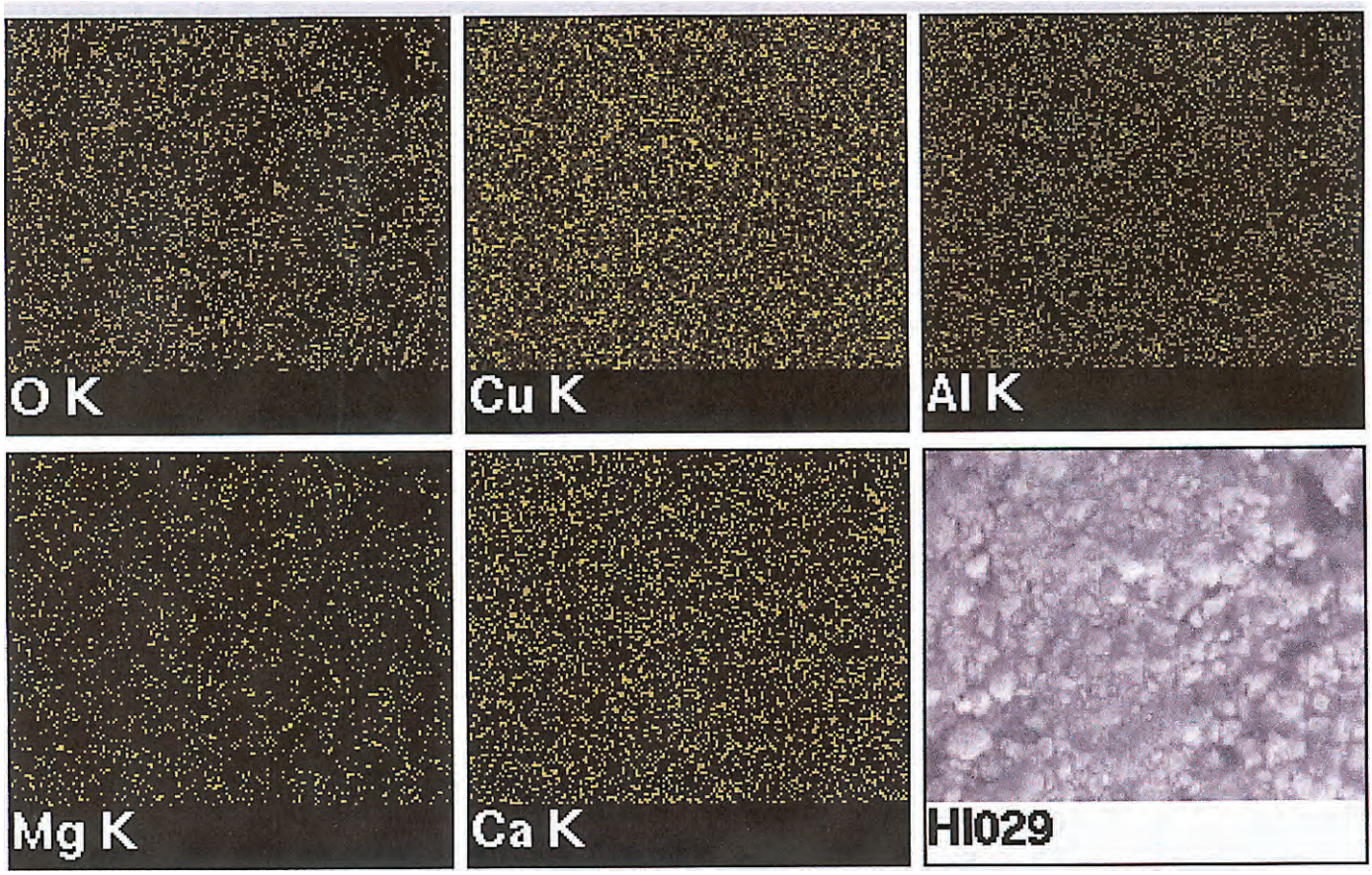

Figure 10. X-ray emission map of the SEM image of sample 05HI029 (shown in lower right).

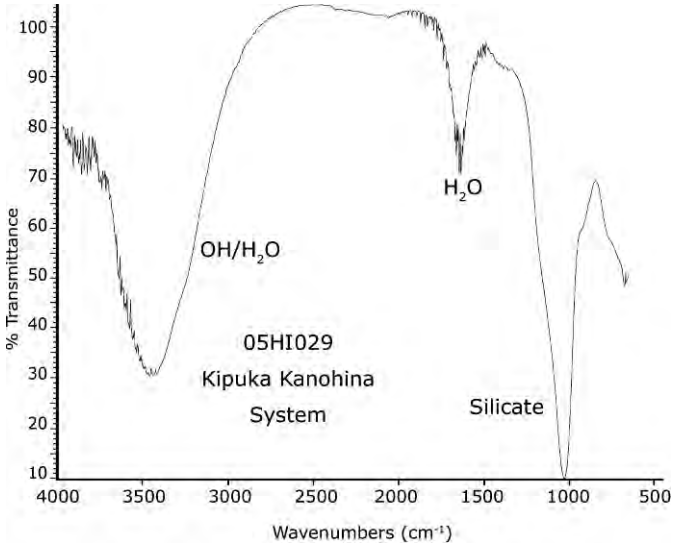

Figure 11. Infrared absorption spectrum for blue-green coating, sample 05HI029.

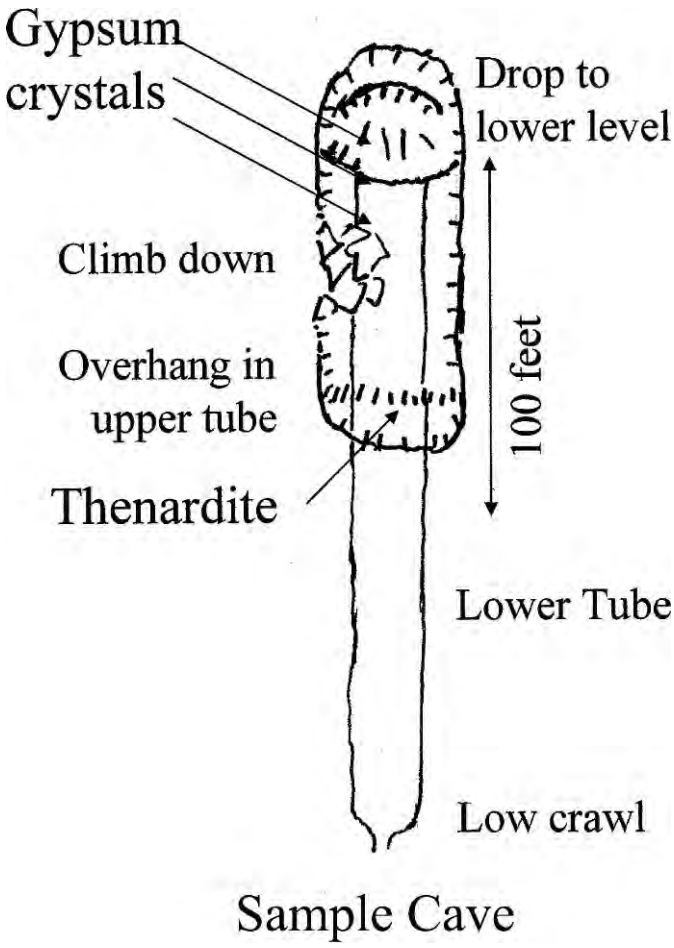

Figure 12. Sketch map of Sample Cave.

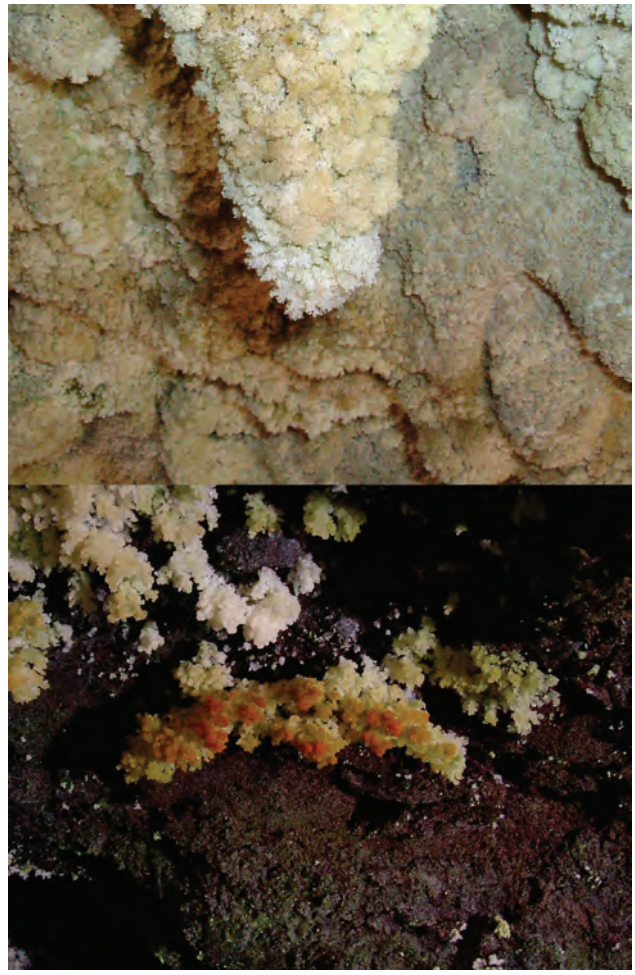

Figure 13. (Upper) Crystal-covered surface near entrance of Sample Cave. (Lower) Orange-tinged crystal mass inside Sample Cave.

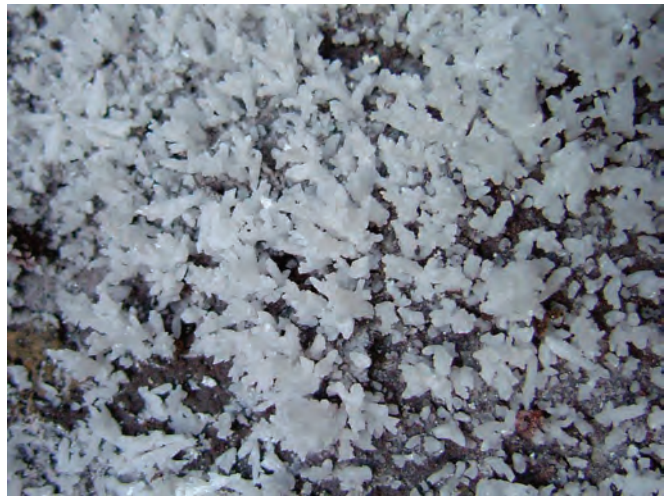

Figure 14. Clear crystals on breakdown block inside drip line of Sample Cave.

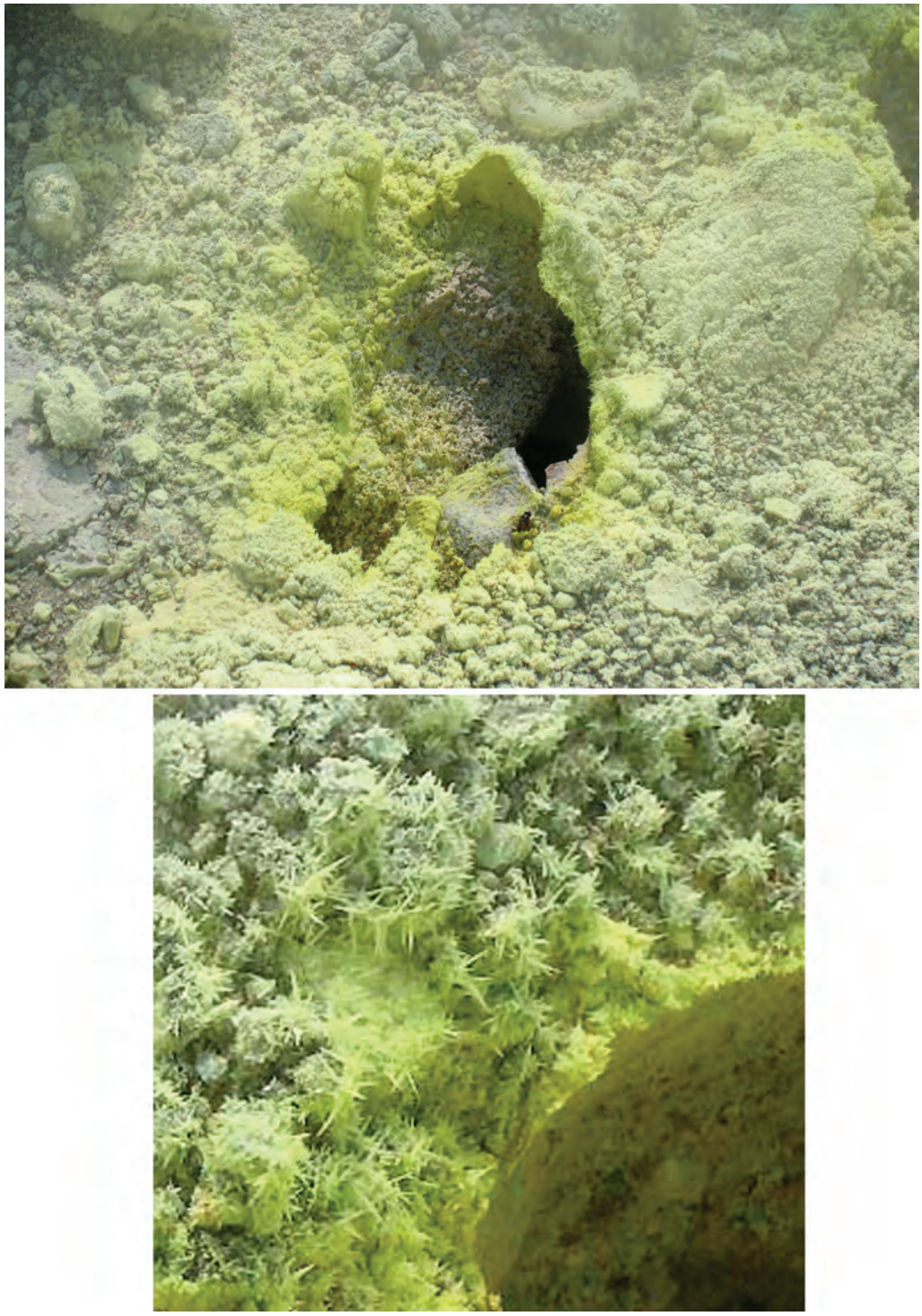

Figure 15. Crystals deposited around small fumarole in Kilauea Caldera.

Lae'apuki Cave was only two-years-old when Porter and his companions did their exploration. Follow-up investigations at regular intervals to observe changes in mineralogy with time and temperature would have been very interesting.

Palmer and Palmer (2006) reported bassanite, $CaSO_4 \cdot \frac{1}{2}H_2O$ from Refuge Cave, part of the Kipuka-Kanohina System. Bassanite is unstable in the presence of water at ambient temperature; it quickly hydrates to form gypsum. Its presence in a cave now cooled to ambient temperature is evidence that some of the gypsum may also have been formed in the presence of high temperature gases and not just as a cold-water deposit formed under present day conditions.

Calcite Speleothems

The mechanism by which calcite speleothems are deposited in limestone caves is well-established and known in considerable detail. Infiltrating rainwater encounters the CO_2-rich soil atmosphere and dissolves CO_2 to concentrations orders of magnitude greater than the atmospheric values. When the acidic CO_2-rich water reaches the soil/limestone contact, there is a reaction and the limestone is dissolved. Those portions of the infiltration water that intersect an underlying cave passage are exposed to the lower CO_2 pressure of the cave atmosphere and excess CO_2 is degassed, thus supersaturating the drip water and forcing the precipitation of $CaCO_3$.

The CO_2 portion of the mechanism should work equally well in volcanic caves. The missing bit of the mechanism is the source of calcium. Instead of limestone, which dissolves readily in acidic groundwater, the source of calcium in volcanic caves is likely from the breakdown of anorthite feldspar (the more calcium-rich side of the plagioclase solid solution series, $Na_xCa_{(1-x)}Al_{(2-x)}$ $Si_{(2+x)}O_8$) in the basaltic rock. Anorthite is the least stable of the common basaltic minerals. It breaks down in water roughly 100 times faster than the pyroxene minerals and 5000 times faster than olivine (Lasaga, 1984). The calcium end-member of the plagioclase series breaks down roughly 100 times faster than the sodium-end member and several thousand times faster than orthoclase, $KAlSi_3O_8$. Although the instability of calcium-rich feldspar provides a ready source of calcium for the deposition of calcite and gypsum, the rates of dissolution are much slower than those of limestone. The absence of massive calcite speleothems (stalactites, stalagmites, and flowstone) may be the result of there being only a weak source of calcium for the seepage water, or it might be due to low CO_2 pressures in the overlying soils. Investigations of the chemistry of the drip water in volcanic caves will be necessary to sort out the possible geochemical mechanisms.

Transition Metal-Containing Minerals

The copper silicate from the Kipuka-Kanohina System and the copper-vanadium silicate from Lama Lua Cave appear to be both fumarole minerals, deposited in pre-existing lava tubes by hot steam or other gases. The source of the copper and vanadium is likely the lava itself. Trace element analyses of basalts in general (Prinz, 1967) and Hawaiian basalts in particular (Wager and Mitchell, 1953) show typical copper concentrations in the range of 100 ppm and vanadium concentrations of several hundred ppm. The transport species is likely to have been a chloride complex. Both copper and vanadium chlorides are volatile at the temperatures of fumarole gases and this would account for stripping relatively pure copper and vanadium compounds from a rock in which the elements were present at only part-per-million quantities. The presence of kainite in the still-hot Lae'apuka Cave is evidence that chloride is present in the gases of young lava tubes.

The failure to identify the copper-vanadium mineral in Lama Lua cave, in spite of a reasonably accurate chemical composition and a reasonably good quality X-ray diffraction pattern, raises the possibility that it is a new mineral. However, a much more extensive characterization effort would be required before a new mineral would be accepted by the International Commission on New Mineral Names.

Acknowledgements

Elizabeth L. White is thanked for her assistance in the field and with preparing the illustrations used in this article. Nevin and Judy Davis showed us mineralized areas in the caves near Kona. Judy Davis sampled some of the caves. Nevin Davis (Figs 4, 8, 13, and 14) and John Wilson (Figs 1 and 3) generously permitted use of some of their photographs in this article. Don Coons guided us to interesting features in the Kapuka Kanohina System. We thank William R. Halliday for an extensive walking tour of the caves of Kilauea Caldera. The X-ray diffraction patterns were measured by Nichole Wonderling and the microprobe analysis by Mark Angelone at Penn State's Materials Characterization Laboratory. I thank Ellen Herman for her assistance with the SEM.

References

Baird, A.K., Mohrig, D.C., and Welday, E.E., 1985, Vapor deposition in basaltic stalactites, Kilauea, Hawaii: Lithos, v. 18, p. 151–160.

Coons, D., 2004, Speleogenesis of the Kipuka-Kanohina Cave System: NSS News, v. 62, p. 42–43.

Davis, N.W., 2006, Bee Cave: Hawaii Speleological Survey Newsletter, no. 19, 6 p.

Elhard, R., and Coons, D., 2004, Mineralogy of the Kipuka Kanohina Cave System: NSS News, v. 62, p. 44–45.

Elhard, R., and Herrera, R., 2004, Caves in our front yard: NSS News, v. 62, p. 36–41.

Forti, P., 2000, Mineralogenic mechanisms and cave minerals in the volcanic caves of Mt. Etna (Sicily, Italy): Mitteilungen des Verbandes der deutschen Höhlen- und Karstforscher e.v. München, v. 46, p. 37–41.

Forti, P., 2005, Genetic processes of cave minerals in volcanic environments: An overview: Journal of Cave and Karst Studies, v. 67, p. 3–13.

Hill, C.A., and Forti, P., 1997, Cave minerals of the world, 2nd Edition, Huntsville, National Speleological Society, 463 p.

Lasaga, A.C., 1984, Chemical kinetics of water-rock interactions: Journal of Geophysical Research, v. 89, p. 4009–4025.

Medville, D., 1997, The lava tubes of north Mauna Loa: NSS News, v. 55, p. 32–43.

Medville, D., 2005, Black Pellet Cave: Hawai'i Speleological Survey Newsletter, no. 17, p. 14–17.

Medville, D., 2006a, Some caves near Kiholo Bay: Hawai'i Speleological Survey Newsletter, no. 20, p. 20–21.

Medville, D., 2006b, The exploration and survey of the Lama Lua System – North Kona, Hawai'i: Hawai'i Speleological Survey Newsletter, no. 20, p. 3–7.

Medville, D., and Davis, N.W., 2007, The exploration and survey of the Lama Lua System – North Kona, Hawai'i: NSS News, v. 65, p. 10–17.

Palmer, P., and Palmer, A., 2006, Mineral deposits in the Refuge Cave, Kipuka Kanohina System, Hawai'i: Hawai'i Speleological Survey Newsletter, no. 19, p. 3–5.

Porter, A., 2000, The initial exploration of Lower Lae'apuki Cave System, Hawai'i Volcanoes National Park: NSS News, v. 58, p. 10–17.

Prinz, M., 1967, Geochemistry of basaltic rocks: Trace elements, *in* Hess, H.H. and Poldervaart, A., eds., Basalts, New York, Wiley Interscience, v. 1, p. 271–323.

Wager, L.R. and Mitchell, R.L., 1953, Trace elements in a suite of Hawaiian lavas: Geochimica et Cosmochimica Acta, v. 3, p. 217–223.

White, W.B., 1997, Thermodynamic equilibrium, kinetics, activation barriers, and reaction mechanisms for chemical reactions in karst terrains: Environmental Geology, v. 30, p. 46–58.

Y. Pan, Z. Hou, and S. Li – Description of a new *Macrobrachium* species (Crustacea: Decapoda: Caridea: Palaemonidae) from a cave in Guangxi, with a synopsis of the stygobiotic Decapoda in China. *Journal of Cave and Karst Studies,* v. 72, no. 2, p. 86–93. DOI: 10.4311/jcks2009lsc0087

DESCRIPTION OF A NEW *MACROBRACHIUM* SPECIES (CRUSTACEA: DECAPODA: CARIDEA: PALAEMONIDAE) FROM A CAVE IN GUANGXI, WITH A SYNOPSIS OF THE STYGOBIOTIC DECAPODA IN CHINA

YITAO PAN[1,2], ZHONGE HOU[1], AND SHUQIANG LI[1*]

Abstract: *Macrobrachium elegantum* is a new species of stygobiotic shrimp discovered in Guangxi, China. The new species is characterized by a transparent body and degenerated eyes and is morphologically similar to *M. lingyunense*. This is an addition to the list of fifteen stygobiotic shrimp previously known from throughout the karst of China.

INTRODUCTION

Karst landforms cover about 33% of China's surface. Caves can be found in most karst areas, especially in Yunnan, Guizhou, and Guangxi provinces. This karst terrain has numerous varieties of cave-dwelling animals, including bats, amphibians, fishes, spiders, and crustaceans (Li, 2007). Geographically disjunct, small, and island-like cave populations in many parts of the world are imperiled by declining water supply and quality as a result of human activities. These include groundwater pumping, tourism, pollution, and nutrient enrichment (Eberhard et al., 2005). Cave species in the Chinese karst regions are threatened by similar factors. Some cave vertebrates have been listed as endangered species and conservation rules have been issued, but stygobiotic invertebrates are poorly studied and less attention has been paid to protecting them.

The study of Chinese cave-dwelling species of Decapoda began about fifteen years ago. A total number of fifteen stygobiotic species of shrimp were recorded (Liang, 2004; Li et al., 2006). In 2008, a scientific expedition to the Guangxi karst regions was organized by the Guangxi Institute of Fisheries and several specimens of stygobiotic Decapoda were collected. Close study of the specimens revealed the presence of a new species of the genus *Macrobrachium* Bate, 1868. In this study, we review the diversity, adaptation, and distribution of cave Decapoda in China and describe the new taxon, *Macrobrachium elegantum* n. sp.

DIVERSITY AND DISTRIBUTION OF STYGOBIOTIC DECAPODA

With the addition of the new species described here, there are 17 stygobiont species of Decapoda recorded in China, of which 15 belong to three genera of the family Atyidae and two to the family Palaemonidae (Table 1). These species are scattered in China's karst regions and there are large areas that have not been fully investigated by scientists (Fig. 1). Therefore we believe that more cave-dwelling decapods will be found in the future.

Compared to the surface biotope, ecosystems in caves are usually characterized by aphotic conditions, tenuous air, and stable temperature. Animals living in such environments often possess the adaptive modifications of troglobites, such as long, slender body and appendages (Espinasa and Vuong, 2008). Cavernicolous species of *Macrobrachium* may invade caves independently, but convergent evolution has resulted in similar life history (Wowor et al., 2009). Cave decapods in China show adaptive changes in eyes, coloration, and body shape. Table 1 provides a list of known species of stygobiotic decapods from China and their different adaptations to the cave environment.

MATERIAL AND METHODS

Specimens were collected by electrofishing, preserved in 75% ethanol, examined using an SZX12-Olympus stereomicroscope, and measured by slide caliper. Detailed observations were made under a BX41-Olympus compound microscope and a BH2-Olympus microscope. All illustrations were produced using a camera lucida. Male pereopods were examined and illustrated after being detached. Size of specimens is indicated by carapace length (CL) measured from the orbital margin to the posterodorsal margin. All measurements are given in millimeters (mm). Terminology for somatic morphology is after Komai and Fujita (2005). All type specimens and other material are deposited in the Institute of Zoology, Chinese Academy of Sciences (IZCAS), Beijing, China.

TAXONOMY

Macrobrachium elegantum n. sp. (Figs. 1–4)

MATERIAL EXAMINED

Holotype: male (IZCAS-DE-005), CL 15.2 mm, an unnamed cave in Xiaorui Village, Ludong Town, Jingxi County

* Corresponding Author, lisq@ioz.ac.cn
[1] Institute of Zoology, Chinese Academy of Sciences, Beijing 100101, China
[2] College of Environment and Resources, Jilin University, Changchun 130012, China

Table 1. The known stygobiotic Decapoda from China.

Species	Type locality	Latitude and Longitude	Habitat and morphological adaptation
		Atyidae	
Caridina guangxiensis Liang and Zhou, 1993	Tianwangshan Cave, Guilin, Guangxi (1)	25.20°N, 110.30°E	Found in groundwater of cave, without light; body pink and transparent, eyes normal, cornea developed.
Caridina feixiana Cai and Liang, 1999	Feixia Cave, Gejiu, Yunnan (2)	23.35°N, 103.15°E	In completely dark zone of cave; eyes normal.
Caridina cavernicola Liang and Zhou, 1993	Lenggu Cave, Du'an, Guangxi (3)	24.20°N, 108.13°E	In groundwater of cave, 30 meters away from entrance, no light; eyes normal, cornea developed.
Caridina dianchiensis Liang and Yan, 1985	Huahong Cave, Kunming, Yunnan (4)	25.67°N, 102.67°E	…
Caridina mengae Liang, 1993	Xiangshui Cave, Panshi, Songtao, Guizhou (5)	28.15°N, 109.2°E	…
Caridina ablepsia Guo, Jiang and Zhang, 1992	Xiaolong Cave, Yongshunwang Village, Hunan (6)	29.00°N, 109.85°E	In groundwater of cave, completely dark; eyes small, reduced, cornea non-pigmented, body ivory.
Caridina semiblepsia Guo, Choy and Gui, 1996	Baojing Cave, Baojing, Hunan (7)	28.70°N, 109.65°E	In completely dark zone of cave; eye-stalk degenerated, body transparent.
Caridina demenica Cai and Li, 1997	Demen Cave, Yongkang Village, Libo, Guizhou (8)	25.37°N, 107.90°E	Eyes reduced with small pigment.
Caridina caverna Liang, Chen and Li, 2005	Xiaoshui Cave, Maolan, Guizhou (9)	25.33°N, 107.93°E	In groundwater of cave, no light; cornea non-pigmented.
Caridina acuta Liang, Chen and Li, 2005	Labiaoqiao Cave, Maolan, Guizhou (10)	25.33°N, 107.93°E	In a cave with weak light; cornea degenerated, with pigment.
Typhlocaridina lanceifrons Liang and Yan, 1981	Daji Cave, Qifeng Mountain, Wuming, Guangxi (11)	23.21°N, 108.21°E	In limpid groundwater of cave, completely dark; the whole body ivory, no eyes, cornea non-pigmented.
Typhlocaridina liui Liang and Zhou, 1993	Paobing Cave, Lingui, Guangxi (12)	25.25°N, 110.05°E	In the entrance of cave, with weak light; eyes degenerated, with 3 black pigments.
Typhlocaridina semityphlata Cai, 1995	A cave in Guilin, Guangxi (13)	25.283°N, 110.283°E	In caves; eyes reduced, pigment in cornea degenerated to a small black dot.
Typhlocaridina lingyunensis Li and Luo, 2001	Lingyun, Guangxi (14)	24.38°N, 106.63°E	Eyes degenerated and small, cornea non-pigmented.
Neocaridina brevidactyla Liang, Chen and Li, 2005	Xiaoshui Cave, Maolan, Guizhou (15)	25.33°N, 107.93°E	In a cave; eyes normal, cornea developed
		Palaemonidae	
Macrobrachium lingyunense Li, Cai and Clarke, 2006	Shadong (Sand cave), Lingyun, Guangxi (16)	24.38°N, 106.63°E	Eyes degenerated, cornea non-pigmented, body transparent.
Macrobrachium elegantum n. sp.	A cave in Jingxi, Guangxi (17)	23.10°N, 106.4°E	In caves; eyes degenerated and small, cornea non-pigmented, body transparent.

(23.1°N, 106.4°E), Guangxi Zhuang Autonomous Region, China; March 3, 2008, collected by Chunguang Zhang.

Paratypes: one male (IZCAS-DE-006), CL 12.8 mm; two females (IZCAS-DE-007, 008), CL 14.7 mm, 15.2 mm, same data as holotype.

Diagnosis

Rostrum straight, tip bifurcate and reaching beyond distal margin of scaphocerite, dorsal margin armed with seven or eight teeth, including three or four on carapace behind orbital margin; teeth placed more widely on anterior part; ventral margin armed with four to six teeth. Inferior orbital lobe typical for genus, produced in roundly triangular, overhung lobe. Antennal spine behind inferior orbital angle; hepatic spine inferior to antennal spine. First to fifth abdominal sternites with distinct transverse ridge, tooth of fifth larger. Telson terminating in sharp tooth posteriorly, with two pairs of dorsolateral spines; terminal

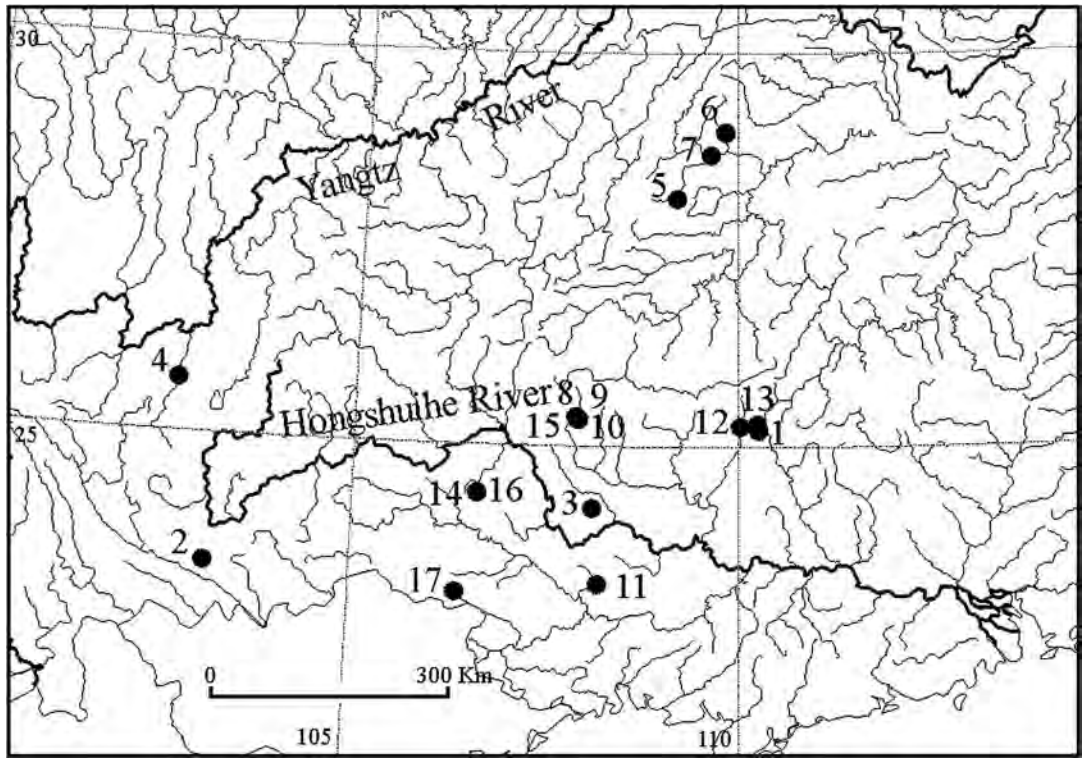

Figure 1. Localities of Chinese stygobiotic Decopoda (the numbers are the same as in Table 1).

tooth not overreaching posterolateral spines. Epistome not bilobed. Eyes small, stalks highly reduced, cornea non-pigmented. Lateral margin of scaphocerite straight. Carpus of first pereopod 1.7 times as long as chela. Second pereopod symmetrically equal, surface of segments smooth; chela about 1.9 times longer than carpus; fingers about 1.6 times longer than palm, dactylus slightly longer than fixed finger, with tips crossing when closed; cutting edges with rows of setae, no tooth. Palm subcylindrical, shorter than carpus, inflated. Carpus subequal in length to merus. Third pereopod slender, reaching beyond distal margin of scaphocerite by 0.3 times the length of propodus, carpus distinctly shorter than propodus.

DESCRIPTION OF HOLOTYPE MALE

Body moderately robust. Rostrum (Fig. 2A–C) straight, tip bifurcate with setule, reaching slightly beyond distal margin of scaphocerite, 0.7 times as long as the carapace. Dorsal margin armed with eight teeth, including four on carapace behind posterior margin of orbit, arising from about 0.4 times the carapace length; anterior teeth larger than posterior, spaces between first, second, and third teeth distinctly wider than others; ventral margin armed with four teeth, rows of plumose setae present between each tooth on dorsal and ventral margin. Inferior orbital angle produced in roundly triangular lobe, conspicuous. Antennal spine (Fig. 2A–B) moderately small, submarginal, situated inferior to inferior orbital angle, tip not reaching anterolateral margin of carapace; hepatic spine smaller than antennal spine, lying slightly inferior to level of it. Surface of carapace (Fig. 2A) smooth, glabrous.

Thoracic sternum narrow; fourth to fifth thoracic sternites with indistinct transverse ridge; sixth to seventh sternites with transverse ridge along posterior border; eighth thoracic sternite with distinct oblique transverse ridges along posterior border.

Abdomen smooth and glabrous (Fig. 3A); first to third and fifth pleurae with posterolateral margins produced roundly, those of fourth with feeble posterior process; sixth abdominal somite 1.4 times as long as fifth somite. First to fifth abdominal sternites with distinct transverse ridges; fourth and fifth abdominal sternites with transverse ridges and median teeth, that of fifth abdominal sternites larger. Telson (Fig. 2E) 1.2 times as long as the sixth abdominal somite, with two pairs of spines (at 70% and 85% of total length measured from posterior tooth, respectively); posterior margin terminating in acute tooth (= posteromedian tooth), flanked by two pairs of spines, inner pair about 3 times longer than lateral pair; four pairs of plumose setae arising from ventral surface of posteromedian tooth; all four pairs of setae as long as inner pair of spines, distinctly longer than lateral pair of spines.

Epistome not bilobed (Fig. 4I).

Eyes highly reduced (Fig. 2A–C); cornea elliptical, small and non-pigmented, eye-stalks degenerated.

Antennular peduncle (Fig. 2B, C) reaching 0.8 times the length of scaphocerite. Basal segment moderately broad, about 2 times as wide as second segment, as long as wide,

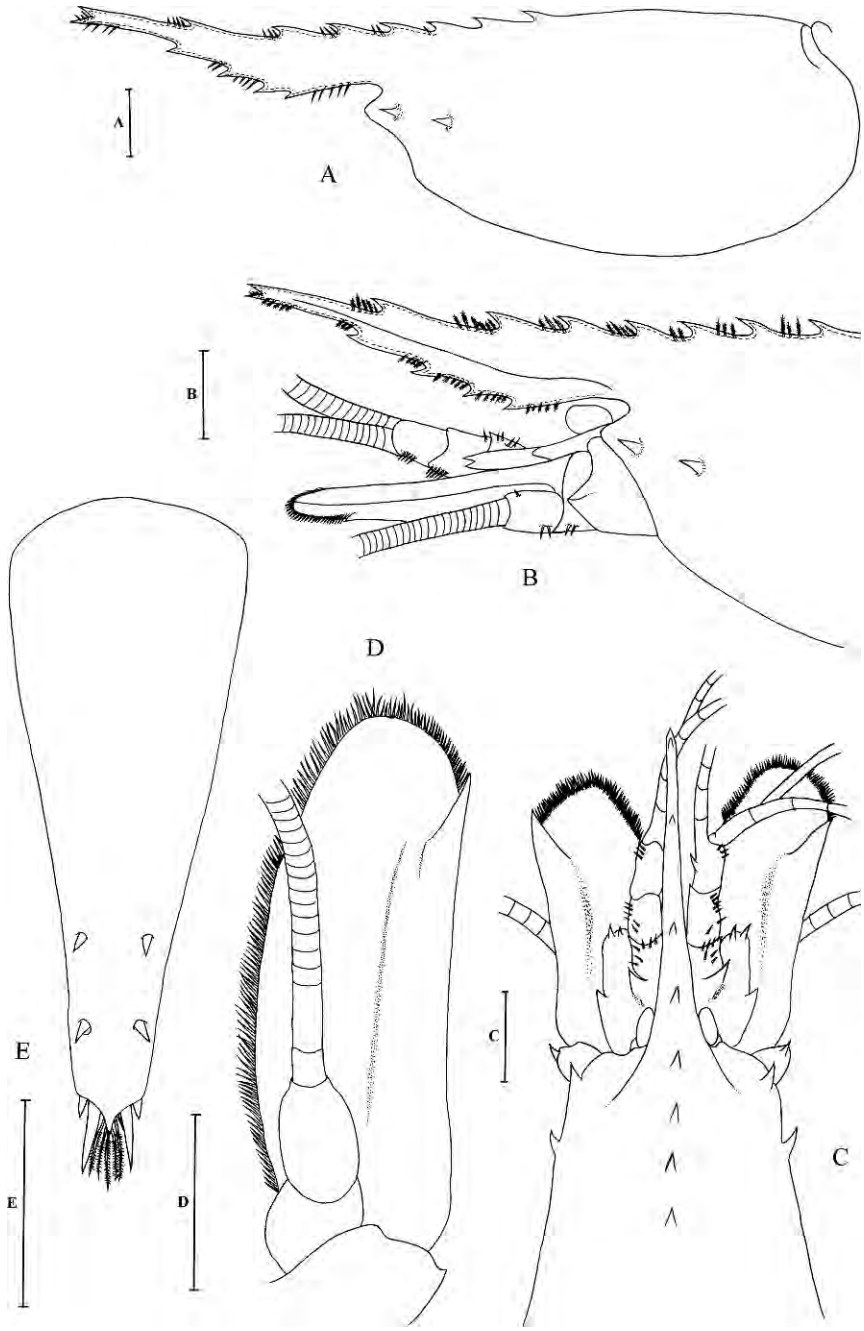

Figure 2. ***Macrobrachium elegantum*** **n sp., holotype, male. A, rostrum and carapace, lateral view. B, rostrum, anterior part of carapace and cephalic appendages, lateral view. C, rostrum, anterior part of carapace and cephalic appendages, dorsal view. D, antenna, ventral view. E, telson, dorsal view. Scale bars: 2 mm.**

lateral margin straight, with a small proximal tooth, anterolateral angle produced in two sharp spines overreaching distal margin of basal segment, dorsal surface weakly concave, with few short setae; ventral edge tapering posteriorly; stylocerite short and sharp, reaching about 0.5 times the length of second segment. Second segment about 0.6 times as long as basal segment, about 1.6 times as long as wide, ventral edge with row of setae. Third segment slightly longer than second segment, about 1.8 times as long as wide. Lateral flagellum biramous, longer ramus 2.5 times the carapace length, shorter ramus (accessory flagellum) about 0.5 times the length of longer ramus.

Antennal peduncle (Fig. 2B, D) with tooth on ventrolateral margin of basicerite. Fifth segment (carpocerite) cylindrical, reaching 30% of scaphocerite length. Scaphocerite (Fig. 2D) about 50% of carapace length, 3 times longer than broad; lateral margin straight, terminating in

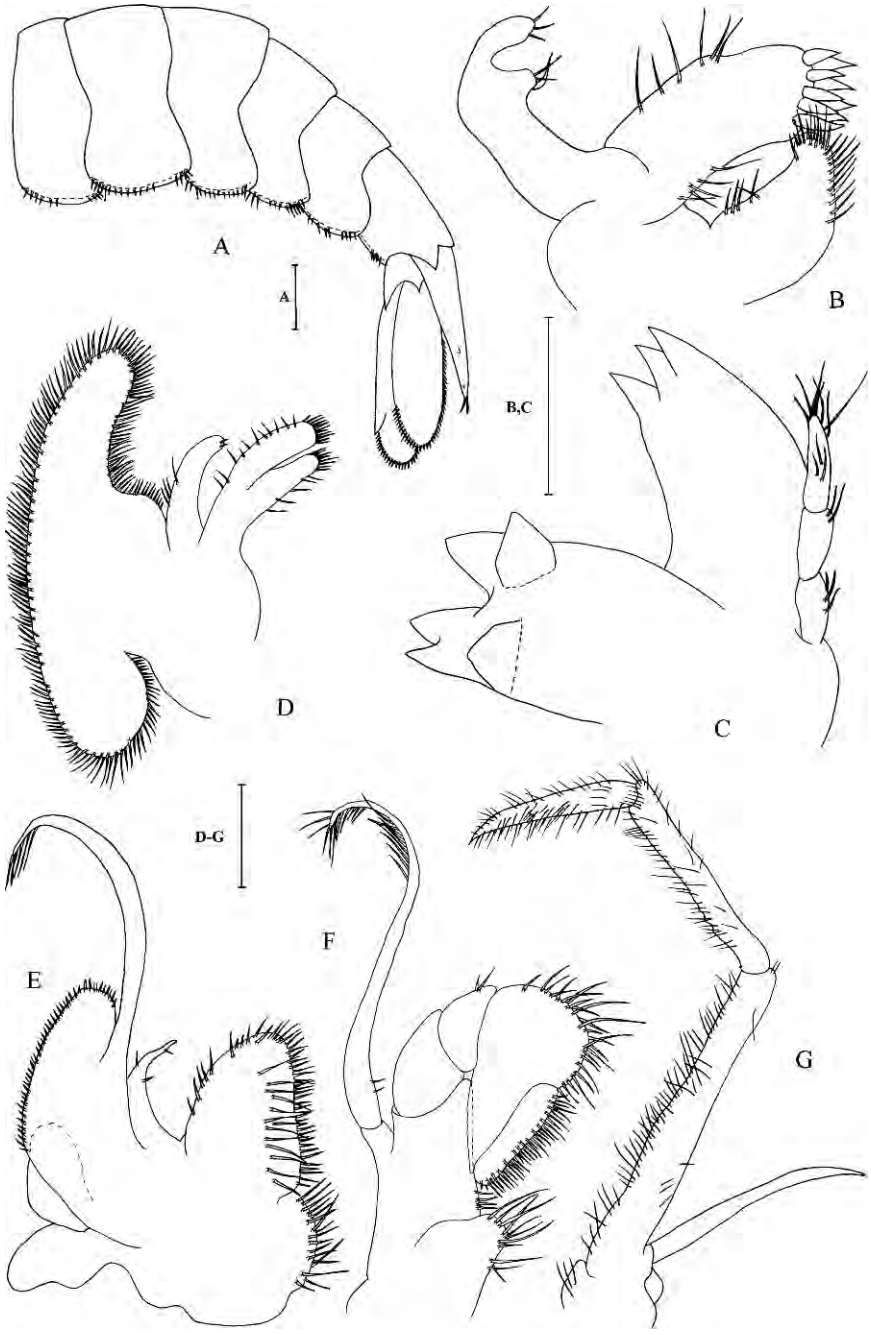

Figure 3. *Macrobrachium elegantum* n. sp. holotype, male. A, abdomen and left uropod, lateral view. B, maxillule. C, mandible. D, maxilla. E, first maxilliped. F, second maxilliped. G, third maxilliped. Scale bars: A, 2 mm; B–G, 1 mm.

small distolateral tooth far exceeded by broadly rounded lamella. Flagellum 1.6 times of body length.

Mouthparts typical for genus. Mandible (Fig. 3C) with slender palp consisting of three articles; incisor process robust, armed with three moderate teeth; molar process robust, truncate distally, with four principal peripheral teeth; maxillule (Fig. 3B) with palp weakly bilobed, outer lobe somewhat elongate; inner lobe short, rounded, two lobes with three setae distally; coxal endite extending as far as basial endite, tapering to truncate tip distally, surface with stiff setae; basial endite trapeziform, broad, with nine large spines and stiff setae on truncate distal margin. Maxilla (Fig. 3D) with coxal endite obsolete; basial endite consisting of two slender lobes, anterior lobe bearing setae on dorsal margin, posterior lobe with setae on ventral margin, both lobes with numerous short setae distally, setae on dorsal and ventral margin longer than those distally; palp with basal part moderately broad, tapering distally; scaphognathite broad, anterior lobe large, posterior lobe moderately narrow, both lobes rounded. First

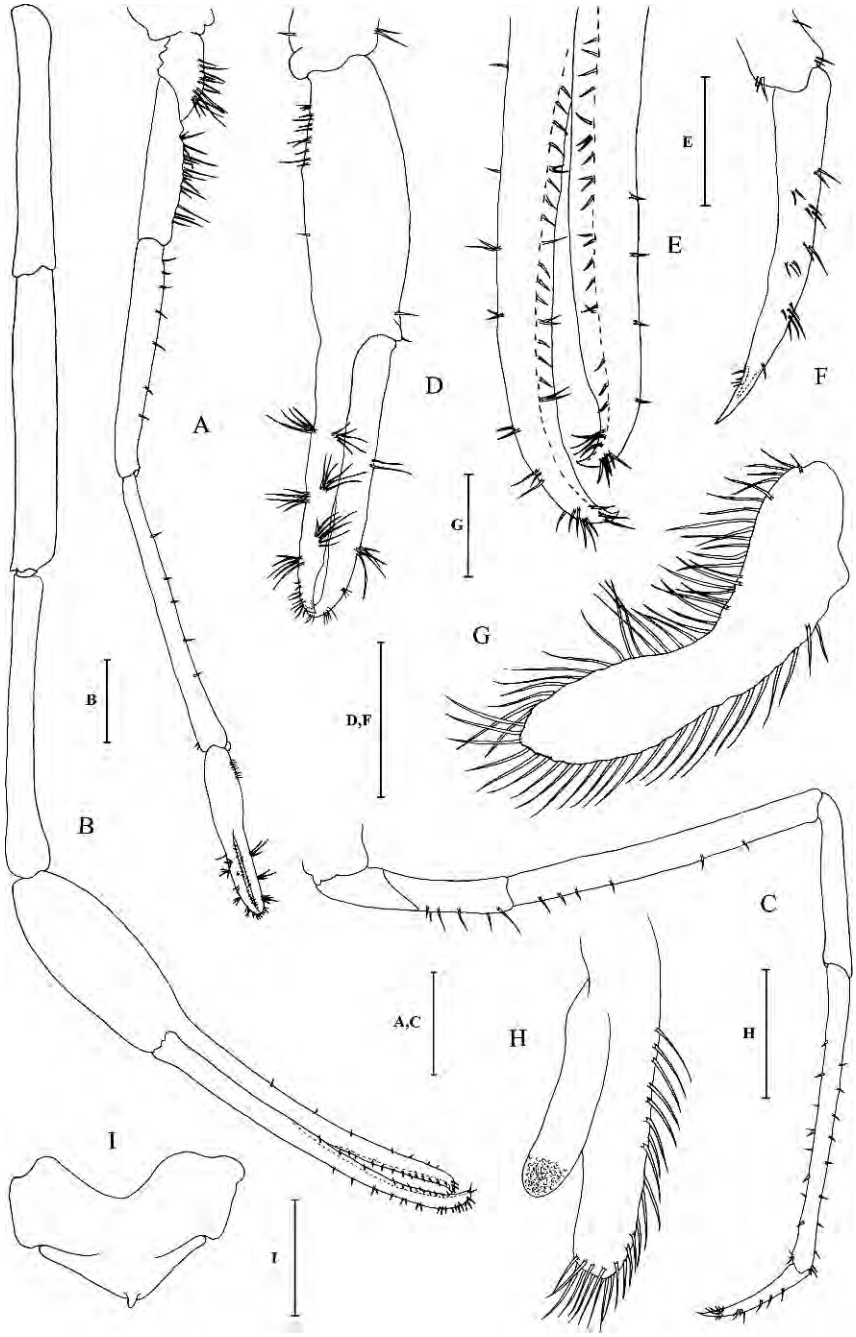

Figure 4. ***Macrobrachium elegantum*** **n. sp. holotype, male. A, first pereopod. B, second pereopod. C, third pereopod. D, chela of first pereopod. E, tips of fingers of second pereopod. F, dactylus of third pereopod. G, endopod of first pleopod. H, appendix interna and appendix masculina of second pleopod. I, epistome. Scale bars: A–C 2 mm, D–F, I, 1 mm; G–H, 0.5 mm.**

maxilliped (Fig. 3E) with setose coxal endite; basial endite subtriangular; palp with few setae, simple and slender, not reaching the distal margin of basial endite; exopod well developed, with long flagellum, caridean lobe moderately broad with row of short setae on margin; epipod with two broad lobes, both tapering distally. Second maxilliped (Fig. 3F) with dactylus and propodus partially fused; ischium and basis fused; coxa with long setae; exopod long and slender, with several setae distally; epipod moderately simple with well-developed podobranch. Third maxilliped (Fig. 3G) with robust endopod; coxa stout, ischiomeral (antepenultimate) segment incompletely fused to basis, combined length about 6.3 times longer than greatest height, with surface bearing tufts of long setae; penultimate segment 0.6 times the length of ischiomeral segment, 6 times longer than distal height, with low protuberances and tufts of setae on ventral margin; ultimate segment 0.8 times the length of carpus, 6 times

longer than greatest height, with numerous stiff setae, exopod well developed, reaching 0.6 times the length of ischiomeral segment.

First pereopod (Fig. 4A) moderately slender, reaching beyond scaphocerite by entire chela and 10% of carpus; chela (Fig. 4D) 5 times longer than width, fingers 1.1 times longer than palm, terminating in small, curved claws; cutting edge smooth; palm subcylindrical, with setae ventrally; carpus 1.6 times longer than chela, 16.3 times longer than wide; merus about 0.8 times as long as carpus, ischium about 0.6 times the length of merus.

Second pereopod (Fig. 4B) symmetrically equal, overreaching distal margin of scaphocerite by length of chela and carpus; chela slender, 6.3 times as long as the greatest width. Surface of dactylus (Fig. 4E) with a few regularly arranged setae; dactylus slender, 2 times the length of palm, terminating in a small curved claw; cutting edge thin; fixed finger with one row of short setae rising from edge subequally spaced, cutting edge thin and smooth; dactylus longer than fixed finger, with tips crossing when closed; fingers not gaping when closed; palm subcylindrical, 2.2 times as long as maximal height, swollen with ventral margin convex. Carpus slightly widened distally, 0.5 times the chela length, 1.5 times the palm length, subequal in length to merus, smooth, without setae on surface, present also on merus and ischium; merus shorter and wider, nearly as long as carpus; ischium 0.9 times the length of merus.

Third pereopod (Fig. 4C) reaching beyond scaphocerite by 30% the length of propodus; dactylus (Fig. 4F) 0.3 times the propodus length, 6.1 times longer than proximal width, slightly curved, ending with small unguis, lateral surface of dactylus with four tufts of short setae and several single setae along dorsal margin; propodus 1.7 times carpus length, 16 times longer than distal width, with one row of short setae on dorsal margin, present also on ventral margin; carpus 0.5 times of merus length, smooth on dorsal margin; ventral margin of merus and ischium with few short setae.

Fourth and fifth pereopods missing.

Endopod (Fig. 4G) of first pleopod about 0.4 times of exopod length, weakly broadened distally, somewhat curved medially, margins fringed with setae and low protuberances; appendix masculina (Fig. 4H) of second pleopod longer than appendix interna, with numerous spiniform bristles on dorsal margin. Appendix interna exceeding 0.7 times of appendix masculina.

Exopod (Fig. 3A) of uropod overreaching tip of telson by 0.3 times of length, lateral margin straight, ending by small acute tooth; endopod slightly shorter than exopod.

DESCRIPTION OF ALLOTYPE (IZCAS-DE-007) FEMALE

Rostrum 0.6 times carapace length, dorsal margin armed with seven or eight teeth, including three or four on carapace posterior to level of orbital margin; ventral margin with four or five teeth. Second pereopod symmetrical; similar in structure with male; dactylus 1.7 times longer than palm; chela 1.7 times longer than carpus; palm shorter than carpus; merus 1.1 times longer than carpus.

DISTRIBUTION

So far, only known from the type locality.

ETYMOLOGY

The species name *elegantum* alludes to its beautiful body shape. It is an adjective agreeing in gender with the (neuter) generic name.

REMARKS

The genus *Macrobrachium* Bate, 1868, is the most diverse genus of freshwater palaemonid shrimps in China (Liu et al., 1990). Most species are found in surface waters, but two occur in caves. The stygobiotic species can be easily distinguished from others by their highly reduced eyes with unpigmented corneas and the absence of eyestalk. The new species is closely related to *M. lingyunense* Li et al. (2006). Both share similar characters in the second pereopod, including smooth surfaces on the segments and a subcylindrical palm. The new species differs from *M. lingyunense* in the following combination of characters: The rostrum reaches beyond the distal margin of the scaphocerite, 0.7 times the carapace length, while in *M. lingyunense* the rostrum reaches just slightly beyond the distal margin of the scaphocerite, 0.5 times the carapace length. The rostrum is straight, with bifurcate tip, while that of *M. lingyunense* is directed forward. The rostrum formula is 3-4+4/4-6, but 3-4+4-5/3-4 in *M. lingyunense*. The palm of the second pereopod is much more inflated than that of congener. The fingers are about twice as long as the palm, the dactylus is longer than fixed finger, and they cross when fingers are closed, with no gaping or tooth, but in *M. lingyunense* the fingers are about 1.5 times longer than the palm, and the cutting edge of dactylus has a small transparent proximal tooth. The chela is 0.5 times the carpus length and 1.5 times the palm length, and the merus is wider, nearly as long as the carpus, while in *M. lingyunense* the chela is 1.9 to 2.1 times longer than the carpus, the palm is shorter than the carpus, and the latter is subequal in length to the merus. And the inferior orbital lobe is subtriangular, which is typical for the genus, while being poorly developed and hardly recognizable in *M. lingyunense*.

ACKNOWLEDGEMENTS

The manuscript benefited greatly from comments by Malcolm S. Field (U. S. Environmental Protection Agency, National Center for Environmental Assessment–Washington Office, Washington, DC), John E. Cooper (North Carolina State Museum of Natural Sciences, USA) and one anonymous reviewer. This study was supported by the National Natural Sciences Foundation of China (NSFC-

30499341/30670239/30870271/30770268/30870473), by the National Science Fund for Fostering Talents in Basic Research (Special Subjects in Animal Taxonomy, NSFC-J0630964/J0109), by the Knowledge Innovation Program of the Chinese Academy of Sciences (KSCX2-YW-Z-008/KSCX3-IOZ-0811), by the Ministry of Science and Technology of the People's Republic of China (MOST grant no. 2006FY120100/2006FY110500), and also partly by the Beijing Natural Science Foundation (5082013).

References

Bate, C.S., 1868, On a new genus, with four new species of freshwater prawns, *in* Proceedings of the Zoological Society of London, v. 1868, p. 363–368, pls. 30, 31.

Cai, Y.X., 1995, A new troglobitic shrimp from China: Acta Zootaxonomica Sinica, v. 20, no. 2, p. 157–160.

Cai, Y.X., and Li, S.Q., 1997, *Caridina demenica*, a new species of troglobitic shrimp (Crustacea: Decapoda: Atyidae) from Guizhou, China: The Raffles Bulletin of Zoology, v. 45, no. 2, p. 315–318.

Cai, Y.X., and Liang, X.Q., 1999, Descriptions of three new species of freshwater shrimps (Crustacea: Decapoda: Atyidae) from Yunnan, Southern China: The Raffles Bulletin of Zoology, v. 47, no. 1, p. 73–80.

Eberhard, S., Leys, R., and Adams, M., 2005, Conservation of subterranean biodiversity in Western Australia: Using molecular genetics to define spatial and temporal relationships in two species of cave-dwelling Ampipoda: Subterranean Biology, v. 3, p. 13–27.

Espinasa, L., and Vuong, N.H., 2008, A new species of cave adapted nicoletiid (Zygentoma: Insecta) from Sistema Huautla, Oaxaca, Mexico: The tenth deepest cave in the world: Journal of Cave and Karst Studies, v. 70, no. 2, p. 73–77.

Guo, Z.L., Choy, S.C., and Gui, Q.M., 1996, *Caridina semiblepsia*, a new species of troglonic shrimp (Crustacea, Decapoda, Atyidae) from Hunan Province, China: The Raffles Bulletin of Zoology, v. 44, no. 1, p. 1–10.

Guo, Z.L., Jiang, H., and Zhang, M.S., 1992, A new species of *Caridina* from Hunan, China (Decapoda, Atyidae): Sichuan Journal of Zoology, v. 11, no. 2, p. 4–6.

Komai, T., and Fujita, Y., 2005, A new stygiobiont species of *Macrobrachium* (Crustacea: Decapoda: Caridea: Palaemonidae) from an anchialine cave on Miyako Island, Ryukyu Islands: Zootaxa, v. 1021, p. 13–27.

Li, D.H., 2007, Cave animals from karst region of Guizhou Province, Beijing, Geological Publishing House, 190 p.

Li, J.C., Cai, Y.X., and Clarke, A., 2006, A new species of troglobitic freshwater prawn of the genus *Macrobrachium* from Southern China (Crustacea: Decapoda: Palaemonidae): The Raffles Bulletin of Zoology, v. 54, no. 2, p. 277–282.

Li, W.X., and Luo, Z.F., 2001, A new troglobitic shrimp from Guangxi: Journal of Guangxi Normal University, v. 19, no. 2, p. 72–74.

Liang, X.Q., 1993, Two new species of *Caridina* from Guizhou, China: Acta Zootaxonomica Sinica, v. 18, no. 1, p. 22–26.

Liang, X.Q., 2004, Fauna Sinica, Invertebrata, Crustacea, Decapoda, Atyidae, Beijing, Science Press, 375 p.

Liang, X.Q., Chen, H.M., and Li, W.X., 2005, Three new species of atyid shrimps (Decapoda, Caridea) from caves of Guizhou, China: Acta Zootaxonomica Sinica, v. 30, no. 3, p. 529–534.

Liang, X.Q., and Yan, S.L., 1981, A new genus and two new species of freshwater prawns (Crustacea, Decapoda) from Guangxi, China: Acta Zootaxonomica Sinica, v. 6, no. 10, p. 1–21.

Liang, X.Q., and Yan, S.L., 1985, Study on *Caridina* (Decapoda, Caridea) from Yunnan, China: Oceanologia and Limnologia Sinica, v. 16, no. 2, p. 164–174.

Liang, X.Q., and Zhou, J., 1993, Study on new atyid shrimps (Decapoda, Caridea) from Guangxi, China: Acta Hydrobiologia Sinica, v. 17, no. 3, p. 231–239.

Liu, R.Y., Liang, X.Q., and Yan, S.L., 1990, A study of the Palaemoninae (Crustacea, Decapoda) From China I. *Macrobrachium*, *Leander* and *Leandrites*: Transactions of the Chinese Crustacean Society II, p. 102–134.

Wowor, D., Muthu, V., Meier, R., Balke, M., Cai, Y.X., and Ng, P.K.L., 2009, Evolution of life history traits in Asian freshwater prawns of the genus *Macrobrachium* (Crustacea: Decapoda: Palaemonidae) based on multilocus molecular phylogenetic analysis: Molecular Phylogenetics and Evolution, v. 52, no. 2, p. 340–350.

C. Denizman, E.C. Brevik, and J. Doolittle – Ground-penetrating radar investigation of a rapidly developed small island in a lake in southern Georgia, USA. *Journal of Cave and Karst Studies,* v. 72, no. 2, p. 94–99. DOI: 10.4311/jcks2008es0060

GROUND-PENETRATING RADAR INVESTIGATION OF A RAPIDLY DEVELOPED SMALL ISLAND IN A LAKE IN SOUTHERN GEORGIA, USA

CAN DENIZMAN[1], ERIC C. BREVIK[2*], AND JIM DOOLITTLE[3]

Abstract: Collapse sinkholes commonly form in karstic limestones of the Floridan aquifer of southern Georgia, USA. The limestones are capped by impermeable strata that can obscure developing sub-surface voids and catastrophically collapse when too much of their underlying support has been removed. We investigated the overnight appearance of an island in a Georgian lake and its possible relationship to the underlying Floridan aquifer using ground-penetrating radar and global-positioning-satellite spot elevations. The island is adjacent to a submerged sinkhole with an arcuate depression and whose development included convergent downward slumping. Compression created by the convergence probably squeezed lake-bottom sediments upward to form the unusual island. Our methodology can be applied to other lakes in karst regions and may prove useful for diagnosing existing or future subsidence risks.

INTRODUCTION

On the morning of October 13, 2006, residents of a small private lake in southern Georgia near the city of Valdosta woke up to discover a new addition to their lake: a small, newly emergent island. Figure 1 shows the mass of earthen materials that emerged from the lake bottom and formed this strange phenomenon. The lake's residents wanted to know what had led to the formation of this island and what it might mean for the future of their lake.

GEOLOGIC SETTING

The Valdosta region in southern Georgia is characterized by karst. Karst in southern Georgia and Florida has developed in a relatively stable tectonic setting and is covered by either thick, impermeable siliciclastics or thin layers of Pleistocene deposits. Unlike tectonically deformed, uplifted, bare karst of many temperate regions such as the Mediterranean, where almost all the drainage takes place underground, or tropical karst with positive features surrounded by doline fields, the karst in southern Georgia displays a gently rolling topography with few, widely spaced, usually shallow depressions. However, this gentle topographic relief and relatively low depression density represent a muted surficial expression of a much denser doline network that is covered by at least several meters of soil material or as much as hundreds of meters of impermeable confining layers (Huddlestun, 1997; Denizman, 1998).

Sinkholes (dolines) are the signature landform in the temperate karst of southern Georgia and Florida. Karst development is active, and modern sinkhole formation is reported frequently, especially during prolonged drought conditions or after heavy rainfall. In some cases, accumulation of low-permeability material within depressions restricts the infiltration of water and results in the formation of ponds and lakes. These materials and processes may retard sinkhole development. Many of the lakes in Florida and southern Georgia occupy basins formed within karstic depressions lined by impermeable material.

Kindinger et al. (1999) describe lake development in sinkhole basins as occurring due to one of two processes, dissolution of underlying limestone or the collapse, subsidence, or slumping of overburden. They then divide the lakes into four geomorphic types based on progressive developmental phases: active, transitional, mature, and polje. Formation of sinkhole-related lakes is controlled by the extent of karst development in the host limestone rock and by the thickness of the overburden or confining unit. Initially, a collapse sinkhole may be open or water-filled depending on the potentiometric level. Later, the sinkhole may be plugged by sediments that have washed into the depression. This process continues until the sinkhole is buried.

HYDROGEOLOGIC SETTING

The Floridan aquifer, one of the most productive karst aquifers of the world, is the principal aquifer in southern Georgia. It consists of a thick sequence of Tertiary carbonate rocks. Because of the relatively high primary porosity coupled with extensive karstic dissolution conduits within the carbonate rocks of the Floridan aquifer, groundwater storage and flow take place through a complex system of intergranular openings and cavities.

Disclaimer: Trade names or commercial products are given solely for the purpose of providing information on the exact equipment used in this study and do not imply recommendation or endorsement by Valdosta State University, Dickinson State University, or the USDA.

* corresponding author
[1] Department of Physics, Astronomy, and Geosciences, Valdosta State University, Valdosta, GA 31698, cdenizma@valdosta.edu
[2] Departments of Natural Sciences and Agriculture and Technical Studies, Dickinson State University, Dickinson, ND 58601, Eric.Brevik@dsu.nodak.edu
[3] USDA-NRCS-NSSC, 11 Campus Boulevard, Suite 200, Newtown Square, PA 19073, jim.doolittle@lin.usda.gov

Figure 1. The island seen in this photograph emerged overnight from a southern Georgia lake on October 13, 2006. The boat in the foreground gives a scale for the above-water size of the feature. All of the materials observed in the emergent island were unconsolidated.

Both diffuse and conduit groundwater flows occur. Most of the cave systems that facilitate conduit groundwater flow are reported to have formed at the contact between the Floridan aquifer and the overlying confining units of the Hawthorn Group (Denizman, 1998).

The siliciclastic rocks of the Hawthorn Group, along with the younger overlying, unconsolidated, impermeable units, create confined conditions throughout much of the area. However, there are numerous places where the confining units are breached by sinkholes. Recharge to the Floridan aquifer is provided by slow leakage through the confining units or by point recharge through collapse depressions that breach the overlying confining unit.

Use of GPR in Karst Settings and Lakes

Ground-penetrating radar (GPR) measures the time it takes for a shortwave electromagnetic pulse to travel from a radar antenna to a subsurface interface and back to the antenna after being reflected off the interface. The greater the contrast in the electrical properties of the materials at the interface, the stronger the reflected pulses will be. High-conductivity materials lead to greater attenuation of radar energy than low-conductivity materials, and therefore, higher conductivity materials lead to shallower effective exploration depths with GPR. Typical effective exploration depths are a few meters, but can be greater than 30 meters if the geologic setting is favorable (i.e., sediments with primarily low conductivity such as dry sands) (Barr, 1993).

GPR tends to work well in southern Georgia because the surficial sediments are principally sands (Truman et al, 1994), which have a low conductivity (Barr, 1993). These sands may overlie clays, which have a higher conductivity than sands, or limestone, which has a similar or lower conductivity than sands (Barr, 1993). In general, the conductivity of these earthen materials is not high enough to cause significant attenuation of the radar energy and restrict penetration depths.

In southern Georgia, contrasting layers of sands, clays, and limestone are often separated by abrupt boundaries or interfaces. The amount of energy that is reflected back to a radar antenna by an interface is dependent upon the contrast in the relative dielectric permittivity (E_r) of the two layers. Abrupt boundaries that separate contrasting materials reflect more energy than gradual boundaries that separate materials with similar E_r. The E_r of soil materials is principally dependent upon moisture content (Annan et al., 1991) and varies with temperature (phase-dependent), density, and antenna frequency (Daniels, 2004).

Because of these favorable electromagnetic properties, GPR has been used extensively in southern Georgia and Florida to map soil features, such as depth and spatial variability of argillic horizons and depth to parent material, water features, such as wetting fronts and water table depths (Truman et al., 1994; Barr, 1993), and geologic features, such as sediment thicknesses, depths to clay beds, and subsurface karst development (Kruse et al., 2006; Wilson, 1995; Collins et al., 1994; Barr, 1993).

GPR has also been used to investigate lakes and reservoirs. Truman et al. (1991) used GPR to map the depth of a reservoir in west-central Georgia, relying on differences in the relative dielectric permittivity of water versus lake-bottom sediments to provide strong and easily recognized reflections. When compared to control measurements, water depths interpreted from radar records showed a strong linear relationship with an R^2 value of 0.989. Barr (1993) used GPR to investigate the hydrogeology of freshwater lakes in Florida, including disturbance of lake-bottom sediments. Other examples of the use of GPR to map freshwater bottom topography and sediments include Buynevich and Fitzgerald (2003), Moorman (2001), Moorman and Michel (1997), Mellett (1995), Sellmann et al. (1992), Izbicki and Parker (1991), Kovacs (1991), and Haeni et al. (1987).

Because southern Georgia is in an active karst zone with fairly shallow limestone bedrock under primarily marine deposits, a karst explanation was deemed most likely in the case of this mysterious island. The past successes using GPR to investigate karst features in the southeastern United States and in freshwater bodies led to the use of GPR as the primary means of investigating this particular unusual geologic occurrence.

Materials and Methods

Survey Equipment and Procedures

The radar unit used was the TerraSIRch Subsurface Interface Radar System-3000, manufactured by Geophysical Survey Systems, Inc. of Salem, New Hampshire (GSSI). The SIR System-3000 weighs about 4.1 kg and is

backpack-portable. A 70-MHz antenna was used in this survey. Within the study lake, the 70-MHz antenna provided adequate depth (greater than 10 m) and acceptable resolution of subsurface features.

Radar records contained in this report were processed with the RADAN for Windows version 5.0 software program developed by GSSI. Processing included setting the initial pulse to time zero, color transformation, header and marker editing, distance normalization, horizontal stacking, migration, filtration, and range gain adjustments (Daniels, 2004).

An Allegro CE field computer (Juniper Systems, North Logan, Utah) and a Garmin Global Positioning System Map 76 receiver (with a CSI Radio Beacon receiver, antenna, and accessories that are fitted into a backpack) (Garmin International, Inc., Olathe, Kansas) were used to record the coordinates of each reference station that was impressed on the radar record. SURFER 8.0 (Golden Software Inc., Golden, Colorado) was used to construct the images of the estimated depths to bottom sediments displayed in this paper.

The radar system and 70-MHz antenna were mounted in a fiberglass boat that was towed behind a pontoon boat. GPR surveys were restricted to the portion of the lake near the island. The island was closely approached, but emerged areas were not surveyed. The boats made eleven traverses across the area, each of different lengths. Locations of traverse lines were arbitrary and were adjusted using identifiable features on the shore and island. Reference points for both GPS and GPR were recorded simultaneously at intervals of 30 seconds.

CALIBRATION OF GPR

Ground-penetrating radar is a time-scaled system. This system measures the time that it takes electromagnetic energy to travel from an antenna to an interface (e.g., soil horizon, top of bedrock, stratigraphic layer) and back. To convert the travel time into a depth scale, either the velocity of pulse propagation or the depth to a reflector must be known. The relationships among depth (D), two-way pulse travel time (T), and velocity of propagation (v) are described in the equation (Daniels, 2004)

$$v = \frac{2D}{T}. \quad (1)$$

The velocity of propagation is principally affected by the E_r of the profiled material(s) according to the equation

$$E_r = \left(\frac{C}{v}\right)^2, \quad (2)$$

where C is the speed of light in vacuum. For water, the E_r is 80 and the v is 0.033 m ns^{-1}. These parameters were used to scale the thickness of the water column or the depth to bottom sediments on the radar records.

With the 70-MHz antenna the lake-bottom sediments were penetrated. Variations in sediments are distinguishable on radar records. However, the compositions and dielectric properties of these layers are unknown. As no borings were made through these sediments, the identity of these layers cannot be verified, nor can their thicknesses be accurately estimated. A constant-depth scale has been used on the accompanying radar records. This scale is based on the dielectric permittivity (80) and pulse propagation velocity (0.033 m ns^{-1}) of fresh water. While the thickness of the water column is accurately portrayed in the accompanying radar records, the scale is inaccurate within the bottom sediments and underlying layers, which, because of lower water contents, should have lower dielectric permittivities and faster pulse propagation velocities.

INVESTIGATION OF ISLAND SEDIMENTS

Eight samples of known volume were collected from the island, and a core was collected to a depth of about 1.5 m. The samples of known volume were analyzed for bulk density by drying the samples for 24 hours at 105 °C. Organic-matter content was determined for these samples using the loss-on-ignition method at 550 °C (Heiri et al., 2001; Dean, 1974). These measurements were done for comparison to other local lake-bottom sediments studied by Leandro et al. (2005).

RESULTS

Radar records were of excellent interpretive quality. Figure 2 is a portion of the radar record from traverse line 6 (see Figure 4 for location). The emergent island was approached closely along this transverse, but was not crossed. This traverse line crosses the impacted area in an east-northeast to west-southwest direction. Although the radar provides a continuous profile of the lake, measurements of the water depth were restricted to reference points (numbered white, vertical lines at the top of the radar record). These lines were impressed on the radar record by the operator at a time interval of about 30 seconds. In Figure 2, the emergent island is most closely approached between reference marks 5 and 6.

In Figure 2, the horizontal, high-amplitude (colored white and grey) reflector at the top of the radar record represents the reflection from the lake's surface. Below the surface reflection, the first series of high-amplitude reflections represents the lake bottom (see point A). On this portion of the radar record, this interface varies in depth from about 1.78 to 7.64 m. Between horizontal reference marks 5 and 6, reflections from this interface are noticeably mixed, lower in signal amplitude (colored red, yellow, and blue), segmented, and dipping towards the northeast and away from a deep sinkhole that is evident between reference marks 6 to 8. Lines have been

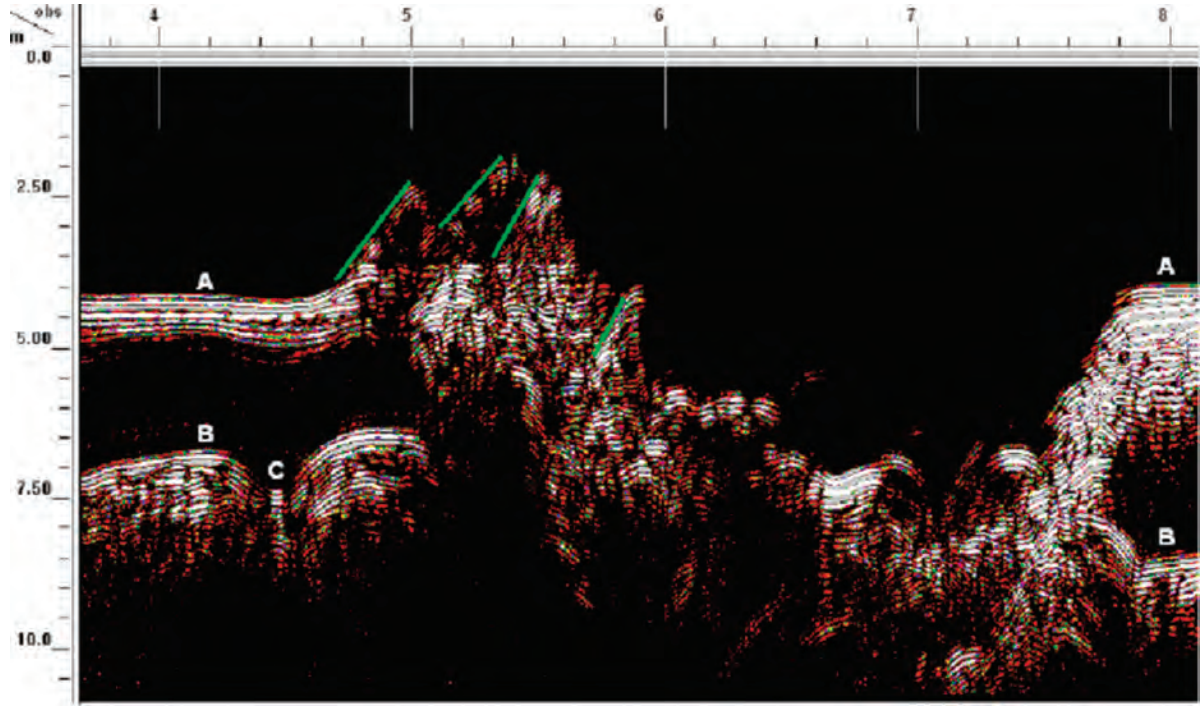

Figure 2. A deep sinkhole and shoved, elevated lake-floor sediments are evident in this portion of the GPR record from traverse line 6. This traverse line crosses the study area in an east-northeast (left side) to west-southwest (right side) direction. A sinkhole can be seen roughly between reference marks 6 and 8. The lake bottom is shown by reflections at point A, the reflection at point B is suspected to represent the top of the local limestone bedrock. A small depression in the surface is indicated at point C.

drawn between reference marks 5 and 6 to draw attention to the downward-dipping reflections from layers of former sub-bottom sediments that have been moved upwards along the eastern rim of the sinkhole. A sharp drop-off is evident near reference mark 8. Here, downward-bending bands of reflectors suggest the collapse of sediments into the sinkhole. Though not verified, it is suspected that the high-amplitude planar reflector at point B represents the upper boundary of the underlying limestone bedrock. If so, a potential cavity in this surface is suggested at point C. The black zone between the depths of about 5 m and 7 m most likely represents fairly uniform lake bottom materials.

Figure 3 is a portion of the radar record from traverse line 11 (see Fig. 4 for location). This traverse line crosses to the west of the emergent island and across the sinkhole from north-northwest to south-southeast. This traverse line is essentially orthogonal to traverse line 6 (shown in Fig. 2). In Figure 3, the emergent island is most closely approached between reference marks 6 and 8. The horizontal, high-amplitude reflector at the top of the radar record represents the reflection from the lake's surface. Below the surface reflection, the first series of high-amplitude reflections represents the lake bottom (see point A). On this portion of the radar record, this interface is essentially horizontal on either side of the sinkhole, but is slightly lower (about 4.05 to 4.10 m below the lake surface) on the left-side (north-northwest) and slightly higher (about 3.9 m below the lake surface) on the right-side (south-southeast). Two conspicuous, high-amplitude, planar subsurface reflectors (see points B and C) separate distinct sub-bottom sedimentary or lithologic facies. Methods of GPR facies analysis are described for unconsolidated sediments by Beres and Haeni (1991). The reflections near the 10-m depth mark along the left side (north-northwest) likely represent limestone bedrock, but this was not confirmed.

Downward-bending bands of reflectors suggest local rotations and slump folding during the collapse of sediments into the sinkhole on its south-southeastern (right-hand) side (Fig. 3). On the north-northwestern (left-hand) side of the sinkhole, near reference mark 4, down-turned bands of reflectors are less evident, and the abrupt truncation of reflectors suggests a much sharper break. Both sides of the sinkhole show layer slumping, with dips toward the center of the sinkhole.

The depths to bottom sediments were calculated using GPR at 169 points, and GPS was used determine locations for the points. The average depth to bottom sediments within the survey area is 3.96 m with a range of 1.09 m to 6.96 m. At one half of the reference points, depths to bottom sediments were between 3.77 m and 4.21 m. While these statistics are useful, a two-dimensional plot of these depth estimates would provide a more coherent picture of

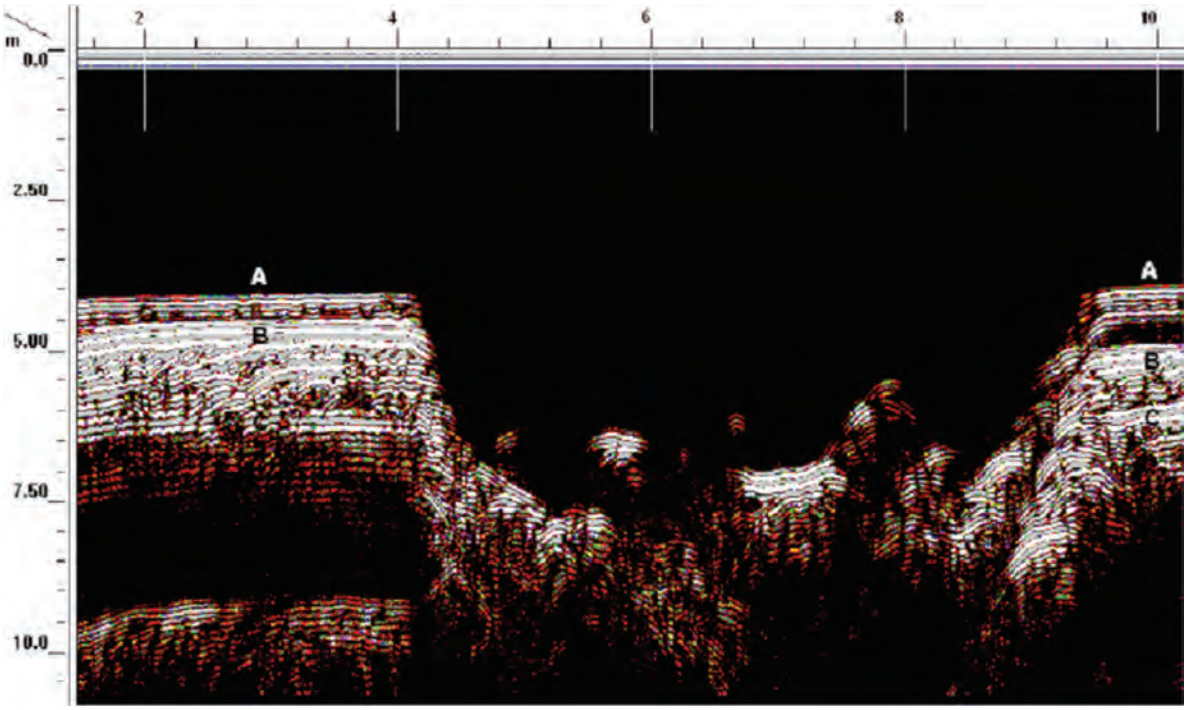

Figure 3. A portion of the radar record from traverse line 11 showing the crater-like feature and collapsed lake-floor sediments. This traverse line crosses to the west of the emergent island and across the crater-like feature from north-northwest to south-southeast. A sinkhole can be seen roughly between reference marks 4 and 10. The lake bottom is shown by reflections at point A. The reflections at points B and C represent separate distinct, sub-bottom sedimentary and/or lithologic facies. The top of the suspected limestone bedrock is shown at a depth of approximately 8–9 m on the left side of the figure.

the emergent island area. Figure 4 shows a two-dimensional contour map of the lake bottom with a contour interval of 50 cm. Portions of the island that emerge from the lake are labeled A. It must be emphasized that data used to prepare Figure 4 were collected only in areas that the boats could reach. No measurements were collected on the emergent island because the sediments were too soft to allow surveying, so the elevations of the emergent portions of the island are estimated.

The eight sediment samples collected from the island had a very low bulk density (average 0.20 g cm^{-3}, standard deviation 0.08 g cm^{-3}) and high organic matter content (average 49%, standard deviation 9.3%). The core sample had a uniform appearance throughout its length. No lithified materials were noted in the island materials. These results are consistent with the composition and bulk density of lake-bottom sediments from other nearby lakes (Leandro et al., 2005).

DISCUSSION AND CONCLUSION

Cover-collapse and cover-subsidence sinkholes are common surficial karst features in temperate karst regions with thick overburden material. Most of the ponds and even some large lakes in Florida and south Georgia are formed by sinkhole-related collapse. Many of them develop in response to subsurface karst development and subsequent collapse of the overburden. However, island formation has never been reported to occur along with these depression processes.

The mysterious island that formed overnight in a Georgia lake is an unusual result of a sinkhole collapse within the highly karstic carbonates underlying the lake bottom. Steep walls of the apparently new sinkhole indicate a sudden collapse of a bedrock cavity around reference mark 8 and upward movement of lake bottom and cavity sediments between reference marks 5 and 6. We propose this unusual feature is composed of lake sediments that were probably scraped off the lake bottom and squeezed upward as they underwent convergent downward slumping into an apparently arcuate-shaped sinkhole throat. Displaced water may have also played a role. As the collapse occurred, enough sediment and rock may have dropped into the collapse to displace a significant amount of water upward. This displaced water may have then ''rafted'' the sediments that compose the emergent island upward into an angled position.

Using the classification of Kindinger et al. (1999), this lake would classify as a lake that developed due to the collapse or subsidence of overburden to form a sinkhole. It is most likely in the transitional development phase. Given that the lake is already present, it is too advanced to be in the active phase, but the creation of the island indicates that karstification is still active in this system.

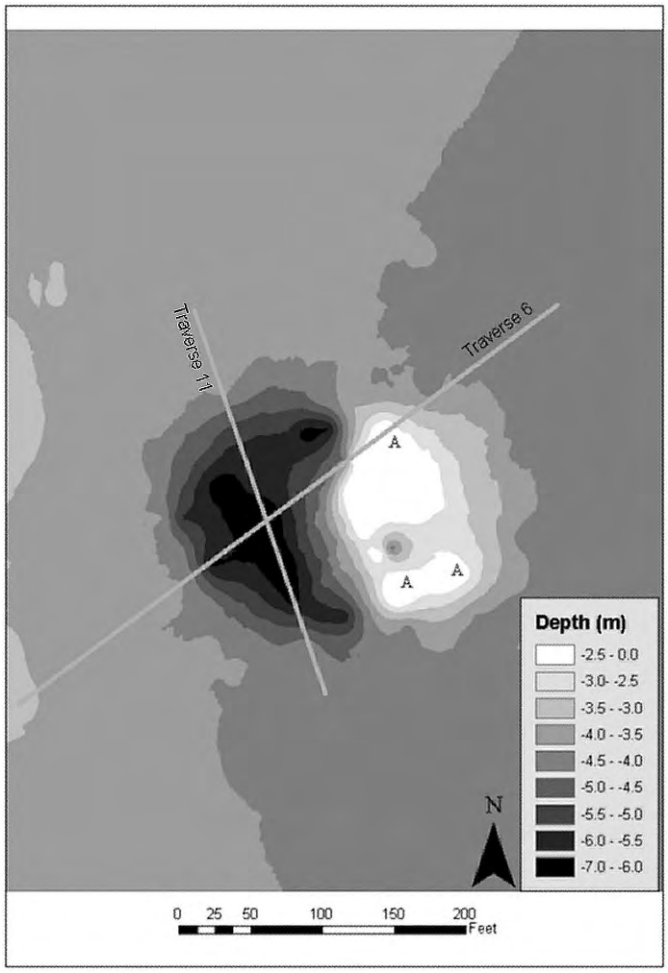

Figure 4. The locations of emergent land are denoted by the letter A in this two-dimensional contour map of the lake-bottom depths in the study area. The locations of the segments of the radar records shown in Figures 2 (Traverse 6) and 3 (Traverse 11) are also indicated.

REFERENCES

Annan, A.P., Cosway, S.W., and Redman, J.D., 1991, Water table detection with ground penetrating radar: Tulsa, Oklahoma, Society of Exploration Geophysicists, Expanded Abstracts 61st Annual Meeting, v. 1, p. 494–495.

Barr, G.L., 1993, Application of ground-penetrating radar methods in determining hydrogeologic conditions in a karst area, west-central Florida: U.S. Geological Survey Water-Resources Investigations Report 92-4141, 26 p.

Beres, M., and Haeni, F.P., 1991, Application of ground-penetrating radar methods in hydrogeologic studies: Ground Water, v. 29, p. 375–386.

Buynevich, I.V., and Fitzgerald, D.M., 2003, High-resolution subsurface (GPR) imaging and sedimentology of coastal ponds, Maine, USA: implications for Holocene back-barrier evolution: Journal of Sedimentary Research, v. 73, no. 4, p. 559–571.

Collins, M.E., Cum, M., and Hanninen, P., 1994, Using ground-penetrating radar to investigate a subsurface karst landscape in north-central Florida: Geoderma, v. 61, p. 1–15.

Daniels, D.J., 2004, Ground penetrating radar, 2nd edition, London, The Institute of Electrical Engineers, 760 p.

Dean, W.E., 1974, Determination of carbonate and organic matter in calcareous sediments and sedimentary rocks by loss on ignition: comparison with other methods: Journal of Sedimentary Petrology, v. 44, no. 1, p. 242–248.

Denizman, C., 1998, Evolution of karst in the lower Suwannee River basin, Florida [Ph.D. thesis]: Gainesville, Fla., University of Florida, 214 p.

Haeni, F.P., McKeegan, D.K., and Capron, D.R., 1987, Ground-penetrating radar study of the thickness and extent of sediments beneath Silver Lake, Berlin and Meriden, Connecticut: US Geological Survey Water-Resources Investigation Report 85-4108, 19 p.

Heiri, O., Lotter, A.F., and Lemcke, G., 2001, Loss on ignition as a method for estimating organic and carbonate content in sediments: reproducibility and comparability of results: Journal of Paleolimnology, v. 25, p. 101–110.

Huddlestun, P.F., 1997, Geologic atlas of the Valdosta area: Atlanta, Georgia Geologic Survey Geologic Atlas 10, 27 p.

Izbicki, J.A., and Parker, G.W., 1991, Water depth and thickness of sediment in reservoirs 1 and 2, Framingham and Ashland, Massachusetts: US Geological Survey Open-File Report 91-508, 18 p.

Kindinger, J.L., Davis, J.B., and Flocks, J.G., 1999, Geology and evolution of lakes in north-central Florida: Environmental Geology, v. 38, no. 4, p. 301–321.

Kovacs, A., 1991, Impulse radar bathymetric profiling in weed-infested fresh water: CRREL Report 91-10, 25 p.

Kruse, S., Grasmueck, M., Weiss, M., and Viggiano, D., 2006, Sinkhole structure imaging in covered karst terrain: Geophysical Research Letters, v. 33, L16405 p.

Leandro, A.M., Wall, A., Hyatt, J.A., and Brevik, E.C., 2005, Identifying spatial trends in the physical properties of sediments, Lake Louise, Georgia [abs.]: Geological Society of America Northeastern Section 40th Annual Meeting, Geological Society of America Abstracts with Programs, v. 37, no. 1, 15 p.

Mellett, J.S., 1995, Profiling of ponds and bogs using ground-penetrating radar: Journal of Paleolimnology, v. 14, p. 233–240.

Moorman, B.J., 2001, Ground-penetrating radar applications in paleolimnology, *in*: Last, W.M., and Smol, J.P., eds., Tracking Environmental Change using Lake Sediments: Physical and Chemical Techniques: Dordrecht, The Netherlands, Kluwer Academic Publishers, p. 1–25.

Moorman, B.J., and Michel, F.A., 1997, Bathymetric mapping and subbottom profiling through lake ice with ground-penetrating radar: Journal of Paleolimnology, v. 18, p. 61–73.

Sellmann, P.V., Delaney, A.J., and Arcone, S.A., 1992, Sub-bottom surveying in lakes with ground-penetrating radar: CRREL Report 92-8.

Truman, C.C., Asmussen, L.E., and Allison, H.D., 1991, Ground-penetrating radar: a tool for mapping reservoirs and lakes: Journal of Soil and Water Conservation, v. 46, no. 5, p. 370–373.

Truman, C.C., Bosch, D.D., Allison, H.D., and Fletcher, R.G., 1994, Uses of ground-penetrating radar in the Georgia Coastal Plain: review of past and current studies: US Department of Agriculture, Agricultural Research Service. ARS-124. 32 p.

Wilson, W.L., 1995, Sinkhole and buried sinkhole densities and new sinkhole frequencies in karst of northwest peninsular Florida, *in*: Beck, B.F., ed., Karst Geohazards: Engineering and Environmental Problems in Karst Terrain: Proceedings of the Fifth Multidisciplinary Conference on Sinkholes and the Engineering and Environmental Impacts of Karst, Gatlinburg, Tennessee, April 2–5: Leiden, The Netherlands, A.A. Balkema, p. 79–91.

J.J. Lewis and T.E. Bowman – The subterranean asellids of Maryland: Description of *Caecidotea nordeni*, new species, and new records of C. holsingeri *and* C. franzi *(Crustacea: Malacostraca: Isopoda). Journal of Cave and Karst Studies,* v. 72, no. 2, p. 100–104. DOI: 10.4311/jcks2009lsc0092

THE SUBTERRANEAN ASELLIDS OF MARYLAND: DESCRIPTION OF *CAECIDOTEA NORDENI*, NEW SPECIES, AND NEW RECORDS OF *C. HOLSINGERI* AND *C. FRANZI* (CRUSTACEA: MALACOSTRACA: ISOPODA)

JULIAN J. LEWIS[1] AND THOMAS E. BOWMAN[2]

Abstract: Five species of subterranean asellid are known from Maryland: *Caecidotea pricei*, *C. franzi*, *C. holsingeri*, *C. mausi* and *C. vandeli*. *Caecidotea nordeni*, n. sp. is a subterranean species described from Washington Co., Maryland and assigned to the *hobbsi* Group. A new locality for *C. franzi* in Kentucky is presented. This species was previously known from two caves in Maryland and Pennsylvania. The newly discovered population represents a range extension of over 400 km. The male pleopod 2 morphology of specimens from a Maryland population of the subterranean asellid *C. holsingeri* is compared with populations from three caves in West Virginia. The range of *C. holsingeri* extends from eastern West Virginia and adjacent Virginia to Garrett Co., Maryland.

INTRODUCTION

This paper is part of a long term project to better understand the systematics of subterranean isopods of the family Asellidae that occur in Maryland. This work started as a collaboration between Dan Feller of the Maryland Department of Natural Resources and Thomas E. Bowman of the Smithsonian Institution. Sadly, Dr. Bowman died before any of their work could come to fruition. I took possession of his materials, and after a long hiatus, the project has started to become productive finally.

My first contribution to the Maryland asellid project was the description of *Caecidotea mausi* Lewis (2009). Four other obligate subterranean species have been recorded from Maryland: *C. pricei* (Levy 1949), *C. franzi* (Holsinger and Steeves, 1971), *C. holsingeri* (Steeves, 1963) and *C. vandeli* (Bresson 1955). Much of what is currently known of the habitat and range of these species was summarized by Lewis (2009). The taxon described below adds a sixth species to Maryland's subterranean asellid fauna.

Another facet of the project was clarification of the ranges of other species already known to occur in Maryland. Few subterranean asellid distribution patterns are well understood due to their cryptic nature and ability to disperse through a variety of groundwater habitats. An example of this is *Caecidotea franzi*, previously known from Pennsylvania and Maryland, but now discovered in Kentucky and extending their range more than 400 km. Considerably less isolated were the isopods from John Friends Cave, Garrett Co., Maryland, identified by Fleming (1972) as *C. holsingeri*. There was some suspicion that the Garrett County population represented an undescribed species. To test that theory, Dr. Bowman compared the male pleopod 2 morphology of the Maryland specimens with other *C. holsingeri* populations in West Virginia. That analysis, as well as mapping the collection sites of *C. holsingeri*, led to elucidation of the range of the species.

FAMILY ASELLIDAE

GENUS *CAECIDOTEA* PACKARD, 1871

CAECIDOTEA NORDENI, NEW SPECIES

FIGS. 1–2, 4

Material Examined: MARYLAND: Washington Co., under rocks in stream, 15.2 km SSE Hancock, 5 Apr 1980, A. Norden, 1♂. The holotype (USNM 337163) is in the collection of the National Museum of Natural History, Smithsonian Institution.

Description of Holotype: Eyeless, unpigmented, 7.8 mm long, body slender, 5× as long as wide. Head 1.5× as wide as long, anterior margin concave, postmandibular lobes slightly produced. Pleotelson slightly longer than wide, sides slightly convex, caudomedial lobe broadly rounded. Mouthparts conforming to diagnosis of genus (Lewis, 2009). Antenna 1 flagellum with 7 articles, distal 3 each bearing a single esthete. Antenna 2 flagellum with 50 articles. Male pereopod 1, propodus about 1.9× as long as wide, palmar margin with large proximal spine, low medial process; dactyl flexor margin with 5 stout spines.

Male pleopod 1 slightly longer than pleopod 2, protopod 1.2× as long as wide, with 2 retinaculae; exopod 1.6× length of protopod, distal margin with 5 elongate plumose setae, lateral margin slightly concave. Pleopod 2, protopod 1.3× as long as wide, elongate plumose seta and short non-plumose seta on mesodistally, 2 short setae distolaterally; exopod, proximal article with 3 short lateral setae (1 plumose), distal article with 8 elongate, plumose

[1] Lewis & Associates, Cave, Karst & Groundwater Biological Consulting LLC, 17903 State Road 60, Borden, IN 47106, lewisbioconsult@aol.com
[2] Curator Emeritus (deceased), National Museum of Natural History, Smithsonian Institution

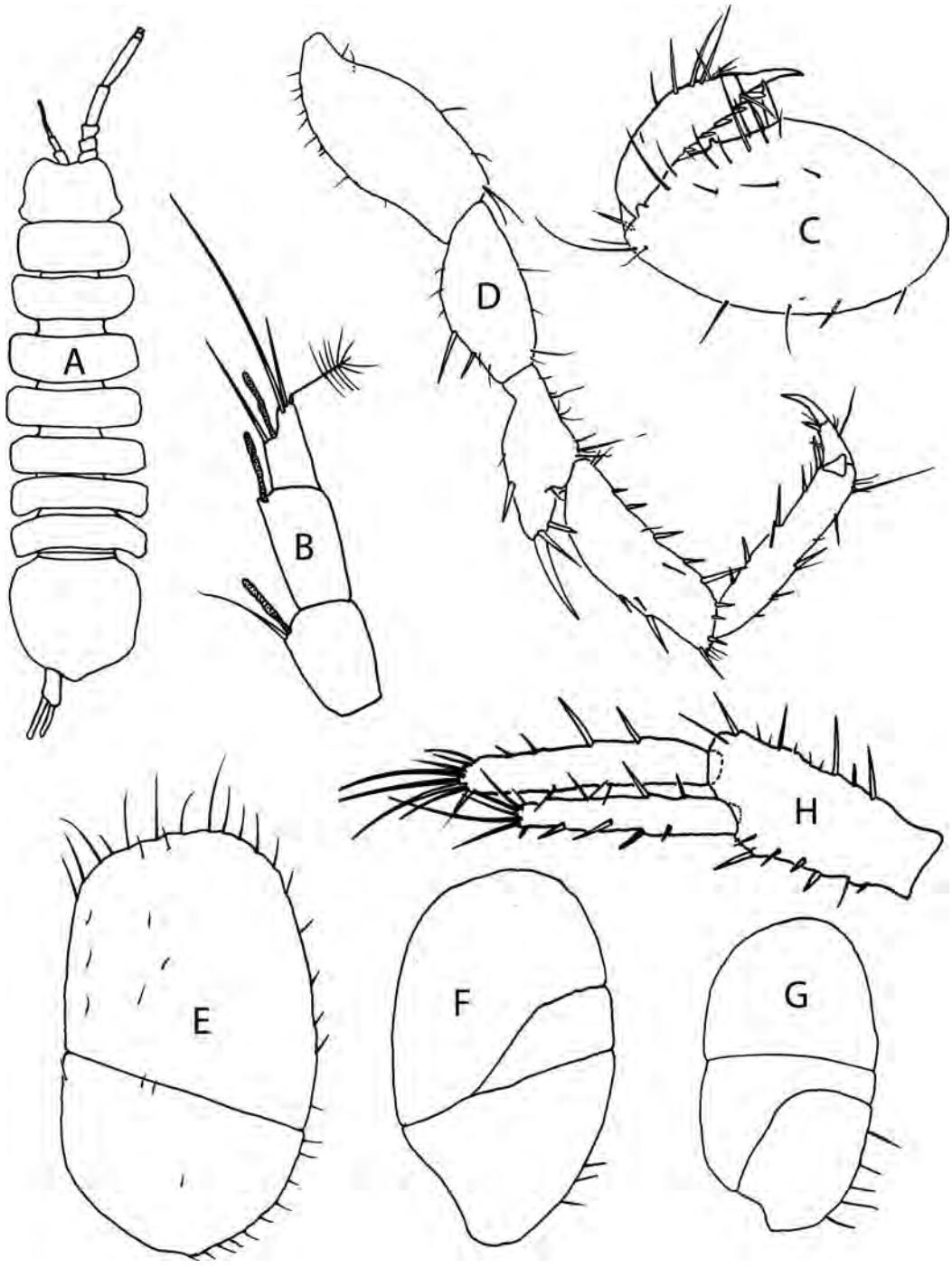

Figure 1. ***Caecidotea nordeni*****, new species: (A) habitus, (B) tip articles, antenna 1, (C) gnathopod, distal articles (D) pereopod 4, (E) pleopod 3 exopod, (F) pleopod 4 exopod, (G) pleopod 5 exopod, (H) uropod.**

setae along margin. Endopod with well developed basal apophysis; tip with short, slightly conical cannula, small scallops laterally, half obscured by broad mesial process in anterior view, caudal process broadly rounded. Pleopod 3 exopod with 18 plumose setae along apical and lateral margin. Pleopod 4 exopod with sigmoid false suture bifurcating mid-length, 3 setae on proximolateral margin. Pleopod 5 with proximal sigmoid false suture, second false sigmoid suture mid-length, 5 setae on proximolateral margin. Uropods 0.67 length of pleotelson, protopod approximately equal in length to endopod, exopod slightly shorter than endopod.

Relationships

Other than lacking large processes on the palmar margin of the pereopod 1 propodus, *C. nordeni* fits the

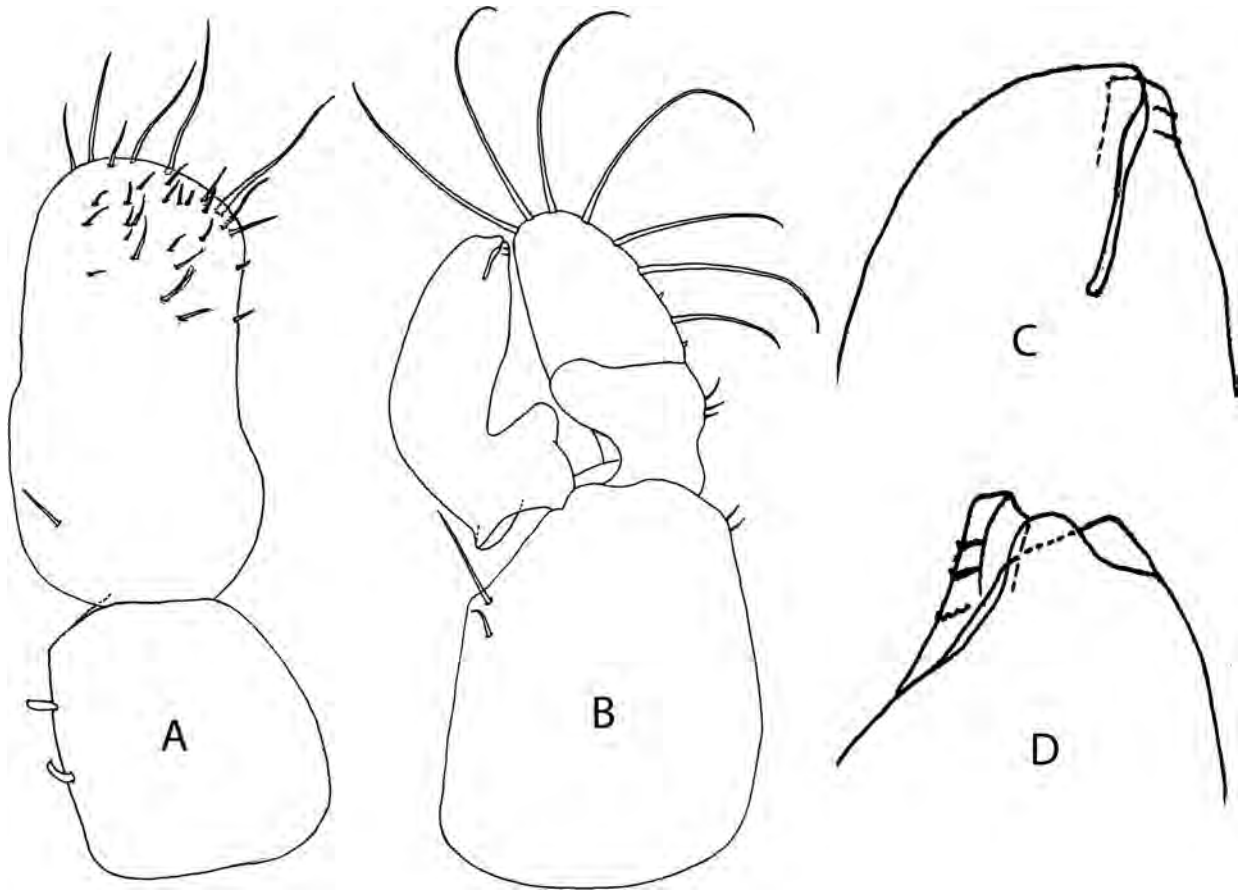

Figure 2. *Caecidotea nordeni*, new species: (A) pleopod 1, (B) pleopod 2, (C) pleopod 2 endopodite tip, anterior, (D) same, posterior.

diagnosis of the *hobbsi* Group (Lewis, 1982). In particular, the male first pleopod exopod with concave lateral margin and elongate plumose setae on the apical margin is quite characteristic of the members of this species group. Likewise, the second pleopod endopodite tip, with a short, blunt cannula partially obstructed from view in the anterior aspect is typical of the *hobbsi* Group. The absence of armature of the pereopod 1 may well be due to the holotype's size, as the processes of the palmar margin usually increase in size with maturity (Bowman and Beckett, 1978). Beyond the placement of *C. nordeni* in the *hobbsi* Group, the species does not bear strong resemblance to any of the other described species.

Etymology

This species is named in honor of the collector, Mr. Arnold Norden. The suggested vernacular name is Norden's groundwater isopod.

Habitat and Range

This subterranean isopod was found in a surface stream, where it presumably had emerged from a groundwater habitat. *Caecidotea nordeni* is known only from the type-locality in Washington Co., Maryland. Franz and Slifer (1971) reported that over half of the 148 caves known in Maryland were located in that county.

CAECIDOTEA FRANZI (HOLSINGER AND STEEVES, 1971)

Material Examined: KENTUCKY: Harlan Co., Sawmill Hollow Cave, 1 km ENE Pine Mountain, James E. Bickford State Nature Preserve, Ellis Laudermilk, 4 Sep 2001, 1♂, 1 ♀; 24 Sep 2001, 1♂, 1 ♀; 1 Oct 2001, 2♂, 1 ♀.

This species was previously described from Millers Cave, Centre Co., Pennsylvania and Crabtree Cave, Garrett Co., Maryland. These caves are approximately 185 km from one another. The appearance of the male gnathopod, pleopod 2 and uropod of the Sawmill Hollow Cave specimens is essentially identical to that illustrated by Holsinger and Steeves (1971). The only significant difference is that the male first pleopod of the Kentucky specimens is not distolaterally produced to the extent shown in the type material. The distal lobes are present in the Sawmill Hollow Cave males and the difference may be a function of curvature of the exopod rather than anatomical.

That the range of *C. franzi* spans 600 km stretches credence. Certainly other subterranean species (e.g., *C. stygia*, *C. kendeighi* and *C. bicrenata*) are found in areas extending as much as 500 km. However, these species are

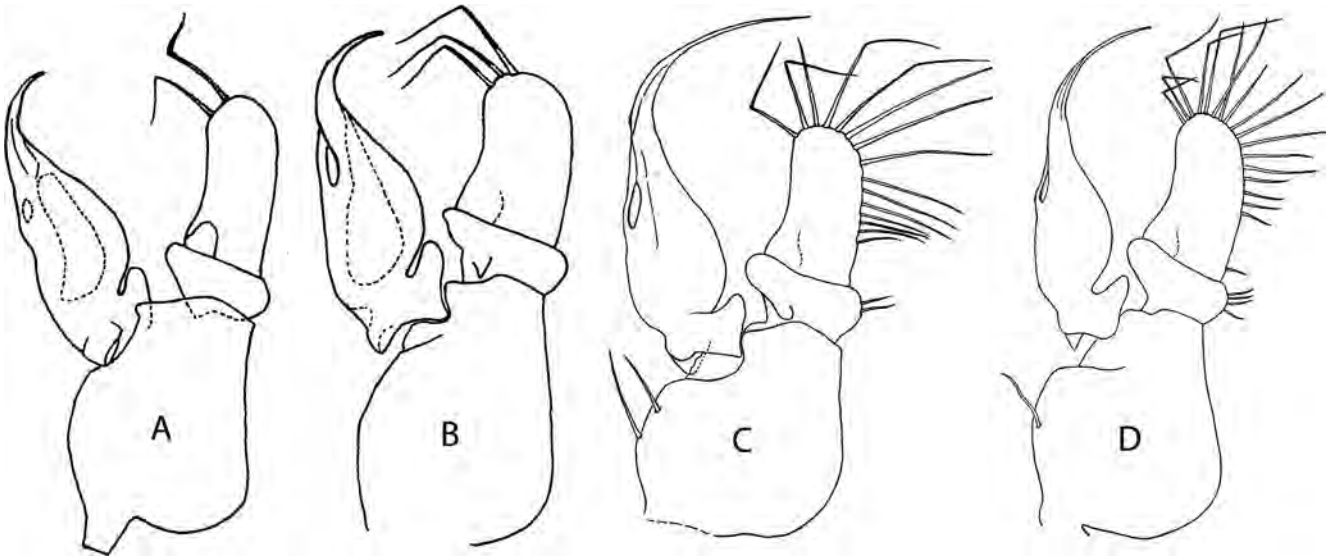

Figure 3. *Caecidotea holsingeri* (Steeves), variation in male pleopod 2: (A) John Friends Cave, Garrett Co., Maryland, (B) Swecker Stream Cave, Pocahontas Co., WV, (C) Piddling Pit Cave, Pocahontas Co., WV, (D) Organ Cave, Greenbrier Co., WV.

recorded from dozens or even hundreds of collection sites across their respective ranges, while *C. franzi* is known from few. The anatomy of specimens examined from the Kentucky population is so similar to the description by Holsinger and Steeves (1971) that despite the distance involved, it is considered intraspecific variation until evidence to the contrary is found.

Caecidotea holsingeri (Steeves, 1963)
Figs. 3–4

Material examined: MARYLAND: Garrett Co., John Friends Cave, 29 Aug 1966, John R. Holsinger, 1♂, 3♀ (USNM 230649); WEST VIRGINIA, Greenbrier Co., Organ Cave, 13 Jul 1987, David Culver, Janine Gibert 8♂♀ (USNM 235213); Pocahontas Co., Piddling Pit Cave, David Culver, Dan Fong, 23 Nov 1990, 3♂♀; Swecker Stream Cave, David Culver, 24 Nov 1990, 3♂♀.

The description by Steeves (1963) was adequate for identification of specimens. Steeves (1969) characterized the range as encompassing eastern West Virginia and the western tip of Maryland. Holsinger and Steeves (1971) added the first Virginia locality. Fleming (1972) and Holsinger et. al (1976) listed 27 caves within that range. Lewis (1980) redescribed *C. holsingeri*, adding details of the morphology and discussing variation. Lewis (2009) added records for Giles and Highland counties, Virginia.

In considering the John Friends Cave population, Thomas Bowman prepared comparative drawings of the male pleopod 2 from three other localities. Other than varying numbers of setae, no significant differences are appreciable. The thread-like cannula terminating the endopodite is fragile and breaks readily, explaining the apparent differences in the length of this structure. A characteristic feature of *C. holsingeri* is the prominent basal apophysis of the male pleopod 2 endopod, which allows the convex lateral edge of the endopod to interlock with the concave exopod (Lewis, 1980, figure 4g).

A plot of the counties in which *C. holsingeri* has been recorded further supports the hypothesis of a single species. This distribution pattern is mirrored by the stygobiont amphipod *Stygobromus emarginatus*. The range map of the

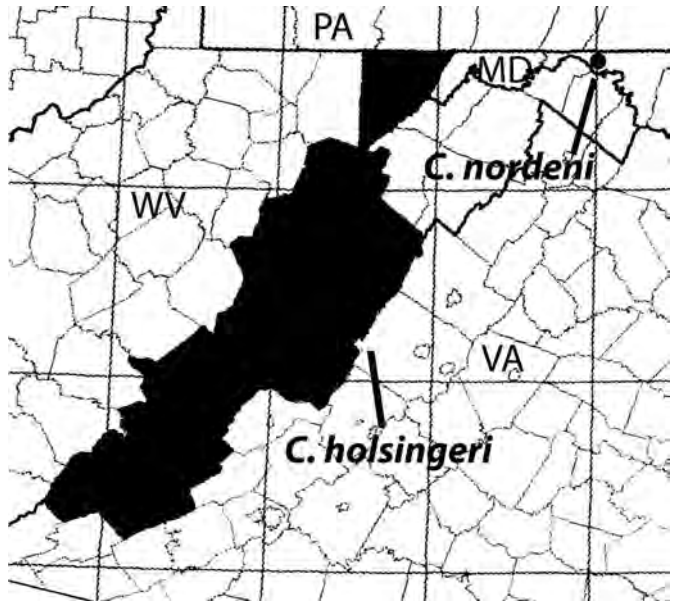

Figure 4. Map of counties of occurrence recorded for *Caecidotea holsingeri* in Virginia, West Virginia and Maryland. The only known locality of *C. nordeni*, n. sp. in Maryland is indicated by a dot.

collection sites for *S. emarginatus* presented by Holsinger (1978) is nearly identical to the one presented here for *C. holsingeri*. Both species are found primarily in caves developed in the Greenbrier Limestone of Mississippian age suggesting that continuous Paleozoic limestones provide a common dispersal corridor for these species.

ACKNOWLEDGMENTS

Dr. Bowman's drawings and other materials were provided to me during a visit to the National Museum of Natural History funded by a Visiting Scientist Grant from the Smithsonian Institution. Ms. Marilyn Schotte sponsored that visit, as well as providing specimens from the museum collections. The manuscript was kindly reviewed by Dr. David C. Culver, Mr. Dan Feller, Dr. John R. Holsinger, Mr. Ellis Laudermilk and Ms. Marilyn Schotte. The description of *Caecidotea nordeni* was funded by the Karst Waters Institute and Cave Conservancy of the Virginias, kindly facilitated by Dr. David C. Culver.

REFERENCES

Bowman, T.E., and Beckett, D.C., 1978, A redescription of the troglobitic isopod, *Caecidotea stygia*, from the environs of Cincinnati, Ohio (Crustacea: Isopoda: Asellidae) *in* Proceedings of the Biological Society of Washington: Washington D.C., v. 91, no. 1, p. 294–302.

Bresson, J., 1955, Aselles de sources et grottes d'Eurasie et d''Amerique du Nord: Archives De Zoologie, Expérimentale et Générale, Notes et Revue, v. 92, p. 45–77.

Fleming, L.E., 1972, The evolution of the eastern North American isopods of the genus *Asellus* (Crustacea: Asellidae), Part I: International Journal of Speleology, v. 4, p. 221–256.

Franz, R., and Slifer, D., 1971, Caves of Maryland: Baltimore, Md., Maryland Geological Survey, Educational Series No. 3, 120 p.

Holsinger, J.R., 1978, Systematics of the subterranean amphipod genus *Stygobromus* (Crangonyctidae), Part II: Species of the eastern United States: Smithsonian Contributions to Zoology, v. 266, p. 1–144.

Holsinger, J.R., and Steeves, H.R. III, 1971, A new species of subterranean isopod crustacean (Asellidae) from the central Appalachians, with remarks on the distribution of other isopods of the region *in* Proceedings of the Biological Society of Washington: Washington, D.C., v. 84, p. 189–200.

Holsinger, J.R., Baroody, R.A., and Culver, D.C., 1976, The invertebrate cave fauna of West Virginia: West Virginia Speleological Survey Bulletin 7, 82 p.

Levy, H., 1949, Two new species of cave isopods from Pennsylvania: Notulae Naturae of the Academy of Natural Sciences of Philadelphia, v. 220, p. 1–6.

Lewis, J.J., 1980, A comparison of *Pseudobaicalasellus* and *Caecidotea*, with a description of *Caecidotea bowmani*, n. sp. (Crustacea: Isopoda: Asellidae) *in* Proceedings of the Biological Society of Washington: Washington, D.C., v. 93, no. 2, p. 314–326.

Lewis, J.J., 1982, A diagnosis of the *Hobbsi* Group, with descriptions of *Caecidotea teresae*, n. sp., and *C. macropropoda* Chase and Blair (Crustacea: Isopoda: Asellidae) *in* Proceedings of the Biological Society of Washington: Washington, D.C., v. 95, p. 338–346.

Lewis, J.J., 2009, Three new species of *Caecidotea*, with a synopsis of the asellids of Virginia (Crustacea: Isopoda: Asellidae), *in* Roble, S.M., and Mitchell, J.C., eds., A lifetime of contributions to Myriapodology and the natural history of Virginia: A festschrift in honor of Richard L. Hoffman's 80th birthday, Martinsville, Va., Virginia Museum of Natural History Special Publication no. 16, Martinsville, Va., p. 251–266.

Packard, A.S., 1871, On the crustaceans and insects, *in* Packard, A.S., and Putnam, F.W., eds., The Mammoth Cave and its inhabitants: American Naturalist, v. 5, no. 12, p. 739–761.

Steeves, H.R. III, 1963, Two new troglobitic asellids from West Virginia: American Midland Naturalist, v. 70, p. 461–465.

Steeves, H.R. III, 1969, The origin and affinities of the troglobitic asellids of the southern Appalachians, *in* Holt, P.C. ed., The distributional history of the biota of the Southern Appalachians, Part I., Invertebrates, Blacksburg, Va., Virginia Polytechnic Institute and State University, Research Division Monograph 1, p. 51–65.

W.A. Shear – *Hesperonemastoma smilax*, n. sp., a remarkable new harvestman from a cave in West Virginia, with comments on other reported cave-dwelling and *Hesperonemastoma* species (Opiliones, Ischyropsalidoidea, Sabaconidae). *Journal of Cave and Karst Studies,* v. 72, no. 2, p. 105–110. DOI: 10.4311/jcks2009lsc0103

HESPERONEMASTOMA SMILAX, N. SP., A REMARKABLE NEW HARVESTMAN FROM A CAVE IN WEST VIRGINIA, WITH COMMENTS ON OTHER REPORTED CAVE-DWELLING *HESPERONEMASTOMA* SPECIES (OPILIONES, ISCHYROPSALIDOIDEA, SABACONIDAE)

WILLIAM A. SHEAR
Biology Department, Hampden-Sydney College, Hampden-Sydney, VA 23943, wshear@hsc.edu

Abstract: *Hesperonemastoma smilax*, n. sp., is a minute, highly troglomorphic harvestman described herein from a single male specimen collected in McClung's Cave, Greenbrier County, West Virginia. *Hesperonemastoma* species described previously from caves are briefly discussed. *H. packardi* (Roewer), first collected in a shallow cave in Utah, is a widely distributed surface-dwelling species found mostly in riparian canyon habitats in northern Utah; it shows no troglomorphic adaptations. *Hesperonemastoma inops* (Packard), described from a cave in Kentucky, is not a species of *Hesperonemastoma*, but most likely a juvenile of *Sabacon cavicolens* (Packard), which was described from the same small cave. *Hesperonemastoma pallidimaculosum* (Goodnight and Goodnight) is a moderately adapted troglobiont known from two caves in Alabama.

INTRODUCTION

Species of the harvestman (Opiliones) genus *Hesperonemastoma* are distributed in three discrete regions: the southern Appalachians of eastern North America, the Rocky Mountains in Utah and Idaho, and the Pacific coastal region from southern California north to the Queen Charlotte Islands, British Columbia, Canada. While three of the six named species inhabit deep forest litter, three species have been reported as collected only in caves. A fourth cave species is described in this article.

All *Hesperonemastoma* species were originally placed in the endemic European/west Asian genus *Nemastoma*. Gruber (1970) demonstrated that these species, in fact, were not members of the family Nemastomatidae and not even of the superfamily Troguloidea. He placed them in the family Ischyropsalididae, which required that they receive a new generic name, *Hesperonemastoma* Gruber 1970. Gruber's treatment was not meant to be complete. It was incidental to the author's interest in *Nemastoma* itself. For recent work on a range of nemastomatid genera, including troglobionts, see Martens (2006).

Of the four *Hesperonemastoma* species associated with caves, the first, *H. packardi*, was described by Packard in 1877 as *Nemastoma troglodytes*, from Clinton's Cave, Lake Point, Tooele County, Utah. Because that name was preoccupied in *Nemastoma*, Roewer changed it to *packardi* in 1914. *Hesperonemastoma inops* (Packard), also originally described as a *Nemastoma* species, was named in 1884 from immature material collected in Bat Cave, Carter County, Kentucky. The specimens are probably no longer extant, and to my knowledge it has not been collected since. Goodnight and Goodnight (1945) described *Nemastoma pallidimaculosum* from Rock House Cave, Marshall County, Alabama; below I report a new record from a cave in an adjacent Alabama county. The description of *H. smilax*, n. sp., in this article is the first description of a new *Hesperonemastoma* species in 64 years.

TAXONOMY

SUPERFAMILY ISCHYROPSALIDOIDEA SIMON 1879

Family Sabaconidae Simon 1879

Hesperonemastoma Gruber 1970

Hesperonemastoma Gruber 1970, p. 129; Shear, 1986, p. 13; Murphree, 1987, p. 94; Cokendolpher and Lee, 1993, p. 6.

Type species: *Nemastoma pallidimaculosum* Goodnight and Goodnight, 1945, by original designation.

Notes: An excellent diagnosis and description of the genus is provided by Gruber (1970). In my cladistic analysis of 1986, based on a rather small number of morphological characters, I placed *Hesperonemastoma* as sister to *Crosbycus* Roewer 1914 and put both in my new family Ceratolasmatidae, opposing a clade composed of the western North American genera *Ceratolasma* Goodnight and Goodnight 1942 and *Acuclavella* Shear 1986. However, recent molecular evidence has challenged this placement, supporting a widely divergent position for *Crosbycus*, and seeming to show *Hesperonemastoma* as close to *Taracus* of the family Sabaconidae Simon 1879 (Shultz and Regier, 2001). A total evidence approach taken by Giribet et al. (2002) differed somewhat, but still placed *Hesperonemastoma* close to *Taracus*. Finally, and conclu-

sively, a multi-locus analysis by Giribet et al. (2009) cemented the relationship of *Hesperonemastoma* to *Taracus*, and Giribet et al. (2009) formalized the transfer of *Hesperonemastoma* to Sabaconidae. Within Sabaconidae, the morphology of *Hesperonemastoma* is extremely divergent. It should be noted, however, that convergence of general body habitus is well known in Opiliones; *Taracus* itself (Sabaconidae), *Ischyropsalis* (Ischyropsalididae), *Nipponopsalis* (Trogulidae), and *Megalopsalis* (Monoscutidae) all resemble one another despite all belonging to separate families and even suborders, perhaps because of a common adaptation for feeding on snails (Nyffeler and Symondson, 2001) or, in the case of the monoscutid, secondary sexual characters of the males. It now seems that the striking similarity of *Hesperonemastoma*, *Crosbycus*, and several genera of Nemastomatidae is also the result of convergence or parallelism. For the time being, a diminished family Ceratolasmatidae and an augmented Sabaconidae are accepted by most harvestmen systematists, but their contents may change drastically in the future (Gruber, 2007; Giribet et al., 2009).

Hesperonemastoma pallidimaculosum (Goodnight and Goodnight)

Nemastoma pallidimaculosa Goodnight and Goodnight, 1945, p. 241, figs. 1, 2.

Nemastoma pallidimaculosum, Roewer, 1951, p. 140 (name corrected to agree in gender with the generic name).

Hesperonemastoma pallidimaculosum, Gruber, 1970, p. 134, figs. 1, 2, 5, 12, 13–15, 18; Cokendolpher and Lee, 1993, p. 6.

Types: Male holotype and two female paratypes from Rock House Cave, 1 mile south of Oleander, Marshall County, Alabama, deposited in the American Museum of Natural History, New York (AMNH).

Notes: Gruber (1970) made this species the type of *Hesperonemastoma* and described and illustrated it in detail. It has been collected only once more since 1945. The decision to make this rare, highly divergent species the type of the genus could be questioned.

The male holotype and paratype have rudimentary, unpigmented eyes. The female paratypes are eyeless, and in addition, the eye tubercle is reduced in size. The name derives from rows of ''light spots'' along the lateral margins of the scute, but in fact these are the impressions on the exoskeleton of the internal apodemes, marked by the absence of the usual granulations of the cuticle, which are darker than their surroundings and quite obvious in this species. These markings occur in all *Hesperonemastoma* species.

New record: ALABAMA: Jackson County, Horseshoe Cave, 6 miles north of Princeton, 30 June 1967, S. Peck and J. Fiske, male (AMNH). This specimen differs from the type males in that the rudimentary eyes have black pigment and the second cheliceromere is somewhat more prolonged dorsally.

Hesperonemastoma packardi (Roewer)

Nemastoma troglodytes Packard 1877, p. 160, fig. 5; 1888, p. 54, figs. 3, 15.

Nemastoma packardi Roewer 1914, p. 163 (new name for *N. troglodytes*); 1923, p. 676; 1951, p. 139.

Hesperonemastoma packardi, Gruber, 1970, p. 142, figs. 3, 6, 24; Cokendolpher and Lee, 1993, p. 6.

Notes: Gruber (1970) was evidently not able to locate the types of *packardi*; I found them in 1971 in the Museum of Comparative Zoology, Harvard University (MCZ), where they were not labeled as types, but the collection data are as reported by Packard (1877). Packard evidently believed he only had females, but the series consists of a male and four females. Restudying the holdings of the MCZ in 2007, I found a second vial, this one containing Packard's original labels and two males and two females. They were not labeled as types but undoubtedly were part of Packard's original series. One of these specimens, a male, has been designated as the lectotype and the others as paralectotypes.

The distinctive dorsal ornamentation of acute, conical abdominal-area tubercles and the lack of any anvil-shaped tubercles distinguishes this species. Packard (1877) thought the eyes and eye tubercle of his specimens were reduced in size, but they seem quite the same as in epigean samples of this and other species.

In the absence of the types, Gruber relied on a male and five females from Rose Lake, Idaho (AMNH). According to the United States Geological Survey database on place names, all place names including ''Rose Lake'' in Idaho are in Kootenai County. This county is in the northern panhandle of Idaho, about 600 miles north of the localities for *packardi* in northern Utah. Based on experience with the distribution of other soil and litter arthropods, I would expect *H. modestum* from this region, not *packardi*, though the collecting of soil and litter animals done by William Leonard and Casey Richart has not revealed any additional *Hesperonemastoma* specimens from northern Idaho. Gruber (1970) illustrates (his fig. 24) the palpal femur of the ID male with a very distinct ventral swelling and glandular area. I did not detect this modification in *packardi* males from Utah, although the femora of the males are slightly thicker than those of the females. I could not verify Gruber's own observation because the single palpus loose in the vial with the ID specimens is from a female. However, this character seems to be variable in *H. modestum*, and the same situation might obtain with *packardi*, assuming that all specimens studied by Gruber as *H. modestum* are actually that species; I have found four undescribed species from within the range of *H. modestum*. The palpal length was exactly the same (2.75 mm) in a *packardi* male and the ID male (as measured by Gruber). My observations of the penis of a *packardi* male from Utah differs from Gruber's of the ID male; he figures the glans with about twenty strongly curved, large basal setae and at least four small distal setae, while my observations of a

male from the *H. packardi* type series show twelve straight, large basal setae and only two small distal setae. Given the generally low interspecific variability in penes in *Hesperonemastoma*, this could be significant. Finally, the ID specimens are entirely smooth and lack the abdominal-area tubercles typical of Utah *packardi*. To further complicate matters, there is a single female conforming to the ID specimens in the AMNH; this female is labeled "Lost Creek Reservoir" without further data. The USGS database contains no such name for any reservoir in Idaho, but "Lost Creek" is a name applied to streams in eight Idaho counties alone, as well as many other places in the northern Rocky Mountains. It is not possible to assign this specimen to a specific locality. It may well be that the ID specimens described by Gruber (1970) are not *packardi* but an undescribed species.

Clinton's Cave, type locality for *packardi*, is west of Lake Point Station, close to the border between Tooele and Salt Lake Counties, Utah, overlooking the Great Salt Lake. Other details of its location are not given here because of conservation concerns. The cave itself is described in detail by Packard (1877). It appears to have been excavated by wave action of the Great Salt Lake during a previous higher stand of shoreline. The cave is relatively shallow; light penetrates, however faintly, throughout. At the time of Packard's visit the cave was also quite dry, and specimens were collected from beneath flat stones on the floor of the cave, where a small amount of moisture had accumulated.

Clinton's Cave is also the type locality of a tiny polydesmidan milliped, *Polydesmus cavicolus* Packard 1877. This species has recently been recollected and actually belongs to an undescribed genus of the family Macrosternodesmidae (Shear and Shelley, in prep.) Neither of the species appears cave-adapted, and their presence in the cave is probably accidental. The collections of the AMNH show that in fact *H. packardi* is relatively abundant and perhaps widely distributed on the surface in northern Utah. Detailed records will be given in the forthcoming revision; most are from the mountains and canyons in the Salt Lake City vicinity, but other regions of Utah remain poorly explored for soil and litter arthropods, and *H. packardi* may turn up in even more localities with further collecting.

In conclusion, *H. packardi* is a widely distributed surface-dwelling, leaf-litter species and is not troglomorphic or distinctly troglophilic.

Hesperonemastoma inops (Packard)

Nemastoma inops Packard 1884, p. 203; 1888, p. 55, fig. 4. Roewer, 1914, p. 168; 1923, p. 677; 1951, p. 139. [Roewer 1923 is not in the reference list]

Hesperonemastoma inops, Gruber, 1970, p. 138; Cokendolpher and Lee, 1993, p. 6.

Types: Two juvenile cotypes from Bat Cave, Carter County, Kentucky. Present whereabouts unknown, probably no longer in existence. Some Packard types, as with *H. packardi*, are in the collections of the MCZ, but neither the types of this species nor of *Phlegmacera (=Sabacon) cavicolens*, described from the same sample, were to be found in either the type collection or the general collection when searched for in 1970 and 1971 (Shear, 1975).

Notes: The original material is probably lost and the species has never been collected again, despite the fact that the Carter County caves are among the most intensively studied in the United States, the record of exploration going back to the early nineteenth century. The description by Packard (1884, 1888) raises doubts as to the position of this species. His description and illustration of the palpus (Packard, 1884, 1888) is completely unlike that of any other species of *Hesperonemastoma* in that the segments are much shorter and thicker and in quite different proportions. Packard (1884) also described *Phlegmacera cavicolens* (now *Sabacon cavicolens*; see Shear, 1975) from the same cave, from specimens collected at the same time. The description of *Nemastoma inops* and the illustration of the palpus fit an immature individual of *Sabacon*; indeed, *inops* is only about a fourth the size of a mature *S. cavicolens* (1 mm long vs. 4 to 5.5 mm for mature female *S. cavicolens*). At this size, immature *S. cavicolens* are white, have poorly pigmented eyes, and the palpi closely resemble Packard's illustration of the *inops* palpus—the enlarged tibia of adults is only a little bigger than the patella in these very young juveniles. In samples of the Pacific coast species of *Hesperonemastoma*, the individuals most commonly incorrectly included as *Hesperonemastoma* are small juveniles of *Sabacon*. Furthermore, Bat Cave is a shallow cave "not suitable for the survival of normal troglobites" (S.B. Peck 2007, pers. comm.). Therefore I confidently hypothesize that *Nemastoma inops* is a synonym of *Sabacon cavicolens*, but in the absence of the original specimens, it's impossible to prove it.

Hesperonemastoma smilax, n. sp.

Figures 1–10.

Suggested vernacular name: McClung's Cave Harvestman.

Type: Male holotype from McClung's Cave, Greenbrier County, West Virginia, collected March 23, 1961, by Lyle G. Conrad, deposited in the Virginia Museum of Natural History (VMNH), Martinsville, Virginia.

Diagnosis: Distinct from other known species of *Hesperonemastoma* in being not only eyeless, but in lacking the eye tubercle; the scute is completely smooth, without the paired tubercles, anvil-shaped tubercles, elevations, or black granules found in other species.

Etymology: The species epithet is a noun in apposition, the generic name of the greenbrier, catclaw vine, or wait-a-minute plant, a pernicious vine with hooked thorns from which the West Virginia county takes its name.

Description: length, 1.0 mm, greatest width 0.55 mm. Cephalic part of scutum nearly flat, eye tubercle absent

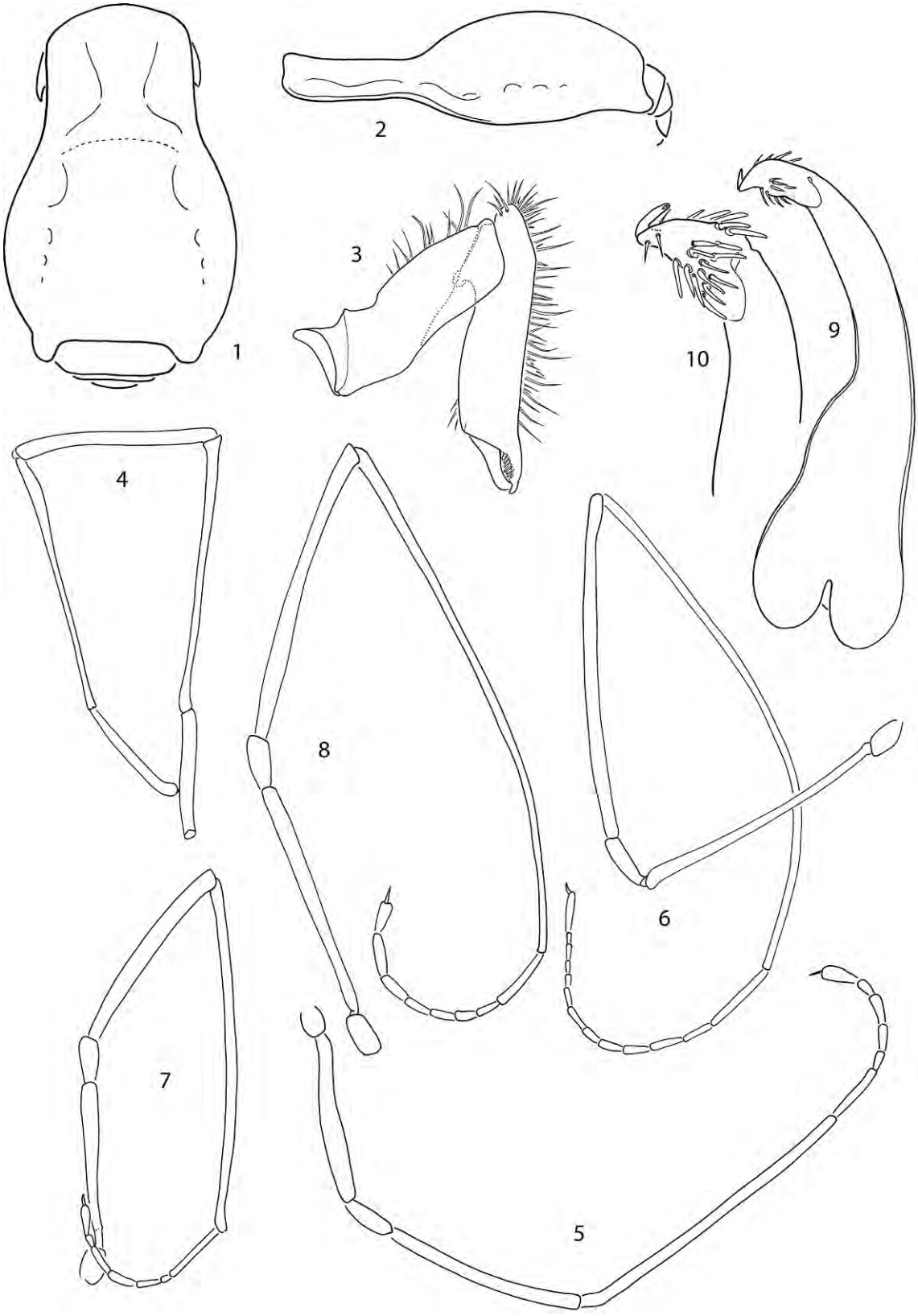

Figures 1 to 10. Male *Hesperonemastoma smilax*, n. sp. (1) body, dorsal view. (2) scutum, lateral view. (3) right chelicera, lateral view. (4) palpus, posterior view. (5) leg 1, posterior view. (6) leg 2, posterior view. (7) leg 3, posterior view. (8) leg 4, posterior view. (9) penis, dorsal view. (10) glans penis, dorsal view.

Table 1. Appendage article lengths in mm of *H. smilax* male holotype.

Appendage	Trochanter	Femur	Patella	Tibia	Metatarsus	Tarsus
Palp	0.6	1.38	1.16	1.34	···	0.7
Leg 1	0.20	0.89	0.30	1.06	1.65	1.06
Leg 2	0.24	1.30	0.27	1.83	2.71	1.95
Leg 3	0.21	1.18	0.39	1.41	2.19	1.34
Leg 4	0.26	1.50	0.35	2.00	3.00	2.00

(Figs. 1, 2); abdominal part of scutum gently domed, smooth, lacking any paired ornament; all surfaces minutely granulate, granules concolorous with intervening cuticle; single large, subtriangular lateral sclerite. Color uniform yellow-tan after long preservation, color in life unknown. Chelicerae (Fig. 3) disproportionately large compared to congeners. Basal cheliceromere 0.5 mm long, 0.16 mm wide, not basally constricted, lacking crest; distal cheliceromere elongate, 0.66 mm long, 0.16 mm wide, slightly elevated above proximal articulation, setal coat most dense on elevated part. Pedipalp 5.18 mm long, thin, with extremely elongate trochanter; palpal hairs scattered, becoming much more dense on tibia and tarsus; claw absent (Fig. 4). Legs (Figs. 5–8) very long, thin; femora and patellae smooth to sparsely setose, lacking sculpture; femora with single basal false articulation; tibiae densely hairy, without false articulations; metatarsi densely hairy, with false articulations distal on metatarsi 2, 4; tarsi with articles as follows: tarsus 1, 6; tarsus 2, 13, tarsus 3, 7; tarsus 4, 8. Legs in order of length in mm: 4 (9.11), 2 (8.30), 1 (6.96), 3 (6.72). Measurements of articles of palpus and legs as in Table 1. Penis (Figs. 9, 10) typical for genus, shaft relatively short, glans set with stout, decurved setae, stylus sharply recurved.

Notes: McClung's Cave is located near Lewisburg, West Virginia. Extensive land holdings surrounding the Lightner Entrance to the cave have recently been purchased by the West Virginia Cave Conservancy. The cave has over 17 miles of mapped passageways, and may possibly be part of a system of four interconnected named caves with more than 77 miles of passageways. The cave has a rich fauna (J. Holsinger, pers. com.; Fong et al., 2007), including troglobionts (two millipeds, a dipluran, a collembolan, a pseudoscorpion, a spider, and a beetle), stygobionts (a flatworm, a snail, an amphipod, and a crayfish) troglophiles (a terrestrial snail, a third milliped, a dipteran, and a second spider and amphipod), and trogloxenes (yet another milliped, a second collembolan, and a cricket). Because of the small size and pale coloration of *H. smilax*, it is unlikely that the species will be collected again without intensive effort. A group of speleobiologists from American University under the direction of David Culver has been closely examining Greenbrier County caves in recent years; even so, they have not found this species again.

The slightly elevated second cheliceromere of this species is similar to that of *H. pallidimaculosum*, but the first cheliceromere lacks the constriction and crest found in that species and generally in other *Hesperonemastoma* (see Figs. 12, 13 in Gruber, 1970). In *H. kepharti* (Crosby and Bishop), a leaf-litter species distributed from northern Alabama to southern Virginia (and the closest to *smilax* geographically), the elevation of the second cheliceromere is much exaggerated and extends dorsal from the articulation of the first and second cheliceromeres to about half the length of the latter. This modification of the chelicerae, however slight or pronounced, seems to separate the species of *Hesperonemastoma* into a western and an eastern clade, since the western species have the proximal part of the second cheliceromere evenly rounded and not at all exceeding the articulation dorsally. The long palpal trochanter and long, thin legs also suggest *pallidimaculosum*, but the elongation is even more pronounced in *smilax*.

Hesperonemastoma smilax shows extreme troglomorphy, in that not only is every trace of eyes gone, the eye tubercle itself is entirely flattened. This character alone would mark it as the most highly modified harvestman troglobiont in North America, since in all others at least a low eye tubercle is present, even if the eyes are entirely reduced. Cuticular ornament has also been reduced; no trace of the abdominal-area tubercles or anvil-shaped tubercles remains, and the small black denticles, so prominently covering the scute and abdominal tergites in the other eastern species, are difficult to see. The cuticle is thin and leathery, as opposed to the hard, black, heavily sclerotized cuticle of surface-dwelling species, and the legs and palpi are extraordinarily long and threadlike. It is clear that this species has undergone a long period of adaptation to its subterranean environment. *H. smilax* occurs approximately 75 miles due north of the northernmost records of the nearest congener, *H. kepharti*, suggesting that *H. smilax* is a relict of a once more northerly distribution of the genus.

As for comparisons with other species from caves, while *Hesperonemastoma packardi* of Utah was collected in a cave, that species has no troglomorphic adaptations, and its occurrence in the cave, as explained above, is clearly accidental. *H. inops* is likely not a member of the genus. *H. pallidimaculosum* is from northern Alabama and differs in its lesser degree of troglomorphy—males have small eyes, and females, while eyeless, retain the eye tubercle. Roewer (1951) described an animal he called *Crosbycus goodnightorum* from Fountain Cave, Madison County, Virginia, and

it is conceivable this could represent yet another troglobiontic *Hesperonemastoma*. However, Rambla (1968) established from the description (the specimens seem to have been lost) that *C. goodnighti* is a juvenile *Nemastoma* (see also Shear, 2008). Subsequent collecting in Fountain Cave has not turned this species up. There are no native *Nemastoma* species in North America and no records of European members of the genus having established themselves in the United States. It is possible the collection from which Roewer worked was mislabeled. For a fuller discussion of *Crosbycus*, see Shear (1986).

Acknowledgments

Thanks to Richard L. Hoffman, Virginia Museum of Natural History, for the loan of the specimens of *Hesperonemastoma smilax*; to Lorenzo Prendini, American Museum of Natural History, for the loan of the type material of *H. pallidimaculosum* and specimens of *H. packardi*, and to Herbert W. Levi, Gonzalo Giribet, and Laura Leibensperger for assistance and loans from the Museum of Comparative Zoology. Thanks also to James C. Cokendolpher, who first recognized *H. smilax* as a new species and so labeled it during a survey of the VMNH collection. This research was supported by the Karst Waters Institute, the Cave Conservancy of Virginia, and the Professional Development Committee of Hampden-Sydney College. I am grateful to David Culver, American University, and two anonymous reviewers for comments on the manuscript and to Culver and John Holsinger for information on the fauna and status of McClung's Cave.

References

Cokendolpher, J.C., and Lee, V.F., 1993, Catalogue of the Cyphopalpatores and Bibliography of the Harvestmen (Arachnida, Opiliones) of Greenland, Canada, USA and Mexico, Lubbock, Texas, privately published, 82 p.

Fong, D.W., Culver, D.C., Hobbs, III, H.H., and Pipan, T., 2007, The Invertebrate Cave Fauna of West Virginia, Second Edition, Barrackville, West Virginia Speleological Survey (bulletin 16), 163 p.

Giribet, G., Edgecombe, G.D., Wheeler, W.C., and Babbitt, C., 2002, Phylogeny and systematic position of Opiliones: a combined analysis of chelicerate relationships using morphological and molecular data: Cladistics, v. 18, p. 5–70.

Giribet, G., Vogt, L., Pérez González, A., Sharma, P., and Kury, A.B., 2009, A multilocus approach to harvestman (Arachnida, Opiliones) phylogeny with emphasis on biogeography and the systematics of Laniatores: Cladistics, v. 25, p. 1–30.

Goodnight, C.J., and Goodnight, M.L., 1945, Phalangida from the United States: Journal of the New York Entomological Society, v. 53, p. 239–245.

Gruber, J., 1970, Die "Nemastoma"-Arten Nordamerikas (Ischyropsalididae, Opiliones, Arachnida): Annales naturhistorisches Museum Wien, v. 74, p. 129–144.

Gruber, J., 2007, Ceratolasmatidae, *in* Pinto-da-Rocha, R., Machado, G., and Giribet, G., eds., Harvestmen, The Biology of Opiliones, Cambridge, Mass., Harvard University Press, p. 136–142.

Martens, J., 2006, Weberknechte aus dem Kaukasus (Arachnida, Opiliones, Nemastomatidae): Senckenbergiana biologica, v. 86, p. 145–210.

Murphree, C.S., 1987, Two leaf-litter phalangids from Short Mountain (Cannon County), Tennessee: Journal of the Tennessee Academy of Sciences, v. 62, p. 93–94.

Nyffeler, M., and Symondson, W.O.C., 2001, Spiders and harvestmen as gastropod predators: Ecological Entomology, v. 26, p. 617–628.

Packard, A.S., 1877, On a new cave fauna in Utah: Bulletin of the United States Geological Survey of the Territories, v. 3, p. 157–169.

Packard, A.S., 1884, New cave arachnids: American Naturalist, v. 18, p. 202–204.

Packard, A.S., 1888, The cave fauna of North America, with remarks on the anatomy of the brain and the blind species: Memoirs of the National Academy of Sciences, v. 4, p. 3–156.

Rambla, M., 1968, Sobre el género *Crosbycus* Roewer, 1914 (Opiliones, fam. Nemastomatidae): Publicaciones del Instituto de Biologia Aplicada, v. 44, p. 65–80.

Roewer, C.F., 1914, Die Familien der Ischyropsalidae und Nemastomatiden der Opiliones-Palpatores: Archive Naturgeschichten, v. 80, p. 99–169.

Roewer, C.F., 1951, Über Nemastomatiden I, weitere Weberknechte XVI: Senckenbergiana, v. 32, p. 96–153.

Shear, W.A., 1975, The opilionid genera *Sabacon* and *Tomicomerus* in America (Opiliones, Troguloidea, Ischyropsalidae): Journal of Arachnology, v. 3, p. 5–29.

Shear, W.A., 1986, A cladistic analysis of the opilionid superfamily Ischyropsalidoidea, with descriptions of the new family Ceratolasmatidae, the new genus *Acuclavella*, and four new species: American Museum Novitates n. 2705, p. 1–34.

Shear, W.A., 2008, Deletions from the North American harvestman (Opiliones) faunal list: *Phalangomma virginicum* Roewer, 1949 is a synonym of *Erebomaster weyerensis* (Packard, 1888) (Travunioidea: Cladonychiidae), and a note on "*Crosbycus" goodnightorum* Roewer, 1951 (Nemastomatidae): Zootaxa, v. 1945, p. 67–68.

Shultz, J.W., and Regier, J.C., 2001, Phylogenetic analysis of Phalangida (Opiliones, Arachnida) using two nuclear protein-encoding genes supports monophyly of Palpatores: Journal of Arachnology, v. 29, p. 189–200.

C.M. Wurster, D.A. McFarlane, M.I. Bird, P. Ascough, and N.B. Athfield – Stable isotopes of subfossil bat guano as a long-term environmental archive: insights from a Grand Canyon cave deposit. *Journal of Cave and Karst Studies,* v. 72, no. 2, p. 111–121. DOI: 10.4311/jcks2009es0109

STABLE ISOTOPES OF SUBFOSSIL BAT GUANO AS A LONG-TERM ENVIRONMENTAL ARCHIVE: INSIGHTS FROM A GRAND CANYON CAVE DEPOSIT

Christopher M. Wurster[1]*, Donald A. McFarlane[2], Michael I. Bird[1], Philippa Ascough[3], and Nancy Beavan Athfield[4]

Abstract: We investigated the utility of subfossil bat guano as a paleoenvironmental archive by comparing elemental ratios and $\delta^{13}C$, $\delta^{15}N$, and δD values of various simple extracts from bulk material. Solvent-extracted guano yielded consistent C:N and N:H ratios, and $\delta^{13}C$ values of solvent-extracted guano exhibited strong covariation with δD values, as well as with the $\delta^{13}C$ values of other simple extracts (bulk guano, bulk lipid). The results suggest that reliable records are easily recovered for $\delta^{13}C$, and also indicate that $\delta^{15}N$ values may have utility as a paleoenvironmental archive. Despite coeval $\delta^{13}C$ values of bulk guano and solvent-extracted guano, ^{14}C ages of the different fractions did not always yield similar ages, indicating that future refinement of a suitable extraction protocol is required. Applying these protocols to an ancient bat guano deposit allowed us to infer that climate at the Grand Canyon during the late Pleistocene was more variable and generally cooler and wetter, relative to Holocene climate. We conclude that guano deposits are an underutilized, yet powerful continental paleoenvironmental archive of climate change for semi-arid and tropical regions.

Introduction

An overlooked, but potentially valuable terrestrial paleoenvironmental record is archived in stable isotope ratios of guano preserved in caves, for which extended Quaternary cave deposits are known to exist (Des Marais et al., 1980; Mizutani et al., 1992b; McFarlane et al., 2002; Bird et al., 2007). To date, several studies have shown $\delta^{13}C$ and $\delta^{15}N$ values of animal feces to be a faithful tracer of dietary sources (e.g., Webb et al., 1998; Sponheimer et al., 2003). Moreover, guano from insectivorous bats is composed mostly of insect exoskeletons containing chitin, and chitin is known to be a resistant biopolymer found in the geological record as long ago as 25 Ma (Stankiewicz et al., 1997). $\delta^{13}C$ and δD values of chitin are well studied and are considered to record dietary and local water sources (e.g., Schimmelmann and DeNiro 1986b; Miller et al., 1988; Webb et al., 1998; Gröcke et al., 2006). Therefore, such a record might be recoverable from guano deposits found in *Tadarida brasiliensis* (the Mexican free-tailed bat) maternity roosts. Additional studies have looked at pollen sequences in guano deposits (Carrión et al., 2006; Maher, 2006), showing that multi-proxy records can be recovered.

The Mexican free-tailed bat is one of the most widely distributed mammals in the western hemisphere, common from the semi-arid and temperate regions of the southern United States to the tropical-humid environments of Brazil (Koopman, 1982; Wilkins, 1989). Up to 90 tons of guano can be deposited annually within individual maternity caves that contain populations numbering greater than one million individuals (Constantine 1970). Guano from insectivorous bats is composed mostly of finely comminuted insect exoskeletons (Jeuniaux, 1971; McFarlane et al., 2002). Chitin is a resistant biomacromolecule (Miller et al., 1988), and guano in arid environments is effectively mummified, virtually arresting bacterial degradation (Mizutani et al., 1992b; Shahack-Gross et al., 2004). Chitin diagenesis proceeds first by degradation of bound proteins, with the remaining chitin apparently transforming over time to aliphatic compounds (Stankiewicz et al., 1998; Briggs, 1999). During at least early diagenesis, stable isotope values of chitin and bat guano remain unchanged over up to 30 years (Schimmelmann et al., 1986; Mizutani et al., 1992b).

The Mexican free-tailed bat is a generalist insectivore with a dietary composition strongly correlated with local insect abundance (Lee and McCracken, 2002). Because insect tissue $\delta^{13}C$ values reflect insect diet (Schimmelmann et al., 1993; Webb et al., 1998) and insect abundance is largely determined by available local vegetation (e.g., Pinder and Kroh, 1987; Warren and Gaston, 1992), spatially integrated variations in vegetation resulting from climate change are archived in the isotope compositions of subfossil guano deposits (Wurster et al., 2007, 2008). C_3, C_4, and CAM photosynthetic pathways control the carbon

* Corresponding author, *christopher.wurster@jcu.edu.au*

[1] School of Earth and Environmental Sciences, James Cook University, PO Box 6811, Cairns QLD 4870, Australia

[2] Keck Science Center, The Claremont Colleges, 925 North Mills Avenue, Claremont, CA 91711, USA

[3] AMS Group, S. U. E. R. C, Scottish Enterprise Technology Park, Rankine Avenue, East Kilbride, G75 0QF, UK

[4] Rafter Radiocarbon, National Isotope Centre, GNS Science, PO Box 31 312, Gracefield, Lower Hutt, New Zealand

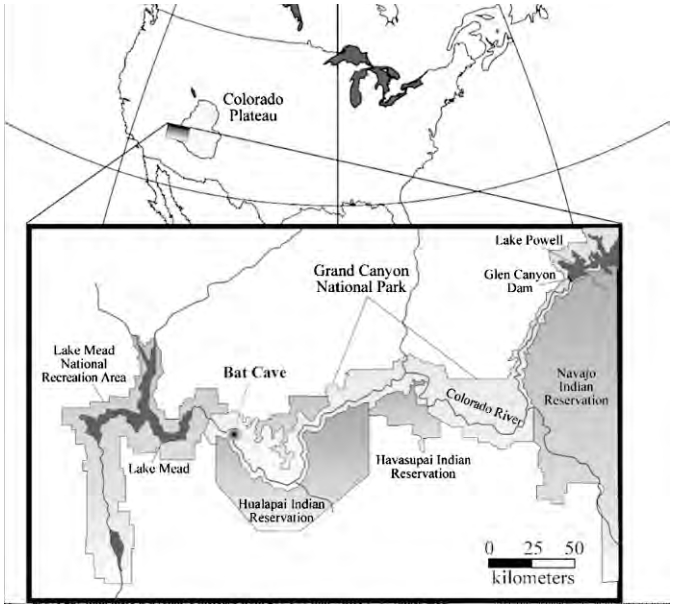

Figure 1. Study area and location of *Tadarida brasiliensis* maternity roost, where a guano core was excavated. Inset map after Bowers et al. 1997.

isotopic composition of plants (Ehleringer et al., 1997), and in semi-arid regions, the relative abundances of these plant types are strongly tied to local climate conditions (Paruelo and Lauenroth, 1996). Wurster et al. (2007) demonstrated a strong correlation between the relative abundance of C_4 grasses and $\delta^{13}C$ values of modern guano from insectivorous bats from Florida to California. Moreover, they found that $\delta^{13}C$ values of guano were most strongly correlated with summer precipitation amount and winter precipitation ratio in the western United States. δD values of insect chitin reflect local environmental water, with relatively higher values indicating higher temperature, greater summer/winter precipitation ratio, and (or) lower relative humidity (Miller et al., 1988; Schimmelmann et al., 1993; Gröcke et al., 2006). Consequently, chitin $\delta^{13}C$ and δD values derived from bat guano deposits are reliable archives of vegetation and regional climate conditions near the site (Wurster et al., 2007, 2008).

We present $\delta^{13}C$, $\delta^{15}N$, and δD profiles from various simple extracts recovered from a long-term guano deposit in the Grand Canyon, USA, to evaluate further the utility of guano as a paleoenvironmental archive. We measured $\delta^{13}C$ and $\delta^{15}N$ values from bulk guano, solvent-extracted guano (separated by relatively high and low C:N ratios), and $\delta^{13}C$ from the solvent extract (bulk lipids). We also measured δD values on solvent-extracted guano. In addition, we present results from AMS ^{14}C dating of bulk guano and solvent-extracted guano. We expand upon results described by Wurster et al., (2008) by comparing results obtained from different chemical fractions and including results from a deeper guano section.

Figure 2. Flow chart of extraction methods to obtain various fractions in this study. See text for treatment details. (MeOH is methyl alcohol.)

MATERIALS AND METHODS

SAMPLE COLLECTION

A bat guano sequence was recovered from Bat Cave, a *Tadarida brasiliensis* maternity roost, located ~700 m above the Colorado River in Grand Canyon National Park, USA, in 1996 (Fig. 1). The sequences were taken in the back chamber, recently excavated to reveal an ancient bat guano deposit. Currently, the bats inhabit the front chamber, but apparently had been blocked by guano deposition from the back a considerable time ago, and thus the surface of the back deposit was not recently deposited. Two 1-m-length 5-cm-diameter pieces of PVC were driven into the guano pile and self-enclosed to extract the tube and guano without need for excavation. A surface sample was collected, termed 96-02, and a sample was taken 1.3-m-deep between the PVC cores, termed 96-03. The deeper PVC core was termed 96-05, and the shallower PVC core was termed 96-04. Collection of each core section resulted in considerable compression of approximately 65%. Each section was opened in the laboratory, wetted with deionized H_2O to prevent mixing during sampling, and scraped until stratigraphy was conspicuous. Two series of samples from the cores were collected and termed Pass 1 and Pass 2. Pass 1 included samples from both core 96-04 and 96-05, but only core 96-04 was resampled in Pass 2. Before Pass 2, core 96-04 was scraped again to reveal intact stratigraphy. Samples were collected at 8-mm-thick intervals for Pass 1. For Pass 2, 4-mm-thick samples were taken from 0 to 260 mm, and 8-mm-thick increments thereafter.

SAMPLE PROCESSING AND EXTRACTION

Several simple extraction procedures were used to isolate various organic matter components from the bulk sample. Abbreviations and a brief summary of the extraction methods are shown in Figure 2.

1. Initially, we followed methods described by Mizutani et al. (1992a) for analysis of bat guano $\delta^{13}C$ values. This consisted of first decarbonating samples for at least three hours in 2N HCl, followed by rinsing to

neutrality with deionized H_2O, and finally lypholization. Between each step in this method, and the other extraction steps described below, samples were sonicated several times in ~15-minute cycles. Samples analyzed using this method are termed bulk guano (BG).

2. To concentrate the organic portion from the mineral fraction, we used heavy-liquid density separation. This method consisted of mixing $ZnCl_2$ in 2N HCl to obtain a liquid with a specific gravity of 2.0. Samples were then decarbonated in this solution, ensuring that the organic portion at the surface remained saturated. After at least three hours, the sample was centrifuged for three minutes and the floatant poured onto a 12-μm metal sieve. The organic portion retained on the sieve was then rinsed to neutrality with deionized H_2O, and lypholized. Material recovered using this method is termed the guano extract (GE).
3. We attempted to isolate natural chitin following methodology from Schimmelmann and DeNiro (1986a). Initial processing was as for the guano extract, but continued by treatment in 1N NaOH at 100 °C for 30 minutes followed by neutralization in deionized H_2O. Finally, we washed the material once in methanol followed by three times in chloroform/methanol 2:1 by volume. After completion of solvent extraction, samples were lypholized. It was determined that the NaOH step resulted in a significant loss of organic material, probably due to the small amounts of starting material, the small particulate size, and the age of the sub-fossil guano. Therefore, this extraction procedure was later performed without use of NaOH. Samples using this method, without the NaOH, are termed the solvent-extracted guano (SEG), with samples sub-divided into high-C:N (SEG_H) and low-C:N (SEG_L) samples. Two samples later determined to have N:H ratios above 2 were discounted in the interpretation, as this may indicate contamination.
4. Finally, the solvent wash from step 3 was placed in a fume hood and permitted to fully evaporate. The recovered extract was collected and termed the solvent extract (SE).

Fourier Transform Infrared Spectroscopy

Fourier-Transform Infrared Spectroscopy is a widely used qualitative technique in the study of natural polymers and is commonly used for molecular-structure investigation of chitin and its derivatives (Duarte et al., 2002). FTIR was used to characterize the SEG, in order to confirm that this fraction represented material derived from natural chitin. For comparison, analyses were also made of fresh commercial bat guano fertilizer from a Mexican desert and a commercially obtained pure sample of *n*-acetyl-d-glucosamine, the monomer of the chitin polymer. Lypholized samples were diluted by grinding with solid KBr and pressed into pellets prior to analysis using a Nicolet FTIR instrument. Absorbance values were determined between 4000 and 400 cm^{-1}, and spectral bands were identified by comparison with published assignments (Duarte et al., 2002; Van de Velde and Kiekens, 2004; Wanjun et al., 2005).

Analysis of $\delta^{13}C$ and δD Values, and C:N and N:H Elemental Ratios

We determined $\delta^{13}C$, $\delta^{15}N$, and weight-percent organic carbon (%C) and nitrogen (%N) by continuous-flow–isotope-ratio mass spectrometry (CF-IRMS) using a ThermoFinnigan Flash 1112 Elemental Analyzer coupled by a ConFlo III to a ThermoFinnigan Delta XL Plus mass spectrometer. All $\delta^{13}C$ and $\delta^{15}N$ values are reported relative to VPDB and AIR, respectively, standardized using three internal laboratory reference materials. Repeat analyses of laboratory standards yielded an external reproducibility of better than ±0.2‰ and 0.3‰ for $\delta^{13}C$ and $\delta^{15}N$ values, respectively. $\delta^{13}C$ values were determined on samples from each extract. For samples from Pass 1, only $\delta^{13}C$ analyses were performed. Both $\delta^{13}C$ and $\delta^{15}N$ analyses were performed for GE and SEG samples from Pass 2, but sample size was small for N_2, with an attendant decrease in reproducibility of $\delta^{15}N$ values and %N. All samples were analyzed at least twice on separate runs, except in cases where not enough material was available.

δD values and weight percent H (%H) were determined by high-temperature flash pyrolysis CF-IRMS using a ThermoFinnigan High Temperature Conversion Elemental Analyzer (TC/EA) coupled through a ThermoFinnigan ConFlo III to a ThermoFinnigan Delta XL Plus mass spectrometer. All δD values are reported relative to VSMOW-SLAP. Repeat analysis of international material IAEA CH-7, NBS-22, and three internal laboratory standards yielded an external reproducibility of better than ± 3‰.

Correction for Labile Hydrogen

δD values were analyzed for solvent-extracted guano samples with correction for labile hydrogen exchange with atmospheric H_2O vapor. Some hydrogen in complex organic matter (that component bonded to N or O) is potentially available for exchange with the atmosphere (e.g., Schimmelmann, 1991; Wassenaar and Hobson, 2000). To correct for this exchangeable hydrogen, two standards (see below) with known δD_n values (nonexchangeable δD values) were permitted to air equilibrate with SEG samples and analyzed together using high temperature pyrolysis CF-IRMS. Standard δD_n values were used to correct for δD_n values of samples (after Wassenaar and Hobson, 2000, 2003).

Because the SEG was assumed to be dominantly composed of chitin, grasshoppers were collected from Saskatoon in September and October of 2002 for one standard, and commercial bat guano was used for the

Table 1. Determination of nonexchangeable δD value of internal reference materials used for comparative equilibration with subfossil solvent extracted guano.

δD_{ta} (‰)	δD_{tb}	Equilibration water δD_{wa} (‰)	Equilibration water δD_{wb} (‰)	δD_n (‰)	f_e
GH					
34	−106	1168	7	−120	0.10
−133	−106	−171	7	−123	0.12
34	−133	1168	−171	−124	0.10
Guano					
70	−54	1168	7	−60	0.09
−69	−54	−171	7	−59	0.07
70	−69	1168	−171	−56	0.09

Note: GH and Guano represent Saskatchewan Grasshopper chitin and fertilizer guano (chitin) standards, respectively. Samples were equilibrated with water with known δD at 25°C and the non-exchangeable δD value and exchangeable hydrogen amount (f_e) determined. Subscripts t, w, n, a, and b, refer to total, water, non-exchangeable, and reference a and b, respectively. All δD values are reported relative to VSMOW in ‰ units. Calculations are performed using equations (3) and (4) in Wassenaar and Hobson (2000) assuming $\alpha = 1.251$. GH and Guano standards were also air-equilibrated with and corrected using known non-exchangeable δD keratin standards previously determined by high temperature equilibration (Wassenaar and Hobson, 2000). Comparisons of both equilibration methods show good agreement. GH and Guano average δD values were −123 ± 4‰ and −59 ± 2‰, respectively, in this experiment. Relative to keratin standards GH and Guano standards were determined to be −128 ± 1‰ and −56±2‰, respectively.

second standard. Natural chitin from each standard was isolated using the SEG method described above (method 3 with the NaOH step included). Because chitin and keratin contain similar amounts of labile hydrogen at 130°C, 15.3 ± 2.9% (Schimmelmann et al., 1993) and 15 ± 3%, respectively (Wassenaar and Hobson, 2003), chitin standard δD_n values were constrained by air equilibration with known keratin standards, determined to be −128 ± 0.9‰ and −56.5 ± 2.3‰ (assuming 80‰ between atmospheric water vapor and organic-matter labile hydrogen) for these grasshopper and guano standards, respectively (Table 1).

As an additional test, these standards were equilibrated with water with known δD value for three weeks at 25°C. After equilibration was complete, samples were immediately frozen using liquid nitrogen upon removal from the water bath. The frozen samples were then placed under vacuum and lypholized. After freeze-drying was complete, samples were kept frozen, removed from vacuum, and immediately transferred to a zero-blank autosampler, where He was introduced to remove atmospheric water vapor. Then the samples were analyzed for δD values using the high temperature pyrolysis method described above. By this procedure, δD_n values of −123 ± 4‰ and −59 ± 2‰, and labile hydrogen values of 11 ± 1% and 8 ± 1% were determined for the grasshopper and guano standards, respectively (Table 1). δD values were calculated using a provisional value of 224‰, estimated assuming a linear interpolation between assumed chitin values of 80‰ at 130°C (after Schimmelmann et al., 1993; Wassenaar and Hobson, 2003), and 256‰ at 0°C (Motz, 2000). Although the water-equilibration test may have allowed a small opportunity for atmospheric water vapor to exchange with equilibrated labile hydrogen, the consistency between standard values determined in this experiment with those determined by equilibration of keratin argues against significant exchange having occurred and confirms the use of these standard values.

Additionally, the 9 to 10% labile hydrogen that we calculated is similar to Motz's (2000) result of 11% at 0°C. δD_n values of samples were determined using δD_n values of standards determined by air-equilibration with keratin standards. A critical assumption is that subfossil solvent-extracted guano has a similar percentage of labile hydrogen. To test this assumption, ten repeat measurements on selected samples over a range of δD values were made over a year apart. All repeat measurements, corrected using guano and grasshopper chitin standards, were within reported analytical precision.

RADIOCARBON DATING

Two bulk guano (BG) samples were taken at the time the sequence was collected, one sample at the surface (96-02) and a second sample at 1.3 meters depth within the deposit (96-03) (corresponding to the surface and end of section 96-04), and sent for AMS radiocarbon dating at Beta Analytic. At a later time, and after initial examination of $\delta^{13}C$ values analyzed from Pass 1, seven additional samples were taken from selected depths from both cores 96-04 and 96-05 and sent to Gliwice Radiocarbon Laboratory for AMS radiocarbon measurement on BG. Because significant age reversals were noted (Fig. 3), we later submitted 11 dates to Rafter Laboratory on the solvent-extracted guano fraction to test the reliability and reproducibility of ^{14}C ages on different extracts. Samples from the deeper part of core 96-05 were often low in carbon, as organic material was much reduced in this section, so several samples from this core were near the limit of sample-size requirements.

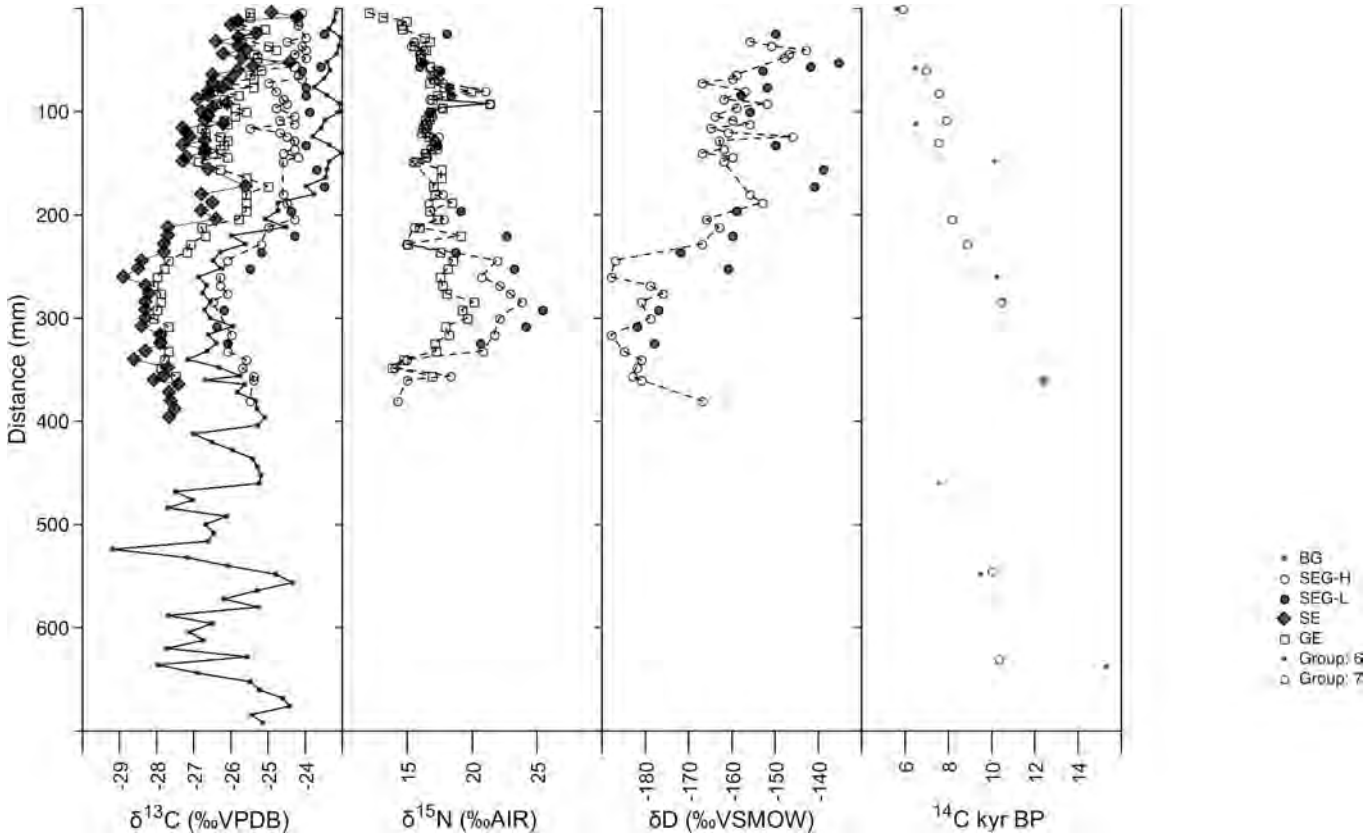

Figure 3. Comparison of stable isotope profiles of various extracts from guano deposit recovered from Bat Cave, Grand Canyon, USA. Stable isotope values for bulk guano (BG); guano extract (GE); solvent extract (SE), solvent extracted guano (SEG_H; and SEG_L). See text for extraction methods.

Results

Isotope Profiles, and Elemental Ratios, and Infrared Spectroscopy

All extracts have $\delta^{13}C$ values that strongly covary with each other and with δD values, suggesting that a primary isotope signal is recoverable from guano material (Table 2; Fig. 3). $\delta^{15}N$ values of solvent-extracted guano samples SEG_L and SEG_H are less strongly covariant with δD and $\delta^{13}C$ values. However, only $\delta^{15}N$ values of guano extract (GE) are not significantly related to any other isotope profile, remaining relatively consistent throughout the core. $\delta^{15}N$ values of GE and SEG profiles are similar for much of the core, but differ from 196 to 332 mm. In this location, the solvents appear to have incorporated nitrogen-bearing compounds that were preferentially depleted in ^{15}N in solvent-extract samples. The resulting pattern shows a large increase in $\delta^{15}N$ values at a time where $\delta^{13}C$ and δD values are most negative.

$\delta^{13}C$ values from bulk guano (BG) are more positive than those from equivalent GE samples. Measurements of $\delta^{13}C$ values from the same aliquot of material have more negative $\delta^{13}C$ values by 1 to 2‰, indicating that there is some fractionation of the sample associated with either density separation or particle size. Of the separated extracts, $\delta^{13}C$ values of SE are the most negative, however, $\delta^{13}C$ values of GE are close to those of the SE, indicating a high lipid content in these samples. Separation of SEG into SEG_L and SEG_H indicates that SEG_L $\delta^{13}C$ values are more positive by about 0.5‰ than equivalent SEG_H samples. Likewise, δD values were approximately 5‰ higher for SEG_L than SEG_H samples.

In general, greatly increased %C and %N of separated extracts confirms that organic matter was concentrated in the floatant, increasing in amounts from 1 to 10% in the case of carbon, and thereby, also enabling nitrogen isotope analysis of the material. However, these results also indicate that not all mineral matter was removed by the density separation. Samples were split for different extracts and isotope analyses, requiring that only small amounts of material could be used for each measurement. Although isotope analyses were generally reproducible at acceptable precisions, amount percents were not as reproducible. In particular, %N for many samples was small, ranging from 0.6 to 4.0%, with an average of 1.6%. The case was similar for %H, which ranged from 0.6 to 2.5%, with an average of 1.3%. To determine if isotopic values are a result of varying organic components, C:N and N:H ratios were compared

Table 2. Regression statistics among stable isotope profiles and elemental ratios for various extracts from a guano deposit recovered from Bat Cave, Grand Canyon, USA.

Guano Extract	Covariate 1	Covariate 2	*F* Value	n	*R*
Pre-Transition					
	$\delta^{13}C_{GE}$	$\delta^{13}C_{SEG}$	259.91[a]	1, 40	0.93
	$\delta^{13}C_{GE}$	$\delta^{13}C_{SE}$	214.65[a]	1, 39	0.91
	$\delta^{13}C_{SEG}$	$\delta^{13}C_{SE}$	217.34[a]	1, 43	0.90
	δD_{SEG}	$\delta^{13}C_{SEG}$	71.26[a]	1, 39	0.75
	$\delta^{15}N_{GE}$	$\delta^{15}N_{SEG}$	68.20[a]	1, 35	0.81
Pre-Transition					
	$\delta^{13}C_{SEG}$	δD_{SEG}	7.85[b]	1, 20	0.51
Transition					
	$\delta^{13}C_{SEG}$	δD_{SEG}	36.2[a]	1, 6	0.93
Post-Transition					
	$\delta^{13}C_{SEG}$	δD_{SEG}	10.99[a]	1, 9	0.83
All Samples					
	C:N	$\delta^{13}C_{GE}$	208.38[a]	1, 59	−0.88
	C:N	$\delta^{13}C_{SEG}$	0.13	1, 38	−0.07
	N:H	$\delta^{13}C_{SEG}$	4.56	1, 34	0.4
	C:N	δD_{SEG}	0.93	1, 38	0.05
	N:H	δD_{SEG}	2.77	1, 34	0.28
Transition					
	C:N	$\delta^{13}C_{SEG}$	0.01	1, 6	−0.47
	C:N	δD_{SEG}	1.00	1, 6	−0.38
	N:H	$\delta^{13}C_{SEG}$	0.93	1, 6	0.37
	N:H	δD_{SEG}	0.99	1, 6	0.38

[a] Significant at or beyond 0.001.
[b] Significant at or beyond 0.025.
Note: Subscripts refer to extraction types (see text for methods) Guano Extract (GE), Solvent Extracted High-C:N Guano (SEG), Solvent Extract (SE).

to $\delta^{13}C$ and δD values (Table 2). Carbon-13 values of the GE have a strong and significant relationship with C:N ratios. However, $\delta^{13}C$ values of the SEG did not have a significant relationship with C:N and N:H ratios. Samples with C:N ratios between 6 and 8, and N:H ratios below 2.5 had no significant relationship with $\delta^{13}C$ nor δD values (Table 2). To further test the effect of diagenesis on the SEG_H, C:N and N:H ratios were grouped into several subdivisions based on a large transition in $\delta^{13}C$, δD, and $\delta^{15}N$ values that occurred from 260 to 150 mm in section 96-04: (1) prior to this transition, (2) within this transition, and (3) after this transition. Neither C:N nor N:H ratios were significantly different among these time periods (Kruskal-Wallis test, $H = 1.58$, $p = 0.45$; $H = 1.85$, $p = 0.40$, respectively), supporting the interpretation that this large isotopic change did not occur due to diagenesis.

Relative to the reference spectrum of *n*-acetyl-*d*-glucosamine, Fourier-transform infrared spectroscopy of fresh bat guano shows a broadening of the IR bands, typical in natural polymers (Duarte et al., 2002). The spectra of both modern comparison materials demonstrated a range of signals relating to the molecular structure of chitin (Fig. 4). Bands at 3448, 3269, and 2934 cm^{-1} represent OH stretching and symmetric NH stretching in secondary amides, respectively, while CH symmetric and asymmetric stretching vibrations were observed between 2828 and 2962 cm^{-1} (Seoudi et al., 2005). Detailed information is contained in the fingerprint region at 900–1700 cm^{-1}. Here, bands at 1653 and 1557 cm^{-1} relate to CO stretching in amide I and N–H deformation of amine II, and at 1381 cm^{-1} to CH bending vibration in chitin (Van de Velde and Kiekens, 2004; Seoudi et al., 2005). Finally, bands at 1030 to 1156 cm^{-1} are diagnostic for ring and bridge C-O-C vibrations in the saccharide monomer (Duarte et al., 2002). The IR spectra of SEG (subfossil bat guano on Figure 4) contained a lower range of signals, which are much broader than the modern samples, but the position of these signals corresponds to the bands that characterize the chitin macromolecule. The merging of bands in the region 1550 to 1690 cm^{-1} indicates a higher degree of deacetylation in SEG than in modern material, while distinct peaks at 1030 to 1156 cm^{-1} are replaced by a broad signal with discernable peaks at 1030 and 1076 cm^{-1}, suggesting partial break up of the polysaccharide structure and rupture of the β-glycosidic-linkages. Overall, the infrared spectra of SEG appear diagnostic of significantly degraded chitin, as reported previously (Wanjun et al., 2005).

RADIOCARBON DATES

Radiocarbon dates do not increase monotonically on bulk guano (BG) samples taken from both sections 96-05

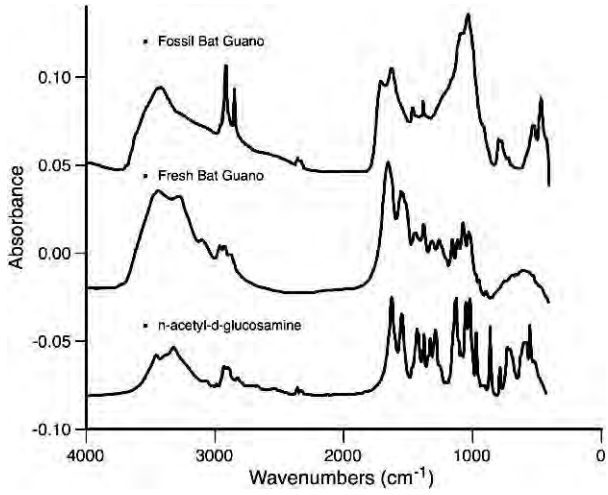

Figure 4. Comparison of infrared spectra of subfossil guano (DAM 96-02), fresh bat guano, and *n*-acetyl-*d*-glucosamine (top to bottom) showing major chitin peaks preserved in subfossil guano.

and 96-04, and thus a reliable chronology cannot be developed for the entire sequence (Table 3; Fig. 3). Two dates from section 96-05 are conspicuously young, and several dates from 58 to 262 mm suggest periods of rapid deposition separated by a hiatus (Table 3, Fig. 3). However, a second set of ^{14}C ages on solvent extracted guano from section 96-04 displayed a more linear deposition rate. Deeper in the deposit, two SEG radiocarbon measurements from core 96-05 also appear to suffer from contamination. These samples are likely to have suffered from small quantities of carbon submitted and are thus more likely to have been contaminated. Moreover, more than seven separate solvent washes were performed on these samples, because coloration of the solvent indicated a high and consistent presence of lipid components, and it is unlikely that all lipids were removed. Many BG dates are similar to SEG dates, again suggesting broad reliability. One measurement from section 96-05 (15,300 ± 100 ^{14}C yr BP uncalibrated, sample GdA-322) suggests a continued relatively linear deposition rate when compared with SEG radiocarbon measurements from section 96-04.

Discussion

$\delta^{13}C$, δD, and $\delta^{15}N$ Values of Guano Extracts

$\delta^{13}C$ values on all extracts show a similar pattern and are strongly covariant (Table 2). δD values measured on the solvent-extracted guano also exhibit a similar pattern with strong covariation. In particular, each isotopic profile displays a distinct stepwise increase between approximately 260 and 150 mm. The similarity and especially the timing of this transition in each isotopic profile, regardless of chemical fraction, argues that this rise is an environmental signal and not a diagenetic effect. Mizutani and Wada (1988) found little overall fractionation in $\delta^{13}C$ during soil organic matter decomposition, in stark contrast to $\delta^{15}N$ values. In this study, $\delta^{15}N$ values are relatively constant, but more positive than the originally deposited guano based on $\delta^{15}N$ values of modern guano (Wurster et al., 2007). This finding is consistent with post-depositional modification to isotopic composition associated with volatilization of ammonia, described previously for seabird guano (Mizutani and Wada, 1988). Although we expected δD values to be more prone to error, there was strong covariation between δD values and $\delta^{13}C$ values. Some contamination was expected from hydrogen released from a residual mineral component because samples were not completely organic. Nonetheless, the strong correlation between δD and $\delta^{13}C$ indicates that the δD profile is not overly influenced by degradation or contamination, with large changes (over 50‰) in δD values that are likely attributable to environmental effects.

Diagenesis and Elemental Ratios

The guano-extract fraction had $\delta^{13}C$ values similar to the solvent-extract fraction, with values strongly correlated with C:N. However, after a complete solvent wash, there was a lack of significant covariation between $\delta^{13}C$ values and C:N ratios of solvent-extracted guano. To further test influence of diagenesis, a nonparametric Kruskal-Wallis test was performed by splitting C:N and N:H ratios in three groups: pre-transition, transition, and post-transition (see results section for definitions). No significant difference was found between these groups and C:N and N:H ratios. $\delta^{13}C$ values are expected to covary with elemental ratios in part because natural chitin is tightly bound to protein and partially de-acetylated, especially in sclerotized insect cuticles (Schimmelmann and DeNiro, 1986a). Both serve to decrease the C:N ratio from the 6.9 value of theoretical *n*-acetyl-*d*-glucosamine. The presence of lipids, however, will serve to increase the C:N ratio. Both the acetyl group of chitin and lipids have more negative $\delta^{13}C$ values compared to the *n*-acetyl-*d*-glucosamine polysaccharide (Schimmelmann and DeNiro, 1986a). Therefore, chemical changes should invariably lead to strong correlations between elemental ratios and isotope values. Because the cores are retrieved from a bat guano cave, insectivorous bat guano is dominantly composed of finely comminuted insect exoskeletons (McFarlane et al., 2002), and the C:N and N:H ratios are close to those of theoretical chitin. It follows that the solvent-extracted guano represents natural chitin from insects deposited by bats through the Holocene, albeit with much of the protein degraded. This was confirmed by the infrared spectra. Therefore, we conclude that $\delta^{13}C$ and δD values of both extracts are reliable for environmental interpretation, but confidence increases when selecting only samples within a narrow C:N range.

Table 3. Subfossil guano samples submitted for radiocarbon dating.

Sample Name	Extract	Conventional ^{14}C age (yr BP ± 1 σ)	Laboratory Number	Laboratory
96-02	BG	5620 ± 70	Beta #95152	Beta Analytic
96-02	SEG	5881 ± 35	NZA 27606	GNS
Section 96-04				
56–60 mm	BG	6490 ± 50	GdA-494	Gliwice
58–62 mm	SEG	6957 ± 35	NZA 27608	GNS
80–84 mm	SEG	7550 ± 50	GdA-696	Gliwice
100–106 mm	SEG	7872 ± 35	NZA 27609	GNS
108–116 mm	BG	6530 ± 35	GdA-540	Gliwice
128–132 mm	SEG	7530 ± 40	GdA-695	Gliwice
144–152 mm	TOC	10130 ± 60	GdA-319	Gliwice
202–206 mm	SEG	8151 ± 35	NZA 27607	GNS
226–230 mm	SEG	8858 ± 35	NZA 28163	GNS
256–264 mm	BG	10230 ± 60	GdA-321	Gliwice
280–288 mm	SEG	10438 ± 45	NZA 27626	GNS
96-03	BG	12400 ± 90	Beta #95153	Beta Analytic
96-03	SEG	12371 ± 55	NZA 27627	GNS
Section 96-05				
96–104 mm	BG	7550 ± 40	GdA-318	Gliwice
180–190 mm	SEG	9991 ± 45	NZA 27628	GNS
184–192 mm	BG	9490 ± 50	GdA-320	Gliwice
270–280 mm	SEG	10323 ± 45	NZA 27629	GNS
274–280 mm	BG	15300 ± 100	GdA-322	Gliwice

Note: A guano sequence was collected in sections. 96-02 refers to a surface sample, Section 96-04 refers to a 1 m PVC pipe driven into the guano sediment, 96-03 refers to a sample collected after section 96-04 was removed, and section 96-05 refers to a second 1 m PVC pipe driven into the sequence at depth. Depths are internally consistent to the section.

Radiocarbon Dates

Washing samples with an alkaline treatment resulted in a large reduction in retrieved organic matter, and therefore, initially only acid treatment, as used in the preparation of bulk guano (BG) samples, was employed at Gliwice radiocarbon facilities. Alkaline treatment is used to remove organics that are considered more mobile, and BG samples should be considered potentially problematic. Later, we investigated the reliability of solvent-extracted guano (SEG) for radiocarbon measurement, because two independent studies had found only acid/solvent treatment necessary to obtain radiocarbon dates on insect cuticles that were consistent with radiocarbon dates on more traditional substances (peat/cellulose) in a well-constrained depositional environment (Hodgins et al., 2001; Tripp et al., 2004). Such a protocol substantially improved our confidence in the chronology, where only one reversal was noted for the upper section (96-04). Although $\delta^{13}C$ values of all fractions we investigated covaried, it may be that a large part of the lipid fraction is contaminated by younger carbon, consistent with its possible diagenetic origin (Briggs, 1999). Further work in tropical guano sequences has suggested improved sample extraction methods that can yield more reliable radiocarbon measurements (Wurster et al., 2009, 2010). Wurster et al. (2009) suggested a radiocarbon pre-treatment for cave guano that included solvent washing and alkaline treatment. They found young-carbon contamination on material that was assumed to be dead on solvent extraction, whereas radiocarbon measurements on SEG and BG with traditional ABA processing from that same material were found to be within 1-sigma error of background. Together these results suggest that in addition to an acid wash, solvent extraction and alkaline treatment should be preformed prior to radiocarbon measurements.

Radiocarbon measurements of SEG from the upper section, 96-04, are considered reliable. However, dates of one BEG and two SEG samples are younger than the radiocarbon measurement from sample 96-03 taken between sections 96-04 and 96-05, leaving only one out of four radiocarbon measurements from core 96-05 older with depth when compared with the 96-04 core. Importantly, there was a large decrease in %C for samples from the lower part of 96-05. Carbon abundances of samples taken throughout the sequence tended to decrease with depth, and so samples from section 96-04 were generally >10%, whereas samples taken from 96-05 were generally below <1%. We consider the radiocarbon measurements on samples with such low carbon abundances to be problematic. Moreover, several lines of reasoning suggest that 96-05 is older than section 96-04: (1)

Carbon abundances tended to decrease with depth, (2) similar $\delta^{13}C$ values of different fractions between end samples of section 96-04 and the beginning section of 96-05 suggest a continuation of the sequence, and (3) Section 96-05 is deeper in the sequence. Taken independently, radiocarbon measurements of section 96-05 can be interpreted as a Holocene section, but the low carbon abundances and distinct $\delta^{13}C$ values (more variable and lower than section 96-04), and depth in the deposit argue against this interpretation. Although, the guano might deform and flow with depth, it is more likely that the radiocarbon measurements are compromised in this deeper section. Thus, we interpret section 96-05 as being late Pleistocene, but cannot provide a better age estimation.

Climate Interpretation Inferred from Stable Isotope Profiles of Bat Guano Deposits

We have previously presented an interpretation of environmental change using $\delta^{13}C$ and δD values of SEG_H part of the solvent-extracted guano (Wurster et al., 2008) from core 96-04. Below, we expand this interpretation by including $\delta^{15}N$ values and extending the $\delta^{13}C$ profile to include the deeper section (96-05). $\delta^{13}C$ values of insect chitin are dependent on the animal's diet (Schimmelmann and DeNiro, 1986b); (Webb et al., 1998). *Tadarida brasiliensis* is an opportunistic feeder, and has been demonstrated to have dietary insect ratios in the same proportion as local availability (Lee and McCracken, 2002). Wurster et al. (2007) demonstrated $\delta^{13}C$ values of insectivorous bats to be a strong predictor of modeled C_4 grass abundance in the western United States. Therefore, $\delta^{13}C$ values of bat guano-derived chitin reflect local vegetation, and any excursions in $\delta^{13}C$ values of subfossil guano will be directly related to changes in average $\delta^{13}C$ values of local vegetation, in turn reflecting local climatic conditions.

δD values of chitin reflect both metabolic and drinking-water sources of insects, and they are correlated with δD values in local precipitation and mean annual temperature (Gröcke et al., 2006). In the Grand Canyon, δD values of the Colorado River are lower than those from regional precipitation (Coplen and Kendall, 2000), reflecting higher latitude and altitude sources in its upper catchment. The total variation in δD values of SEG_H is over 50‰, and this cannot be accounted for solely by a change in mean temperature (e.g., Miller et al., 1988). Instead, changing δD values of subfossil bat guano likely indicates a change in source or seasonality of precipitation or in plant water-use preference. Higher δD values of SEG_H are expected from a greater summer precipitation fraction (more relative monsoonal moisture). Additionally, changing plant preference for summer δD values may be incorporated in the signal, which would likely occur if there were an increase in the relative abundance of C_4 vegetation (Schwinning et al., 2002, 2003). Therefore, higher δD values reflect one or more of higher temperatures, lower humidity, and higher summer precipitation fraction. Coeval increases in $\delta^{13}C$ and δD values are thought to reflect increased monsoonal activity (Wurster et al., 2007, 2008).

We previously interpreted environmental change using SEG_H $\delta^{13}C$ and δD isotope profiles from core 96-04 (ca. 5,000 to 12,000 ^{14}C yr BP) (Wurster et al., 2008). Grand Canyon climate was interpreted to be cool and possibly drier during the Younger Dryas stade, but modern monsoonal conditions arrived gradually by 9 calibrated ka BP. $\delta^{15}N$ values of chitin have been linked to arthropod trophic level and diet (Schimmelmann et al., 1998), therefore changing $\delta^{15}N$ values of bat guano through time may broadly indicate changing dietary sources and trophic level. Relatively high $\delta^{15}N$ values are not uncommon in semi-arid regions. Modern bat guano $\delta^{15}N$ values are reported to be 14 to 20‰ in New Mexico, USA, and Sonora, Mexico (Mizutani et al., 1992a; McFarlane et al., 1995), and $\delta^{15}N$ values of bat muscle tissue are 15 to 20‰ in arid regions of Venezuela (Nassar et al., 2003). Mammals in more arid regions typically have higher $\delta^{15}N$ values (e.g., Sealy et al., 1987), possibly through an increased recycling of body nitrogen with increased water conservation (e.g., Sponheimer et al., 2003). Although, comparatively little work has been done on insect $\delta^{15}N$ values, increased $\delta^{15}N$ values may be linked with increasing aridity. $\delta^{15}N$ values of solvent-extracted guano show a large increase in $\delta^{15}N$ values at a time when $\delta^{13}C$ and δD values are most negative. Although δD values are generally more negative below relative to above 228 mm, there is a relative increase from 268 to 300 mm where $\delta^{15}N$ values are maximal, and radiocarbon measurements indicate this depositional period to be coincident with the Younger Dryas stade. If higher $\delta^{15}N$ values of SEG_H are a reflection of moisture stress, then these data can be interpreted as additional support for Wurster et al.'s (2008) contention of a drier Younger Dryas stade in the Grand Canyon interpreted from an increase in δD values at this time.

Although complete confidence in radiocarbon dates is lacking for core 96-05, the available evidence suggests this guano deposit captures a period greater than ~12.4 ^{14}C ka and extends into the late Pleistocene. Below 400 cm, $\delta^{13}C$ values from bulk guano are lower and more variable then above. Unfortunately, radiocarbon results from low-%C samples are less reliable and limit our current ability to further interpret climate change beyond 12.4 ^{14}C ka. However, previous studies in the region using other proxies have found the late Pleistocene to be cooler and wetter, but these studies provide only low-resolution data (Thompson et al., 1993; Cole and Arundel, 2005). We plan further investigation of the bat guano deposit reported on in this study, which may yet yield a sequential record of climate change to better understand Late Pleistocene and possibly LGM climate.

Conclusions

Diagenesis does not appear to have significantly masked an interpretable environmental signal in $\delta^{13}C$ or

δD profiles of bulk guano, guano extract, solvent-extracted guano, or solvent extract from this long-term guano deposit in the southwestern US. Although diagenetic influences cannot be completely ruled out, both the covariations among various extracts and the lack of significant covariation between elemental ratios and isotope values for the extracts, as well as the lack of significant differences between elemental ratios and age attest to a lack of significant diagenetic influence. Solvent-extracted guano with C:N ratios within a limited range is the best chemical fraction for detailed analysis, because elemental ratios in the material can be used as a guide to the likelihood of diagenesis or contamination. Solvent extracts may be bacterially and/or post-depositionally derived, although the strong and significant covariation with the SEG, at least for $\delta^{13}C$ values, suggests that the SE may nonetheless be a satisfactory material for rapid analysis. $\delta^{13}C$ values of the GE fractions are the most unreliable, because they tend to be unduly influenced by the proportion of lipids present, but despite this complication, the large changes observed in this fraction are still broadly related to environmental change. Although radiocarbon dates on BG are not necessarily reliable and a definitive protocol still needs to be developed in order to provide full confidence in the chronology of the deeper sections of the core, we conclude in general terms that climate in the Grand Canyon during the latest Pleistocene was cooler and wetter, with more variability than was the case during the Holocene.

ACKNOWLEDGEMENTS

We thank A. Zazzo, E. Dufour, and A. Deifendorf for discussions, and are grateful to R. Keeler and A. Fincham for assistance in the field and T. Prokopiuk, J. Scott, S. Francis, I. González-Alvarez, and Kelly Sutton for analytical assistance. Geological Society of America, National Speleological Society, Syracuse University, Sigma Xi, Karst Research Grant, and NERC Large Grant NE/D001501 supported this research. The guano core was collected under a National Parks permit to D. A. McFarlane.

REFERENCES

Bird, M.I., Boobyer, E.M., Bryant, C., Lewis, H.A., Paz, V., and Stephens, W.E., 2007, A long record of environmental change from bat guano deposits in Makangit Cave, Palawan, Philippines: Earth and Environmental Science Transactions of the Royal Society of Edinburgh, v. 98, p. 59–69.

Bowers, J.E., Webb, R.H., and Pierson, E.A., 1997, Succession of desert plants on debris flow terraces, Grand Canyon, Arizona, USA: Journal of Arid Environments, v. 36, p. 67–86.

Briggs, D.E.G., 1999, Molecular taphonomy of animal and plant cuticles: selective preservation and diagenesis: Philosophical Transactions of the Royal Society B: Biological Sciences, v. 354, p. 7–17.

Carrión, J.S., Scott, L., and Marais, E., 2006, Environmental implications of pollen spectra in bat droppings from southeastern Spain and potential for palaeoenvironmental reconstructions: Review of Palaeobotany and Palynology, v. 140, p. 175–186.

Cole, K.L., and Arundel, S.T., 2005, Carbon isotopes from fossil packrat pellets and elevational movements of Utah agave plants reveal the Younger Dryas cold period in Grand Canyon, Arizona: Geology, v. 33, p. 713–716.

Constantine, D.G., 1970, Bats in relation to the health, welfare, and economy of man: Biology of Bats, v. 2, p. 319–449.

Coplen, T.B., and Kendall, C., 2000, Stable hydrogen and oxygen isotope ratios for selected sites of the U.S. Geological Survey's NASQAN and benchmark surface-water networks: U.S. Geological Survey, Open-File Report 00–160, p. 38–44.

Des Marais, D.J., Mitchell, J.M., Meinschein, W.G., and Hayes, J.M., 1980, The carbon isotope biogeochemistry of the individual hydrocarbons in bat guano and the ecology of the insectivorous bats in the region of Carlsbad, New Mexico: Geochimica et Cosmochimica Acta, v. 44, p. 2075–2086.

Duarte, M.L., Ferreira, M.C., Marvão, M.R., and Rocha, J., 2002, An optimised method to determine the degree of acetylation of chitin and chitosan by FTIR spectroscopy: International Journal of Biological Macromolecules, v. 31, p. 1–8.

Ehleringer, J.R., Cerling, T.E., and Helliker, B.R., 1997, C_4 photosynthesis, Atmospheric CO_2, and climate: Oecologia, v. 112, p. 285–299.

Gröcke, D.R., Schimmelmann, A., Elias, S., and Miller, R.F., 2006, Stable hydrogen-isotope ratios in beetle chitin: preliminary European data and re-interpretation of North American data: Quaternary Science Reviews, v. 25, p. 1850–1864.

Hodgins, G.W.L., Thorpe, J.L., Coope, G.R., and Hedges, R.E.M., 2001, Protocol development for purification and characterization of subfossil insect chitin for stable isotopic analysis and radiocarbon dating: Radiocarbon, v. 43, p. 199–208.

Jeuniaux, C., 1971, Chitinous structures, *in* Florkin, M., and Stotz, E., eds., Comprehensive biochemistry, v. 26C, Amsterdam, Elsevier, p. 595–632.

Koopman, K.F., 1982, Biogeography of the bats of South America, *in* Mares, A.A., and Genoways, H., eds., Mammalian biology in South America, Special Publications, Pymatuning Laboratory of Ecology, University of Pittsburgh, v. 6, p. 273–302.

Lee, Y.F., and McCracken, G.F., 2002, Foraging activity and food resource use of Brazilian free-tailed bats, *Tadarida brasiliensis* (Molossidae): Ecoscience, v. 9, p. 306–313.

Maher, L.J., 2006, Environmental information from guano palynology of insectivorous bats of the central part of the United States of America: Palaeogeography, Palaeoclimatology, Palaeoecology, v. 237, p. 19–31.

McFarlane, D.A., Keeler, R.C., and Mizutani, H., 1995, Ammonia volatilization in a Mexican bat cave ecosystem: Biogeochemistry, v. 30, p. 1–8.

McFarlane, D.A., Lundberg, J., and Fincham, A.G., 2002, A late Quaternary paleoecological record from caves of southern Jamaica, West Indies: Journal of Cave and Karst Studies, v. 64, p. 117–125.

Miller, R.F., Fritz, P., and Morgan, A.V., 1988, Climatic implications of D/H ratios in beetle chitin: Palaeogeography, Palaeoclimatology, Palaeoecology, v. 66, p. 277–288.

Mizutani, H., McFarlane, D.A., and Kabaya, Y., 1992a, Carbon and nitrogen isotopic signatures of bat guanos as a record of past environments: Mass Spectroscopy, v. 40, p. 67–82.

Mizutani, H., McFarlane, D.A., and Kabaya, Y., 1992b, Nitrogen and carbon isotope studies of a bat guano core from Eagle Creek Cave, Arizona, USA: Mass Spectrometry, v. 40, p. 57–65.

Mizutani, H., and Wada, E., 1988, Nitrogen and carbon Isotope ratios in seabird rookeries and their ecological Iimplications: Ecology, v. 69, p. 340–349.

Motz, J.E., 2000, Oxygen and hydrogen isotopes in fossil insect chitin as paleoenvironmental indicators [PhD dissertation]: Waterloo, University of Waterloo, 152 p.

Nassar, J.M., Beck, H., Sternberg, L.S.L., and Fleming, T.H., 2003, Dependence on cacti and agaves in nectar-feeding bats from Venezuelan arid zones: Journal of Mammalogy, v. 84, p. 106–116.

Paruelo, J.M., and Lauenroth, W.K., 1996, Relative abundance of plant functional types in grasslands and shrublands of North America: Ecological Applications, v. 6, p. 1212–1224.

Pinder, III, J.E., and Kroh, G.C., 1987, Insect herbivory and photosynthetic pathways in old-field ecosystems: Ecology, v. 68, p. 254–259.

Schimmelmann, A., 1991, Determination of the concentration and stable isotopic composition of nonexchangeable hydrogen in organic matter: Analytical Chemistry, v. 63, p. 2456–2459.

Schimmelmann, A., and DeNiro, M.J., 1986a, Stable isotopic studies on chitin, measurements on chitin/chitosan isolates and d-glucosamine hydrochloride from chitin, *in* Muzzarelli, R., Jeuniauz, C., and Gooday, G., eds., Chitin in nature and technology, New York, Plenum, p. 357–364.

Schimmelmann, A., and DeNiro, M.J., 1986b, Stable isotopic studies on chitin. II: The $^{13}C/^{12}C$ and $^{15}N/^{14}N$ ratios in arthropod chitin: Contributions in Marine Science, v. 29, p. 113–130.

Schimmelmann, A., DeNiro, M.J., Poulicek, M., Voss-Foucart, M.F., Goffinet, G., and Jeuniaux, C., 1986, Stable isotope composition of chitin from arthropods recovered in archaeological contexts as palaeoenvironmental indicators: Journal of Archaeological Science, v. 13, p. 553–566.

Schimmelmann, A., Miller, R.F., and Leavitt, S.W., 1993, Hydrogen isotopic exchange and stable isotope ratios in cellulose: Wood, chitin, and amino compounds: Geophysical Monograph-American Geophysical Union, v. 78, p. 367–367.

Schimmelmann, A., Wintsch, R.P., Lewan, M.D., and DeNiro, M.J., 1998, Chitin: Forgotten source of nitrogen: From modern chitin to thermally mature kerogen: Lessons from nitrogen isotope ratios, *in* Stankiewicz, B.A., and van Bergen, P.F., eds., Nitrogen-containing macromoleculesin the biosphere and geosphere, ACS Symposium Series 707, Washington, D.C., American Chemical Society, p. 226–242.

Schwinning, S., Davis, K., Richardson, L., and Ehleringer, J.R., 2002, Deuterium enriched irrigation indicates different forms of rain use in shrub/grass species of the Colorado Plateau: Oecologia, v. 130, p. 345–355.

Schwinning, S., Starr, B.I., and Ehleringer, J.R., 2003, Dominant cold desert plants do not partition warm season precipitation by event size: Oecologia, v. 136, p. 252–260.

Sealy, J.C., van der Merwe, N.J., Lee-Thorp, J.A., and Lanham, J.L., 1987, Nitrogen isotopic ecology in southern Africa: implications for environmental and dietary tracing: Geochimica et Cosmochimica Acta, v. 51, p. 2707–2717.

Seoudi, R., Nada, A.M.A., Elmongy, S.A., and Hamed, S.S., 2005, Fourier transform infrared spectroscopic and AC electrical conductivity studies of chitin and its derivatives: Journal of Applied Polymer Science, v. 98, p. 936–943.

Shahack-Gross, R., Berna, F., Karkanas, P., and Weiner, S., 2004, Bat guano and preservation of archaeological remains in cave sites: Journal of Archaeological Science, v. 31, p. 1259–1272.

Sponheimer, M., Robinson, T., Ayliffe, L., Roeder, B., Hammer, J., Passey, B., West, A., Cerling, T., Dearing, D., and Ehleringer, J., 2003, Nitrogen isotopes in mammalian herbivores: hair $\delta^{15}N$ values from a controlled feeding study: International Journal of Osteoarchaeology, v. 13, p. 80–87.

Stankiewicz, B.A., Briggs, D.E.G., Evershed, R.P., Flannery, M.B., and Wuttke, M., 1997, Preservation of chitin in 25-million-year-old fossils: Science, v. 276, 1541 p.

Stankiewicz, B.A., Poinar, H.N., Briggs, D.E.G., Evershed, R.P., and Poinar, G.O., 1998, Chemical preservation of plants and insects in natural resins, *in* Proceedings, Biological Sciences, v. 265, p. 641–647.

Thompson, R.S., Whitlock, C., Bartlein, P.J., Harrison, S.P., and Spaulding, W.G., 1993, Climatic changes in the western United States since 18,000 yr BP, *in* Wright, H.E. Hr., Kutzbach, J.E., Webb, III, T., Ruddiman, W.F., Street-Perrott, F.A., and Bartlein, P.J., eds., Global climates since the last glacial maximum, Minneapolis, University of Minnesota Press, p. 468–513.

Tripp, J.A., Higham, T.F.G., and Hedges, R.E.M., 2004, A pretreatment procedure for the AMS radiocarbon dating of sub-fossil insect remains: Radiocarbon, v. 46, p. 147–154.

Van de Velde, K., and Kiekens, P., 2004, Structure analysis and degree of substitution of chitin, chitosan and dibutyrylchitin by FT-IR spectroscopy and solid state ^{13}C NMR: Carbohydrate Polymers, v. 58, p. 409–416.

Wanjun, T., Cunxin, W., and Donghua, C., 2005, Kinetic studies on the pyrolysis of chitin and chitosan: Polymer Degradation and Stability, v. 87, p. 389–394.

Warren, P.H., and Gaston, K.J., 1992, Predator-prey ratios: A special case of a general pattern?: Royal Society of London B, v. 338, p. 113–130.

Wassenaar, L.I., and Hobson, K.A., 2000, Improved method for determining the stable-hydrogen isotopic composition (δD) of complex organic materials of environmental interest: Environmental Science and Technology, v. 34, p. 2354–2360.

Wassenaar, L.I., and Hobson, K.A., 2003, Comparative equilibration and online technique for determination of non-exchangeable hydrogen of keratins for use in animal migration studies: Isotopes in Environmental and Health Studies, v. 39, p. 211–217.

Webb, S.C., Hedges, R.E.M., and Simpson, S.J., 1998, Diet quality influences the $\delta^{13}C$ and $\delta^{15}N$ of locusts and their biochemical components: Journal of Experimental Biology, v. 201, p. 2903–2911.

Wilkins, K.T., 1989, *Tadarida brasiliensis*: Mammalian Species, v. 331, p. 1–10.

Wurster, C.M., McFarlane, D.A., and Bird, M.I., 2007, Spatial and temporal expression of vegetation and atmospheric variability from stable carbon and nitrogen isotope analysis of bat guano in the southern United States: Geochimica et Cosmochima Acta, v. 71, p. 3302–3310.

Wurster, C.M., Patterson, W.P., McFarlane, D.A., Wassenaar, L.I., Hobson, K.A., Athfield, N.B., and Bird, M.I., 2008, Stable carbon and hydrogen isotopes from bat guano in the Grand Canyon, USA, reveal Younger Dryas and 8.2 ka events: Geology, v. 36, p. 683–686.

Wurster, C.M., Bird, M.I., Bull, I.D., Bryant, C., and Ascough, P., 2009, A protocol for radiocarbon dating tropical subfossil cave guano: Radiocarbon, v. 51, p. 1–10.

Wurster, C.M., Saiz, G., Calder, A., and Bird, M.I., 2010, Recovery of organic matter from mineral-rich sediment and soils for stable isotope analyses using static dense media: Rapid Communications in Mass Spectrometry, v. 24, p. 165–168.

C.G. Diedrich and J.P. Copeland – Upper Pleistocene *Gulo gulo* (Linné, 1758) remains from the Srbsko Chlum-Komin hyena den cave in the Bohemian Karst, Czech Republic, with comparisons to contemporary wolverines. *Journal of Cave and Karst Studies,* v. 72, no. 2, p. 122–127. DOI: 10.4311/jcks2008pa0070

UPPER PLEISTOCENE *GULO GULO* (LINNÉ, 1758) REMAINS FROM THE SRBSKO CHLUM-KOMIN HYENA DEN CAVE IN THE BOHEMIAN KARST, CZECH REPUBLIC, WITH COMPARISONS TO CONTEMPORARY WOLVERINES

Cajus G. Diedrich[1] and Jeffrey P. Copeland[2]

Abstract: Wolverine bone material is described from the famous Upper Pleistocene cave Srbsko Chlum-Komin in the Bohemian Karst, Czech Republic, along with an overview of recently known Czech sites. The *Gulo gulo* Linné material was found in one of the largest Ice Age spotted-hyena dens in Europe. As a result of non-systematic excavations, the taphonomy is partly unclear. Lower-jaw remains indicate a minimum of three wolverines. Two of the mandibles are cracked, which is most likely the result of carnivore scavenging. The absence of juvenile *G. gulo* suggests possible importation of the wolverines by hyenas *Crocuta crocuta spelaea* Goldfuss.

Introduction

The vertical caves of the Chlum quarry near Srbsko in Central Bohemia, Czech Republic (Fig. 1) provide sediments and bone rich caves ranging from Middle to Upper Pleistocene (Diedrich and Žák, 2006). The most important Upper Pleistocene site in the Bohemian Karst, and arguably in Europe, is the vertical cave Srbsko Chlum-Komin (Fig. 1). During the Upper Pleistocene, the Ice Age spotted hyena *Crocuta crocuta spelaea* (Goldfuss, 1823) is believed to have imported large quantities of prey remains into the Komin Cave, including complete carcasses. This site provides the largest deposit of hyena-den bone material in Europe. A general overview of the fauna was given by Diedrich and Žák, (2006).

Geological and Taphonomical Setting

The Chlum-Komin Cave was originally discovered and poorly excavated between 1958 and 1972, primarily by a local speleoclub, and unfortunately, without documentation. Mammal deposition was first thought to be of trapped animals, animals that dropped into the cave, or bones that washed in (Beneš, 1970). Diedrich and Žák (2006) concluded that a clan of the Late Pleistocene spotted hyena *C. crocuta spelaea* used this cave over generations as their den, as evidenced by the abundant presence of hyena bones or partial skeletons, their coprolite material, and chewed and cracked prey bones. The Komin Cave is more or less sloping and in some parts vertical; the entrance was destroyed by the quarry activities. The Komin is connected to a larger, horizontal cave system. Diedrich and Žák (2006) argued that this chimney did not function as a trap and was clearly accessible to hyenas. The Komin contained 3,569 macromammal bones, most notably 350 remains of hyena bones constituting five partial hyena skeletons, including three juveniles, one adult male, and one adult female. Evidence of crushed hyena long bones indicate hyena cub raising and cannibalism as well (Diedrich and Žák, 2006). Prey remains consisted of Przewalski horse (*Equus ferus przewalskii*, including one embryo skeleton), (Diedrich and Zák, 2006), woolly rhinoceros (*Coelodonta antiquitatis*), steppe bison (*Bison priscus*), reindeer (*Rangifer tarandus*), chamoix (*Rupricapra rupricapra*), ibex (*Capra ibex*), wolf (*Canis lupus*), and the herein detailed wolverine material (*Gulo gulo*) (Fig. 2). Finally, the presence of a two- to three-year-old lioness (*Panthera leo spelaea*) with a skull injury, as well as a lion cub about one year of age (Diedrich, 2009a), may indicate either antagonistic conflicts between hyenas and lions in the cave itself or the importation of these individuals as hyena prey.

Chewing and cracking of bones by hyenas is particularly evident on specimens of woolly rhinoceros and steppe bison, as is evidence of hyena cannibalism (Diedrich and Žák, 2006; Diedrich, 2007). This site was also believed to have been used by common foxes (*Vulpes vulpes*). Tens of thousands of micromammal bones have been identified from fox scat and snowy owl (*Nyctea scandiaca*) pellets in the Komin Cave.

Systematic Palaeontology

Sixteen wolverine bones collected from this cave are housed at the National Museum Prague and Museum of the Bohemian Karst Beroun.

Family *Mustelidae* Swainson, 1835
Genus *Gulo* Pallas, 1780
Gulo gulo (Linné, 1758)

Four mandibles of at least three individual adult-to-senile wolverines are represented (Figs. 3, 4.1–4.4). Two of

[1] Cajus G. Diedrich, PaleoLogic, Nansenstr. 8, D-33790 Halle/Westphalia, Germany; cdiedri@gmx.net
[2] Jeffrey P. Copeland, USDA Forest Service, Rocky Mountain Research Station, 800 E. Beckwith, Missoula, Montana 59801, USA; jpcopeland@fs.fed.us

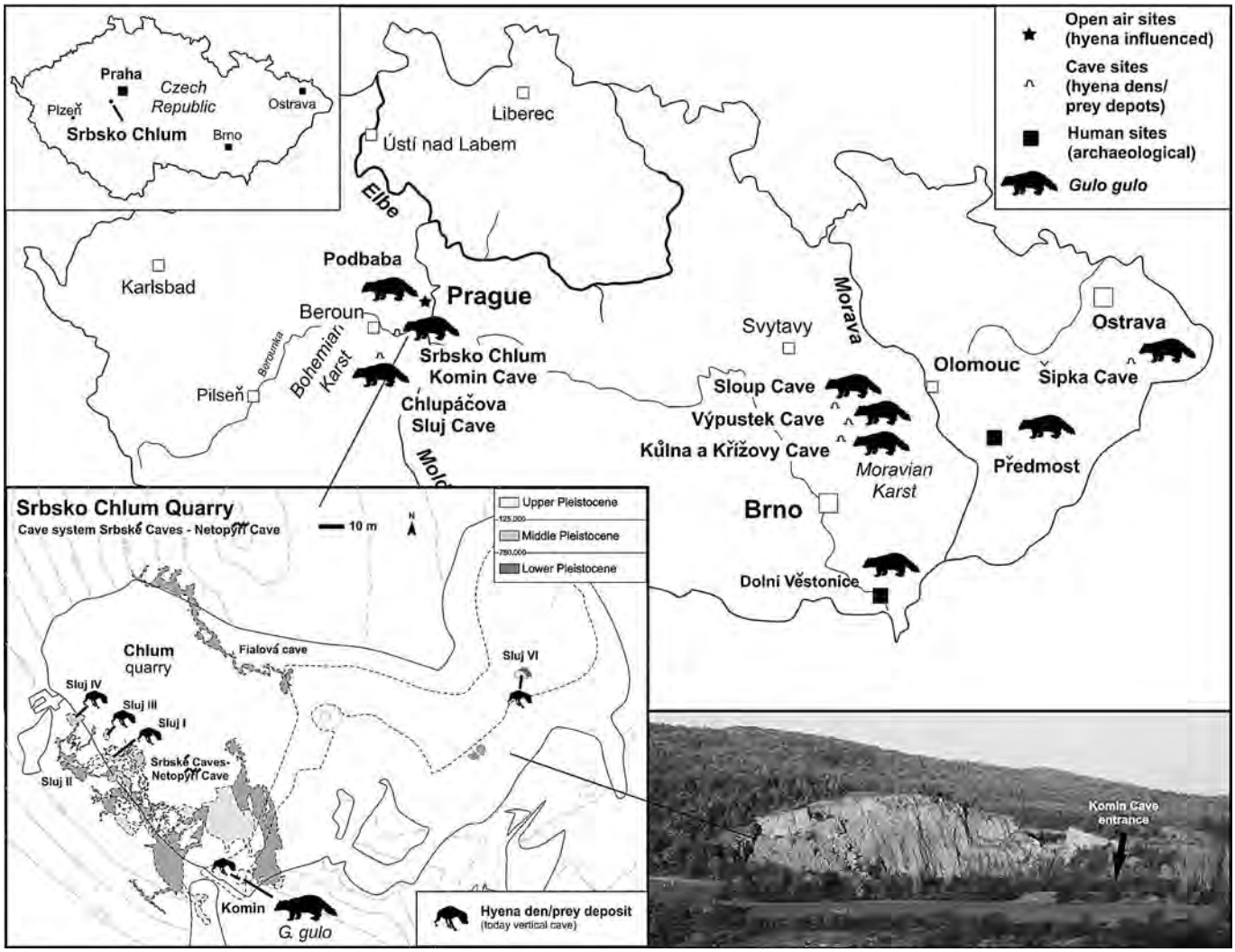

Figure 1. Positions of wolverine *G. gulo* (Linné, 1758) sites in Czech Republic focusing on the Bohemian Karst and adjacent areas around Prague, Czech Republic. Srbsko quarry caves have provided thousands of bones from the Middle to Upper Pleistocene.

them are nearly complete, lacking only incisor teeth. The other two (Figs. 4.3 and 4.4) were cracked by carnivores, with the ramus missing. One mandible is from an adult animal (Fig. 4.2), two are from old-age adult wolverines (Figs. 4.1 and 4.3), and the fourth represents an older individual, as evidenced by severely worn teeth (Fig. 4.4). A single canine tooth without half of the used cusp (Fig. 4.5) is, again, from an older animal. Additionally, two incisor teeth (not figured, Table 1) are from adult-to-senile animals.

The postcranial material is from adult-to-senile individuals and consists of a right complete radius (Fig. 4.6) and a right complete ulna (Fig. 4.7). Two metacarpi, one recently damaged (Fig. 4.12) and one complete left Mc IV (Fig. 4.13), are from the manus skeleton. The hind limb bones include a distally incomplete left femur (Fig. 4.8) that was damaged during the excavations. Also the right and left tibia bones (Figs. 4.9 and 4.10) are similar in length (14.6 cm), indicating they may have come from the same individual. A right astragal is complete (Fig. 4.11). Finally, from the pedal skeleton, the right Metatarsus IV (Fig. 4.14) was found in the sediment dump in front of the cave during a sieving program in 2005. A fractured femur and metacarpus appeared freshly broken.

Discussion

Processing of samples from the Srbsko-Komin hyena den showed that about 60% of the sediment was hyena coprolite material. Some of the excrements were pellet aggregates, while others were single large pellets of up to 8 cm. These single large pellets were drop-shaped, round or oval and flat on the attachment sides, the shape of the entire pellet depends on the moisture and amount of phosphate obtained by swallowing bone fragments. Bone fragments generally adhere to bone compacta and spongi-

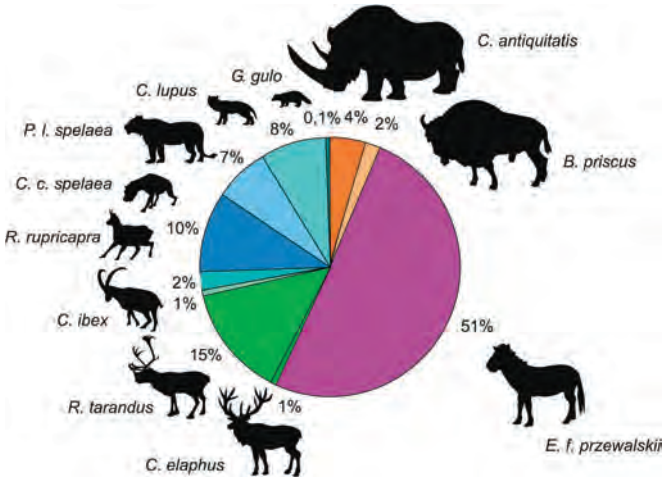

Figure 2. Percentages of hyena *Crocuta crocuta spelaea* (Goldfuss) prey remains in the Srbsko Chlum-Komín vertical cave (n = 3,569 bones) (after Diedrich and Žák, 2006).

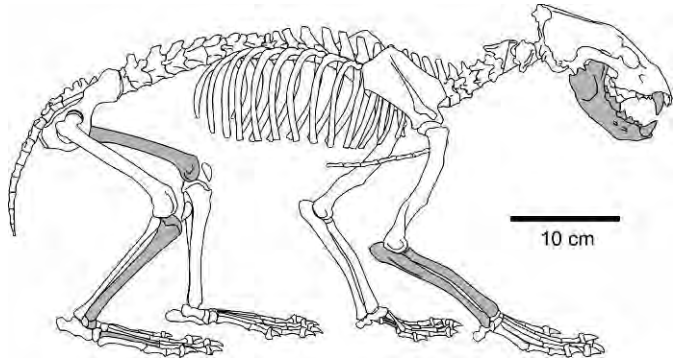

Figure 3. Anatomical locations of bones of three adult-to-senile *Gulo gulo* (Linné, 1758) individuals from the Upper Pleistocene Srbsko Chlum-Komin Cave, Bohemian Karst, Czech Republic. See Figure 4 and Table 1 for details on the bones.

osa fragments, which are then rounded by stomach acids (Diedrich, 2006; Diedrich and Žák, 2006). Such pellets were often trampled, building a phosphatic yellow-to-white layer in the cave sediments. The fecal pellet markings (Bearder and Randall, 1978; Fosse et al., 1998; Diedrich and Žák, 2006) and the megafauna assemblage, with its preservation, along with the large quantity of hyena remains, confirm the site as a well-frequented and long-term hyena-den cave site (Diedrich and Žák, 2006).

We compared the wolverine bone material to modern wolverines of Canada (Collection of Archeozoology, University Alberta, Canada), a well-preserved skeleton from the Salzofenhöhle in the Tote Gebirge (Pacher and Döppes, 1997), Pleistocene material from the catalogue of the Middle European sites (Döppes, 2001), and material from the German Perick Caves (Diedrich and Döppes, 2004). The small complete mandibles (lengths 10.7 to 10.9 cm) indicate females (Döppes, 2001), as do the tibiae and the radius. The ulna was consistent with the length of larger males. The other material is not useful for sex identification. All material appears to be from adult animals; juveniles are absent. Predation or scavenging on wolverines is evident primarily in the mandible remains, which were cracked out of the skulls by hyenas or other carnivores (e.g., Diedrich, 2006). A few wolverine skull fragments were also discovered, although postcranial bones are generally intact and show no evidence of chewing.

The presence of wolverine in the Komin is most likely due to predation or scavenging. Wolverines, as scavenging carnivores themselves, may have been drawn to carrion in the cave, such as reindeers (Fig. 5), which also have been found in the Srbsko Komin Cave, leaving them vulnerable to larger predators such as hyenas, or they may have been preyed upon and transported to the cave. While the ecology of Pleistocene wolverines is unclear, contemporary wolverines are not known to use caves for anything other than periodic resting or foraging sites (Magoun and Copeland, 1998). Wolverines produce their young during winter, and reproductive den sites are most commonly reported as occurring within the snow layer or associated with woody debris or boulder structures beneath the snow layer (Magoun and Copeland, 1998). Overhanging cliffs and shallow caves are occasionally used as secondary dens and rendezvous sites (Magoun and Copeland, 1998), but use of caves that are protected enough to preserve the remains of either wolverines or their prey has not been reported for modern wolverines. Additionally, reproductive den sites of contemporary wolverines are often characterized by the presence of latrine sites wherein large numbers of scats are present. Had caves been used as reproductive dens by Pleistocene wolverines, one might expect the presence of such latrines. The lack of wolverine corprolites in the Komin also precludes the possibility that wolverines fell into vertical passageways, as has been reported by White et al. (1984) and Parmalee (1967), which can not be concluded for the Srbsko-Cave at all. Predation

→

Figure 4. *Gulo gulo* (Linné, 1758) remains from the Upper Pleistocene Srbsko Chlum-Komin Cave, Bohemian Karst, Czech Republic. NMP = National Museum Prague. 1. Right mandible of an adult animal (NMP No. R 4376), lateral. 2. Right mandible of an adult animal (NMP No. R 4377), lateral. 3. Left mandible of an adult animal (NMP No. R 4858), lateral. 4. Right mandible of a senile animal (NMP No. R 4853), lateral. 5. Canine of a senile animal (NMP No. R 4202), lateral. 6. Right radius of an adult-senile animal (NMP No. R 4257), cranial. 7. Right ulna of an adult-senile animal (NMP No. R 4256), lateral. 8. Left femur of an adult-senile animal (NMP No. Ra 3764), cranial. 9. Right tibia of an adult-senile animal (NMP

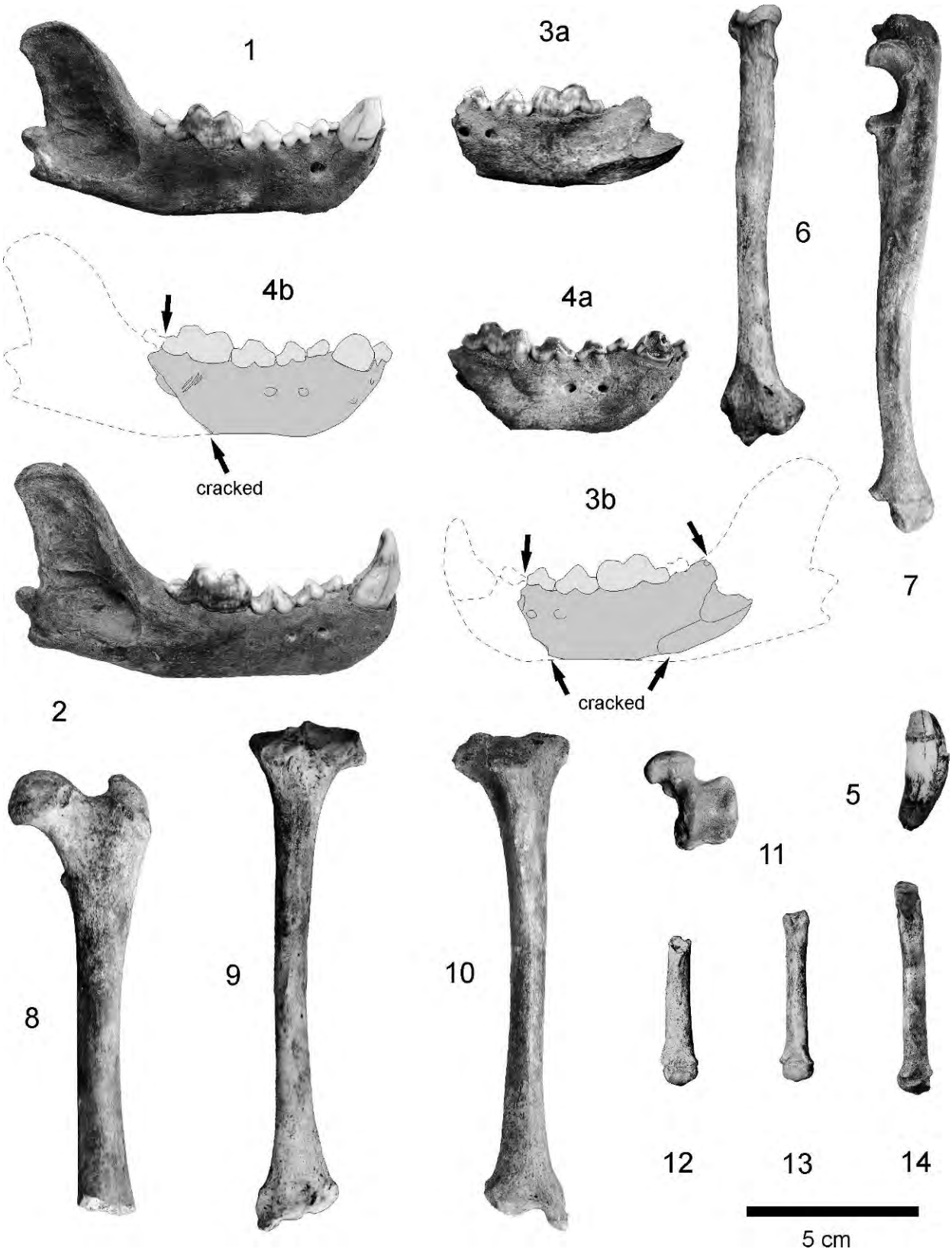

No. Ra 3765), caudal. 10. Right tibia of an adult-senile animal (NMP No. R 5320), cranial. 11. Right astragal of an adult-senile animal (NMP No. R 4378), dorsal. 12. Metacarpal bone fragment (NMP No. R 4204), cranial. 13. Left metacarpal IV of an adult-senile animal (NMP No. R 4203), cranial. 14. Right metatarsal IV (Museum of the Bohemian Karst Beroun without number), cranial.

Table 1. *Gulo gulo* (Linné, 1758) bone remains from the Upper Pleistocene Srbsko-Chlum-Komin Cave, Bohemian Karst, Czech Republic.

No.	Coll.-No.	Locality and Collector	Bone Type	Remarks	Left	Right	Individual Age	Photoplate Original	Collection
1	R 4376	Chlum-Komin (Beneš 1968)	Mandible (length 8.7 cm)	Nearly complete, without $I_{1–3}$		x	Senile	x	National Museum Prague
2	R 4377	Chlum-Komin (Beneš 1968)	Mandible (length 8.9 cm)	Nearly complete, without $I_{1–3}$, M_2		x	High Adult	x	National Museum Prague
3	R 4858	Chlum-Komin (Beneš 1971)	Mandible	With $P_{3–4}$, M_1	x		Senile	x	National Museum Prague
4	R 4853	Chlum-Komin (Beneš 1971)	Mandible	Without ramus, and I_1, M_2		x	Senile	x	National Museum Prague
5	R 4202	Chlum-Komin (Beneš 1964)	Canine	Incomplete			Senile	x	National Museum Prague
6	R 5317	Chlum-Komin (Beneš 1968)	I_2	Incomplete	x		Adult/Senile		National Museum Prague
7	R 4855	Chlum-Komin (Beneš 1971)	I_3	Incomplete		x	Adult/Senile		National Museum Prague
8	R 4257	Chlum-Komin (Beneš 1965)	Radius (length 10.3 cm)	Complete		x	Adult/Senile	x	National Museum Prague
9	R 4256	Chlum-Komin (Beneš 1964)	Ulna (length 12.2 cm)	Complete		x	Adult/Senile	x	National Museum Prague
10	R 4204	Chlum-Komin (Beneš 1964)	Metacarpus	Fragment			?	x	National Museum Prague
11	R 4203	Chlum-Komin (Beneš 1964)	Metacarpus	IV	x		Adult/Senile	x	National Museum Prague
12	Ra 3764	Chlum-Komin (Fejfar 1964)	Femur	Without distal joint	x		Adult/Senile	x	National Museum Prague
13	Ra 3765	Chlum-Komin (Fejfar 1964)	Tibia (length 11.6 cm)	Complete		x	Adult/Senile	x	National Museum Prague
14	R 5320	Chlum-Komin (Beneš 1972)	Tibia (length 11.6 cm)	Complete		x	Adult/Senile	x	National Museum Prague
15	R 4378	Chlum-Komin (Beneš 1968)	Astragalus	Complete		x	Adult/Senile	x	National Museum Prague
16	Srbsko-G1	Chlum-Komin (Diedrich 2005)	Metatarsus	IV		x	Adult/Senile	x	Museum Bohemian Karst Beroun

upon wolverines by conspecifics (Persson, 2003; Krebs et al., 2004), mountain lions (*Puma concolor*) (Krebs et al., 2004), and wolves (Burkholder, 1962) indicates the vulnerability of the species to large predators, which likely included the European hyena during the Late Pleistocene. The practice of modern African spotted hyenas (*Crocuta crocuta crocuta*) to kill and scavenge other predators up to lion sizes is evidenced by numerous descriptions of the bones of prey species at modern hyena dens (Sutcliffe, 1970; Kruuk, 1972; Scott and Klein, 1981) and recently proven for Late Pleistocene (*Crocuta crocuta spelaea*) hyena dens (Diedrich, 2009a). The lack of wolverine corprolites and the association of chewed wolverine bones with numerous other macromammal remains in other prey-storage cave sites (Diedrich and Žák, 2006) support our contention that wolverines were most likely killed at or near the cave and transported there to be eaten by hyenas, such as recently proposed for two other Late Pleistocene

Figure 5. Wolverine on reindeer carcass near the Srbsko Chlum-Komin Cave, Bohemian Karst, Czech Republic (illustration courtesy of G. "Rinaldino" Teichmann by permission).

hyena den sites, the Sloup Cave (Czech Republic: Diedrich, 2009b), and the Perick Caves (Germany: Diedrich, 2008).

Acknowledgements

Access to the collection and loans of bone material from the Museum of the Bohemian Karst Beroun was possible by the support of I. Jančaříková. The head of the Department of Palaeontology, K. Zagoršek, supported our study of their Pleistocene collection. The Speleological Club Praha, especially K. Ryšánek, facilitated trips to the Srbsko-Chlum Cave. K. Žák shared his knowledge of Bohemian Caves. M. Schwartz and J. Squires provided useful comments on early versions of the manuscript.

References

Bearder, S.K., and Randall, R.M., 1978, The use of fecal marking sites by spotted hyaenas and civets: Carnivore, v. 1, p. 32–48.

Beneš, J., 1970, Pleistocénní savci z Chlumu u Srbska (Čechy): Časopis Národního Muzea, Oddíl přírodovědný, v. 137, no. 3/4, p. 17–26.

Burkholder, B.L., 1962, Observations concerning wolverine: Journal of Mammalogy, v. 43, p. 263–264.

Diedrich, C., 2006, The *Crocuta crocuta spelaea* (Goldfuss 1823) population from the early Upper Pleistocene hyena open air prey deposit site Biedensteg near Bad Wildungen (Hess, NW Germany) and contribution to their phylogenetic position, coprolites and prey: Cranium, v. 23, no. 1, p. 1–15.

Diedrich, C., 2007, Bone crackers and carcass accumulators in Central Bohemia—Late Pleistocene hyenas and their cave den and prey depot types: Scripta Facultatis Scientiarum Universitatis Masarykianae Geology, v. 35, p. 91–96.

Diedrich, C., 2008, Die letzen Vielfraße *Gulo gulo* (Linné, 1758) aus den Perick- und Rösenbecker Höhlen im Sauerländer Karst: Mitteilungen des Verbandes der deutschen Höhlen- und Karstforscher, v. 54, no. 2, p. 36–44.

Diedrich, C., 2009a, Steppe lion remains imported by Ice Age spotted hyenas into the Late Pleistocene Perick Caves hyena den in Northern Germany: Quaternary Research, v. 71, no. 3, p. 361–374.

Diedrich, C., 2009b, A Late Pleistocene wolverine *Gulo gulo* (Linné, 1758) skeleton remain from the Sloup Cave in the Moravian Karst, Czech Republic: Annalen des Naturhistorischen Museums Wien, v. 110A, p. 123–132.

Diedrich, C., and Döppes, D., 2004, Oberpleistozäne Vielfraßreste (*Gulo gulo* Linné 1758) aus dem Perick-Höhlensystem im Sauerland (NW Deutschland): Philippia, v. 11, no. 4, p. 335–342.

Diedrich, C., and Žák, K., 2006, Prey deposits and den sites of the Upper Pleistocene hyena *Crocuta crocuta spelaea* (Goldfuss 1823) in horizontal and vertical caves of the Bohemian Karst (Czech Republic): Bulletin of Geosciences, v. 81, no. 4, p. 237–276.

Döppes, D., 2001, *Gulo gulo* (Mustelidae, Mammalia) im Jungpleistozän Mitteleuropas: Beiträge zur Paläontologie, v. 26, p. 1–95.

Fosse, P., Brugal, J.P., Guadelli, J.L., Michel, P., and Tournepiche, J.F., 1998, Les repaires d' hyenes des cavernes en Europe occidentale: presentation et comparisons de quelques assemblages osseux, *in* Economie Prehistorique: Les comportements de substance au Paleolithique, XVIII Rencontres internationales d' Archeologie et d' Historie d' Antibes, Sophia Antipolis, Editions APDCA, p. 44–61.

Krebs, J., Lofroth, E., Copeland, J., Banci, V., Golden, H., Magoun, A., Mulders, R., and Shults, B., 2004, Synthesis of survival rates and causes of mortality in North American wolverine: Journal of Wildlife Management, v. 68, p. 493–502.

Kruuk, H., 1972, The Spotted Hyena: A story of predation and social behavior, Chiciago, University of Chicago Press, 352 p.

Magoun, A.J., and Copeland, J.P., 1998, Characteristics of wolverine reproductive den sites: Journal of Wildlife Management, v. 62, no. 4, p. 1313–1320.

Pacher, M., and Döppes, D., 1997, Zwei Faunenelemente aus pleistozänen Höhlenfundstellen des Toten Gebirges: *Canis lupus* L. und *Gulo gulo* L.: Geologische und Paläontologische Mitteilungen Innsbruck, v. 22, p. 129–151.

Parmalee, P.W., 1967, A recent cave bone deposit in south-western Illinois: Bulletin of the National Speleological Society, v. 29, p. 119–147.

Persson, J., 2003, The role of intraspecific predation in the survival of juvenile wolverines *Gulo gulo*: Wildlife Biology, v. 9, p. 21–28.

Scott, L., and Klein, R.G., 1981, A hyena accumulated bone assemblage from late holocene deposits at Deelpan, Orange Free State, South Africa: Annals of the South African Museum, v. 86, p. 217–227.

Sutcliffe, A.J., 1970, Spotted Hyena: Crusher, gnawer, digester and collector of bones: Nature, v. 227, p. 110–113.

White, J.A., McDonald, H.G., Anderson, E., and Soiset, J.M., 1984, Lava blisters as carnivore traps, *in* Genoways, H.H., and Dawson, M.R., eds., Contributions in Quaternary Vertebrate Paleontology: A Volume in Memorial to John E. Guilday, Pittsburgh, Carnegie Museum of Natural History Special Publication 8, p. 241–256.

BOOK REVIEW

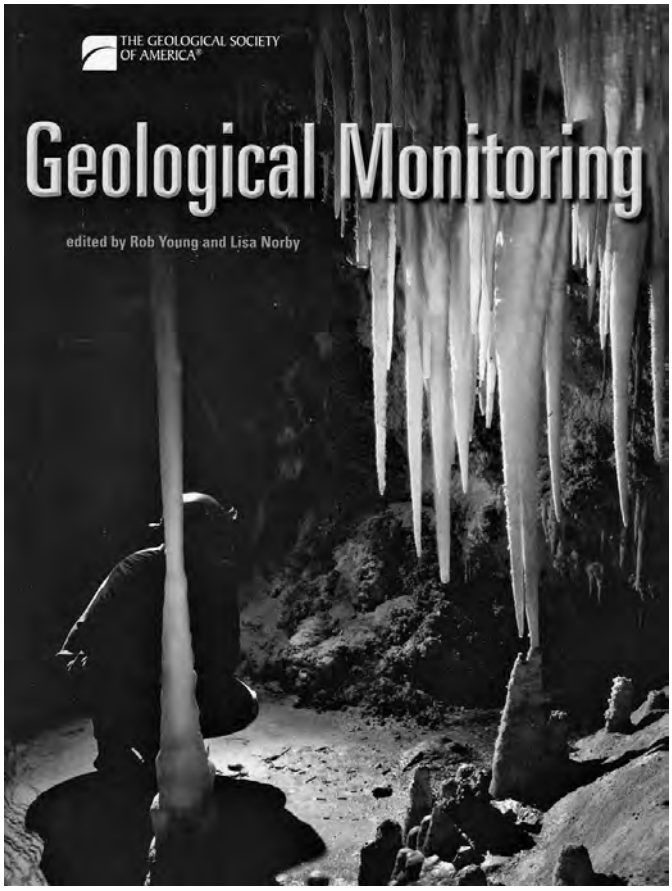

Geological Monitoring

Rob Young and Lisa Norby, editors, 2009. Boulder, Colorado, Geological Society of America, 305 p. ISBN 978-0-8137-6032-2, softbound, 8.5 × 11 inches, $80 ($56 for GSA members). Order at www.geosociety.org/bookstore.

This is a guide for resource managers who need to establish the status of the geological features and the effects of processes affecting them on the lands they supervise. Funded by the Geologic Resources Division of the National Park Service and published by the Geological Society of America, it has strong credentials. This is not a guide to inventorying resources, but a description of methods for their long-term monitoring. Methods of studying the most common geological features are described, with case studies.

The selected topics include features and processes of the following types: aeolian, spelean, coastal, fluvial, geothermal, glacial, marine, paleontological, permafrost, seismic, slope-movement, and volcanic. The book is well illustrated with photos, maps, and diagrams, mostly in color, and there is a nice cover shot of Carlsbad Cavern by Ron Kerbo, former NPS Cave Specialist. Each chapter begins with a detailed introduction to the topic, including a description of stresses to the resource. ''Vital Signs'' are then covered_i.e., processes and features to monitor and methods for doing so. Approaches are graded according to their technical and financial demands.

The chapter on caves is by Rick Toomey of Mammoth Cave National Park. He stresses inventorying and recurrent, long-term research. Specific topics include (1) meteorology and its effect on speleothems; (2) airborne sediments, including natural and anthropogenic; (3) visitor impacts (everything from deliberate breakage to lampenflora), with LIDAR and photomonitoring as promising approaches; (4) ice; (5) cave drips and pools (quantity and chemistry); (6) cave microbiology; (7) cave stability (breakdown, etc.); (8) mineral growth; (9) surface expressions and processes; (10) regional groundwater patterns, quantity, and chemistry; and (11) subterranean fluvial processes (brief coverage, so as not to overlap with the chapter specifically on this topic). References are mainly non-technical and aimed toward management issues. The other chapters deal mainly with geology and physical processes, with the discussion of cave microbiology in this chapter a welcome exception.

Although few other authors even mention caves and karst, they describe features, processes, and monitoring techniques that speleologists will find pertinent. This is particularly true for the fluvial, glacial, geothermal, and volcanic chapters. The chapter on volcanoes ignores lava caves, in preference to such topics as land stability and gas emissions, but vulcanospeleologists will still find much of value.

This book is not designed for entertainment, nor is it an introductory text. Appropriately, the arrangement of topics is formulaic, as in a cook-book. Those who need it most are resource managers who desire a guide to establishing their own programs and strategies. Students and researchers can also learn of potential projects, measurement techniques, and approaches to data analysis.

Reviewed by Arthur N. Palmer, Department of Earth Sciences, State University of New York, Oneonta, NY 13820-4015 (palmeran@oneonta.edu).

DOI: 10.4311/jcks2010br0156

GUIDE TO AUTHORS

The *Journal of Cave and Karst Studies* is a multidisciplinary journal devoted to cave and karst research. The *Journal* is seeking original, unpublished manuscripts concerning the scientific study of caves or other karst features. Authors do not need to be members of the National Speleological Society, but preference is given to manuscripts of importance to North American speleology.

LANGUAGES: The *Journal of Cave and Karst Studies* uses American-style English as its standard language and spelling style, with the exception of allowing a second abstract in another language when room allows. In the case of proper names, the *Journal* tries to accommodate other spellings and punctuation styles. In cases where the Editor-in-Chief finds it appropriate to use non-English words outside of proper names (generally where no equivalent English word exists), the *Journal* italicizes them. However, the common abbreviations i.e., e.g., et al., and etc. should appear in roman text. Authors are encouraged to write for our combined professional and amateur readerships.

CONTENT: Each paper will contain a title with the authors' names and addresses, an abstract, and the text of the paper, including a summary or conclusions section. Acknowledgments and references follow the text.

ABSTRACTS: An abstract stating the essential points and results must accompany all articles. An abstract is a summary, not a promise of what topics are covered in the paper.

STYLE: The *Journal* consults The Chicago Manual of Style on most general style issues.

REFERENCES: In the text, references to previously published work should be followed by the relevant author's name and date (and page number, when appropriate) in parentheses. All cited references are alphabetical at the end of the manuscript with senior author's last name first, followed by date of publication, title, publisher, volume, and page numbers. Geological Society of America format should be used (see http://www.geosociety.org/pubs/geoguid5.htm). Please do not abbreviate periodical titles. Web references are acceptable when deemed appropriate. The references should follow the style of: Author (or publisher), year, Webpage title: Publisher (if a specific author is available), full URL (e.g., http://www.usgs.gov/citguide.html) and date when the web site was accessed in brackets; for example [accessed July 16, 2002]. If there are specific authors given, use their name and list the responsible organization as publisher. Because of the ephemeral nature of websites, please provide the specific date. Citations within the text should read: (Author, Year).

SUBMISSION: Effective July 2007, all manuscripts are to be submitted via AllenTrack, a web-based system for online submission. The web address is http://jcks.allentrack2.net. Instructions are provided at that address. At your first visit, you will be prompted to establish a login and password, after which you will enter information about your manuscript (e.g., authors and addresses, manuscript title, abstract, etc.). You will then enter your manuscript, tables, and figure files separately or all together as part of the manuscript. Manuscript files can be uploaded as DOC, WPD, RTF, TXT, or LaTeX. A DOC template with additional manuscript specifications may be downloaded. (Note: LaTeX files should not use any unusual style files; a LaTeX template and BiBTeX file for the *Journal* may be downloaded or obtained from the Editor-in-Chief.) Table files can be uploaded as DOC, WPD, RTF, TXT, or LaTeX files, and figure files can be uploaded as TIFF, EPS, AI, or CDR files. Alternatively, authors may submit manuscripts as PDF or HTML files, but if the manuscript is accepted for publication, the manuscript will need to be submitted as one of the accepted file types listed above. Manuscripts must be typed, double spaced, and single-sided. Manuscripts should be no longer than 6,000 words plus tables and figures, but exceptions are permitted on a case-by-case basis. Authors of accepted papers exceeding this limit may have to pay a current page charge for the extra pages unless decided otherwise by the Editor-in-Chief. Extensive supporting data will be placed on the *Journal*'s website with a paper copy placed in the NSS archives and library. The data that are used within a paper must be made available. Authors may be required to provide supporting data in a fundamental format, such as ASCII for text data or comma-delimited ASCII for tabular data.

DISCUSSIONS: Critical discussions of papers previously published in the *Journal* are welcome. Authors will be given an opportunity to reply. Discussions and replies must be limited to a maximum of 1000 words and discussions will be subject to review before publication. Discussions must be within 6 months after the original article appears.

MEASUREMENTS: All measurements will be in Systeme Internationale (metric) except when quoting historical references. Other units will be allowed where necessary if placed in parentheses and following the SI units.

FIGURES: Figures and lettering must be neat and legible. Figure captions should be on a separate sheet of paper and not within the figure. Figures should be numbered in sequence and referred to in the text by inserting (Fig. x). Most figures will be reduced, hence the lettering should be large. Photographs must be sharp and high contrast. Color will generally only be printed at author's expense.

TABLES: See http://www.caves.org/pub/journal/PDF/Tables.pdf to get guidelines for table layout.

COPYRIGHT AND AUTHOR'S RESPONSIBILITIES: It is the author's responsibility to clear any copyright or acknowledgement matters concerning text, tables, or figures used. Authors should also ensure adequate attention to sensitive or legal issues such as land owner and land manager concerns or policies.

PROCESS: All submitted manuscripts are sent out to at least two experts in the field. Reviewed manuscripts are then returned to the author for consideration of the referees' remarks and revision, where appropriate. Revised manuscripts are returned to the appropriate Associate Editor who then recommends acceptance or rejection. The Editor-in-Chief makes final decisions regarding publication. Upon acceptance, the senior author will be sent one set of PDF proofs for review. Examine the current issue for more information about the format used.

ELECTRONIC FILES: The *Journal* is printed at high resolution. Illustrations must be a minimum of 300 dpi for acceptance.

Journal of Cave and Karst Studies

Volume 72 Number 2 August 2010